PREDICTION OF CUTTING COEFFICIENTS DURING ORTHOGONAL METAL CUTTING PROCESS USING FEA APPROACH

PREDICTION OF CUTTING COEFFICIENTS DURING ORTHOGONAL METAL CUTTING PROCESS USING FEA APPROACH

By

Tarek Kershah, B.Sc.

A Thesis

Submitted to the School of Graduate Studies

in Partial Fulfillment of the Requirements

for the Degree

Master of Applied Sciences

McMaster University

MASTER OF APPLIED SCIENCE (2013)	McMaster University
Mechanical Engineering Department	Hamilton, Ontario

TITLE	PREDICTION OF CUTTING COEFFICIENTS DURING ORTHOGONAL METAL CUTTING PROCESS USING FEA APPROACH
AUTHOR	Tarek Kershah, B.Sc. (Alexandria University, Egypt)
SUPERVISORS	Dr. Eu-Gene Ng Dr. M. A. Elbestawi
NUMBER OF PAGES	xvii, 86

Abstract

Finite element analysis (FEA) employs a science-based approach in which the complete machining process can be simulated and optimized before resorting to costly and time-consuming experimental trials. In this work, cutting coefficient of AISI 1045 steel will be estimated using finite element modelling using Arbitrary Lagrangian Formulation (ALE). The estimated values are then experimentally validated. A parametric study is carried out after in order to investigate how some cutting parameters can affect the cutting coefficients. The process parameters to be varied include feed rate, cutting speed, and cutting edge radius.

Acknowledgements

I would like to express my deep gratitude to both of my supervisors, Dr. Eu-Gene Ng, and Dr. Mohamed Elbestawi. I sincerely appreciate their continuous guidance, patience and support throughout the preparation of this dissertation.

Special thanks are due to Dr. Philip Koshy, and Dr. Stephen Veldhuis for their valuable help, discussions and insightful suggestions.

I would like to thank the Mechanical Engineering machine shop technicians, Terry, Jim, Ron, Mike, and Michael for their help and guidance during experimental work throughout my research.

I would like to thank my colleagues Keyvan, Nima, Mahmoud, and Ganesh for their valuable help whenever needed.

I would like to thank NSERC CANRIMT and Discovery grant for providing financial support for this research.

At the end, I would like to thank my parents for their understanding, patience and continuous support throughout my work at McMaster University.

Table of Contents

List of Figures

List of Tables

Nomenclature and List of Symbols

v : Cutting speed (m min^{-1})
vc: Chip velocity (m min^{-1})
f : Feed rate (mm rev^{-1})
t : Undeformed chip thickness (mm)
tm : Minimum Chip thickness (mm)
w : Width of cut (mm)
Fc : Cutting force (N)
F_f : Feed force (N)
F_z : Axial force (N)
Kc: Cutting coefficient in cutting direction
K_f : Cutting coefficient in feed direction
α : Tool rake angle (deg)
β : Friction angle (deg)
μ : Coefficient of friction COF (-)
COF : Coefficient of friction (-)
ρ_e : Tool cutting edge radius (μm)
σ : Normal flow stress (MPa)
Ac : Uncut chip area (mm^2)
ALE : Arbitrary Lagrangian Eulerian
AISI: American Iron and Steel Institute
ANSI: American National Standards Institute
A : Material constant (MPa)
B : Material constant (MPa)
C : Strain rate index (-)
ε: Plastic strain (-)
ε_0: Plastic strain rate (s^{-1})
$\dot{\varepsilon}$: Reference plastic strain rate (s^{-1})
T : Temperature (ºC)
T_r: Reference temperature (ºC)
T_m: Workpiece material melting temperature (ºC)
m : Thermal index (-)
n : Strain hardening index (-)
ρ : Density (kg m^{-3})
α : (When used for material property) Thermal expansion (ºC^{-1})
c_p : Specific heat capacity (J kg^{-1} ºC^{-1})
k : Thermal conductivity (W m^{-1} ºC^{-1})
PSZ: Primary Shear Zone
SSZ: Secondary Shear Zone
CVD : Chemical vapor deposition
PVD : Physical vapor deposition
CNC : Computer numerical control
PCBN: Polycrystalline Cubic Boron Nitride
HRC: Rockwell Hardness

Chapter 1 Introduction

1.1 Background

Finite Element Analysis (FEA) has been widely used in simulating metal cutting process. Metal cutting process involves high temperatures and strain rates, which make Johnson-Cook [1] material model the preferred material model that can simulate these exceptional conditions. It has been noticed that there are many parameters that could affect the resulting forces during metal cutting, such as the workpiece material, the tool geometry, feed rates, and cutting speeds and many others factors. The resulting force per unit area is called the cutting coefficients. Many approaches have been used in order to predict the relation between these parameters and the resulting cutting coefficients. Some researchers used empirical models to estimate the cutting coefficients [2]; others used analytical models [3]. Over the last two decades researches used either mechanistic models [4] or FEA models [5]. FEA models have improved through years, and today it is showing relatively accurate and repeatable results when simulating metal cutting process. One advantage for using FEA models is the ability to include as many cutting parameters as possible including very complex parameters such as cutting edge radius. Another advantage is that FEA is an efficient tool when time and cost are of an essence as opposed to experimental approaches. Using FEA also helps to reduce experimental calibration.

In this work a number of FEA models are built in order to estimate the cutting coefficients resulting from metal cutting. FEA cutting models will then be experimentally validated.

1.2 Objectives

The main objective of the current research is to use FEA models in order to estimate the cutting coefficients, and study the effect of some cutting parameters on these cutting coefficients. This is done through two different phases, for two different cutting edge geometries:

- Phase I: The main objective for phase I is to validate the FEM model by comparing the cutting force Fc and feed force F_f with the experimental results.
- Phase II: The main objective for phase II is to study the effect of certain cutting parameters on the cutting coefficients.

Chapter 2 Literature Review

2.1 Estimation of Cutting Coefficients

The cutting coefficients determine the force required per unit area of material to be removed. Estimation of cutting coefficients during metal cutting is of great importance due to the fact that these coefficients determines the resulting cutting forces, and are used in mathematical dynamic models that study the dynamics of the machine tools including vibrations and chatter [6] [7]. Figure 2-1 shows the orthogonal cutting forces and its respective angles.

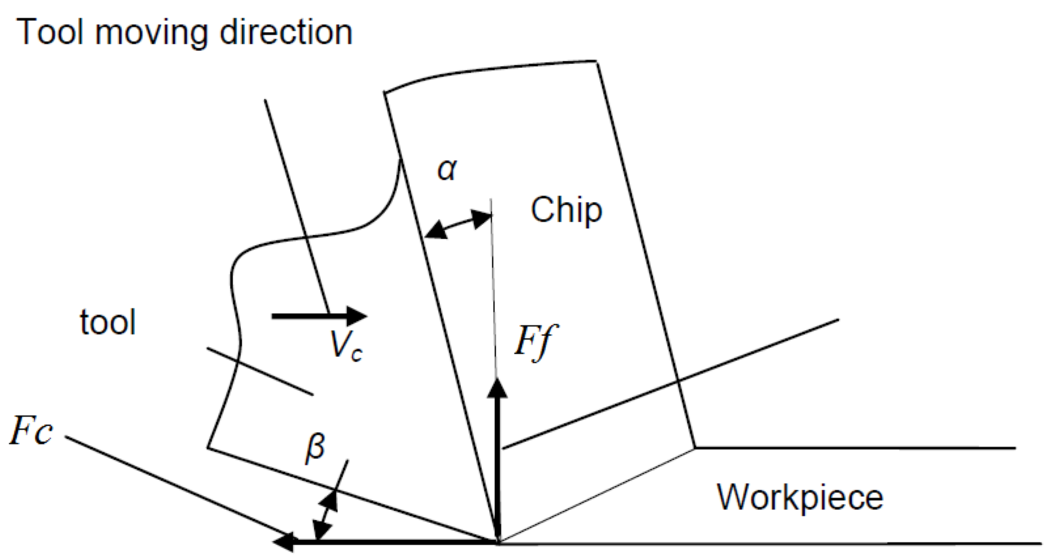

Figure 2-1: Orthogonal cutting forces and angles, α: rake angle, β: clearance angle, F_f: feed force, Fc: cutting force [8]

It should be noted that orthogonal metal cutting assumes that the tool has a plane cutting face and a cutting edge that is perpendicular to the cutting speed (*v*) and chip velocity (*vc*) vectors, Figure 2-2.

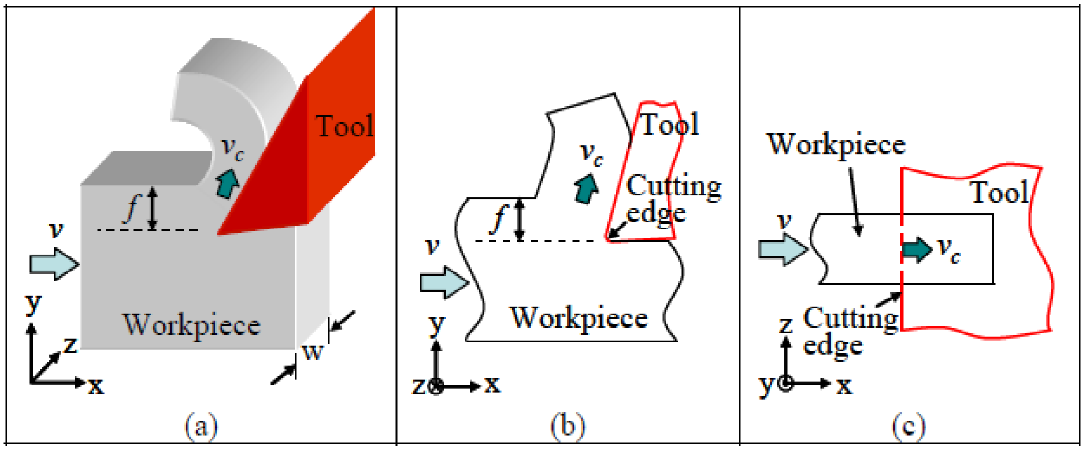

Figure 2-2: Orthogonal machining process. (a) 3-dimensional view. (b) Front view. (c) Top view. [9]

These cutting coefficients are functions of many parameters including cutting speed, feed rate, cutting edge radius, rake angle, clearance angle, and workpiece hardness.

Different types of models were used in the literature in order to estimate these cutting coefficients which can be classified into four major categories [10]:

- Empirical Models
- Analytical Models
- Mechanistic Models
- Finite element analysis Models

2.1.1 Empirical Models

The empirical models focus on deriving the cutting coefficients by using steady state cutting tests [11], dynamic cutting tests [12], and time-series methods [13]. Kienzel [2] developed an empirical models based on large number of experiments. The limitation of experiments is its empirical nature that requires change every time any of the cutting conditions or geometry or material is changed. Furthermore experiments are costly.

2.1.2 Analytical Models

For analytical models, Merchant [3], Lee and Shaffer [14] used a single shear plane theory. Whereas Oxley et al. [15] used the shear zone theory. Their approaches were to model the physical mechanisms that take place during the cutting process in order to predict the cutting forces. However, the main limitation of the analytical models is the high strain rates, high temperature gradients, and combined elastic and plastic deformations. Consequently most of analytical models are unable to predict the cutting forces accurately.

2.1.3 Mechanistic Models

The main concept behind the mechanistic methods is that the cutting forces are proportional to the uncut chip area *Ac*, equation (2.1). The constant of proportionality is the cutting coefficients, which depends on the cutting conditions, cutting geometry, and material properties as mentioned earlier.

$$F \; \alpha \; Ac \ldots\ldots\ldots \quad (2.1)$$

Early work was done by Koenigsberger and Sabberwal [16]. Fu et al. [17] developed a mechanistic model for predicting forces generated during face milling operation, while Chandrasekharan et al. [18] developed a mechanistic approach to predict the cutting forces in drilling. Kapoor et al [19] did an extensive work to show the fundamental elements of the basic mechanistic model; the work showed how the chip load and chip flow are calculated, with a description for workpiece-tool intersection model, and how the model is calibrated. Huang and Liang [4] developed a mechanistic model to model the cutting forces under hard turning conditions, where a genetic algorithm was applied to identify the coefficients. They also presented the modeling of the cutting forces due to chip formation. The tool wear effect was considered in their work.

2.1.4 Finite Element Analysis Models

Using finite elements model to predict cutting forces and cutting coefficients has been widely used by researchers since early 70's. This type of modelling is very promising due to the great breakthroughs in software and hardware needed for such simulations. Three different types of finite element formulations are commonly used in FEM cutting models:

- Lagrangian formulation
- Eulerian formulation
- Arbitary-Lagrangian Eulerian (ALE) formulation

Each of them has its own advantages and limitation, and depending on the cutting process simulated and the expected results one of them is chosen depending on these advantages and limitations.

2.1.4.1 Lagrangian Formulation

Lagrangian approach is usually used for modeling processes with little deformations as in solid-mechanics analysis. In Lagrangian formulations the FE mesh grids are attached completely to the material. Figure 2-3 (a) shows the initial position for the element mesh grid and material. Figure 2-3 (b) shows the final deformed material; the element mesh grids are still attached to the material and are deformed with the material deformation.

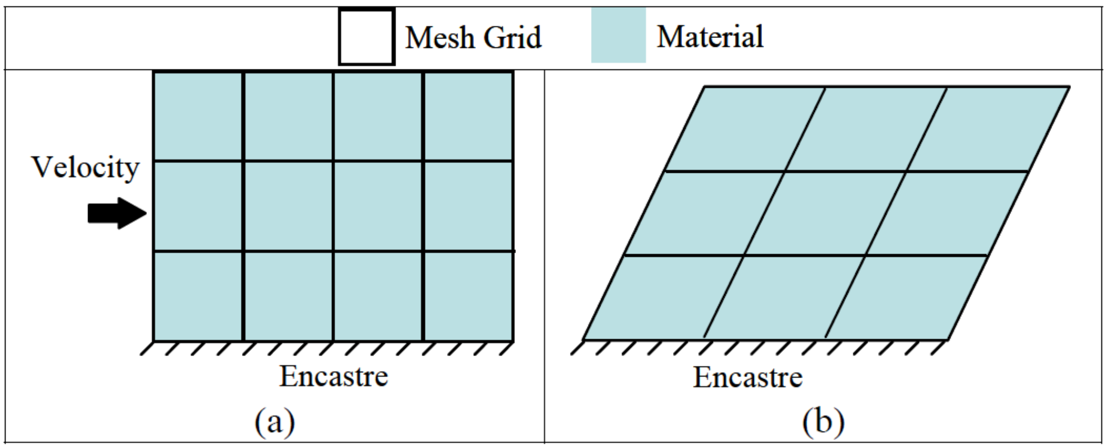

Figure 2-3: Initial position of mesh grids and material. (b) Both material and element mesh grid deformation after the velocity is applied [9]

Lagrangian formulation has been commonly used for simulating cutting process. Klamecki [20] was one of the pioneering researchers to employ the Lagrangian formulation technique to model metal cutting process. Figure 2-4 (a) shows a typical example of the initial mesh and boundary condition used in Lagrangian approach. As shown there is a predefined parting line below the uncut chip thickness t_o. The element along this thin defined parting line will be deleted as the tool cut through the workpiece. Figure 2-4 (b) shows an example of how the chip is formed as the tool cuts through the workpiece, where no initial chip geometry assumptions are required.

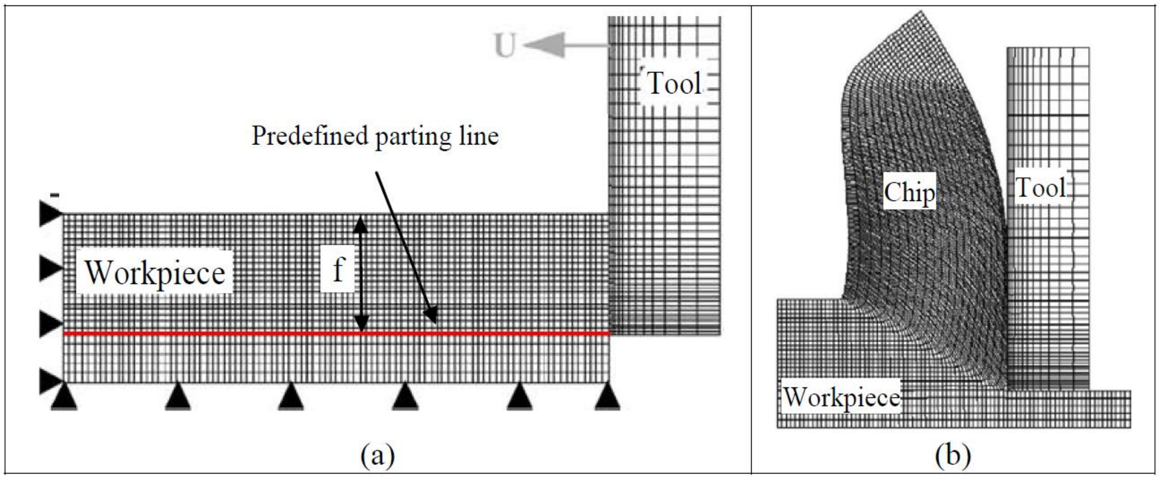

Figure 2-4: Initial boundary condition and geometry when using Lagrangian formulation in FE cutting models. (b) Continuous chip formation using Lagrangian formulation [21]

There are two main drawbacks for the Lagrangian formulation; the first drawback is the needs for a predefined parting line to prevent severe mesh distortion. However there should be a damage criterion for the predefined parting line, choosing the type and value of damage criterion has great influence on the results obtained from the FE model. After performing detailed analysis on material separation criteria, Huang and Black [22] concluded that neither the geometrical nor the physical criterion could simulate the initial cutting accurately. The other limitation of Lagrangian formulation is that the cutting edge radius cannot be simulated due to the presence of the partition line. If for instance the cutting edge radius is simulated, this will result in severe mesh distortion and simulation termination. Therefore the tool should be considered perfectly sharp $\rho e = 0^{o}$. However, this will hinder a lot of useful information like the size effect phenomenon and ploughing, which are of great importance on the cutting forces and coefficients, especially in the feed direction, where it will be underestimated [23].

2.1.4.2 Eulerian Formulation

In Eulerian formulation material are not attached to the FE mesh grids as opposed to Lagrangian formulation. Material has the ability to flow through the mesh grids which is fixed spatially. Figure 2-5 shows simple illustrations of the mesh grids and material flow when the Eulerian approach is employed. Figure 2-5 (a) shows the initial mesh grid and position of the material; Figure 2-5 (b) shows the final position of the mesh grid and the material flow when velocity is being applied. Since the mesh is fixed spatially, no mesh distortion occurs and consequently, no remeshing is required.

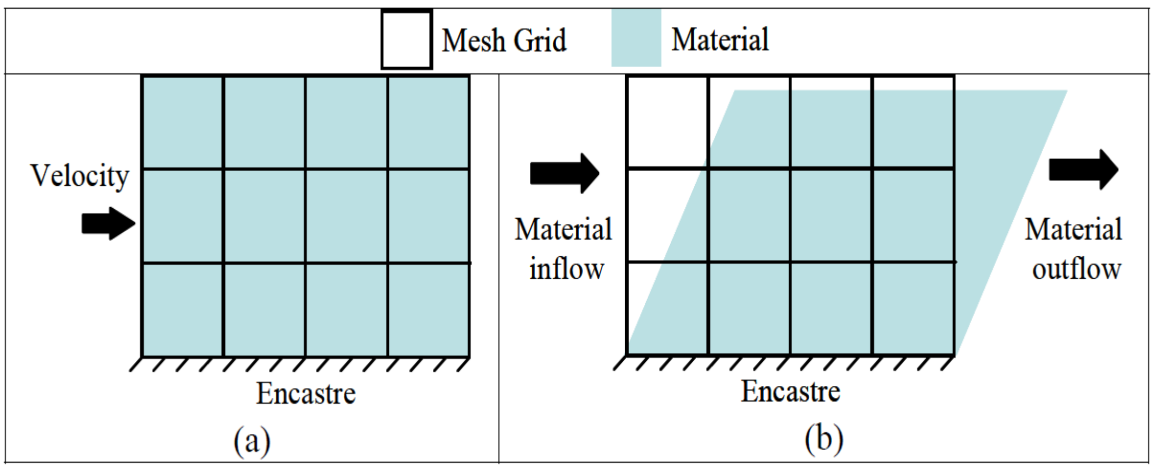

Figure 2-5: Initial position of mesh grids and material. (b) Final position of mesh grid and material flow when using Eulerian formulation [9]

Due to the fact that no predefined parting line is required with a damage criterion, it is now possible to include the cutting edge radius without expecting any severe mesh distortion. However, in order to do that a prior estimation for the chip geometry and the tool-chip contact length should be done. Figure 2-6 shows the initial geometry for Eularian formulation.

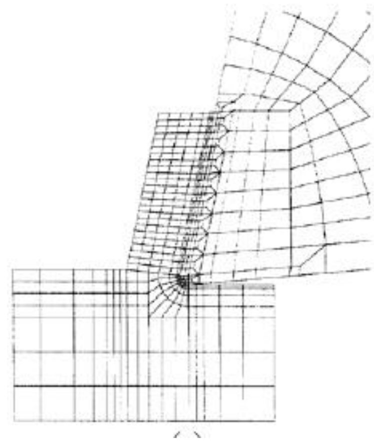

Figure 2-6: Example of initial geometry using Eulerian formulation [24]

Usui et al. [25] was one of the pioneers who used Eulerian formulation method to simulate cutting forces. Raczy [26] used Eulerian formulation to build a FE cutting model that included the tool cutting edge geometry; to predict the stress and strain distributions in the material. To overcome the problem of prior estimation for the chip geometry and the tool-chip contact length, Childs [27] and Kim [24] did number of iterative procedures including changing boundary conditions and mesh design until convergence is achieved.

Eularian formulation assume a viscoplastic material model with no elastic properties included, therefore residual stress analysis on the surface of the workpiece cannot be performed [28]

2.1.4.3 Arbitrary Lagrangian Eulerian Formulation (ALE)

It can be seen that both the Lagrangian and the Eulerian methods are not very efficient methods as far as some characteristics of cutting process are concerned. ALE is a third formulation approach that somehow combines these two methods together in order to eliminate their drawbacks and use their advantages in the best possible way. In an ALE analysis, the FEA mesh is neither attached to the material nor fixed spatially in space.

The mesh has an independent motion from the material. In order to reduce the severe mesh deformation of the workpiece material during deformation, Miguelez [29], Arrazola [30] and Ozel [31] used the adaptive mesh option to allow the remeshing of the workpiece material. However, the adaptive mesh option could not fully reduce the mesh distortion especially around the tool tip. Miguelez [29] and Ozel [31] solved the severe mesh distortion problem around the tool cutting edge radius by using very fine mesh around the tool cutting edge radius. A detailed ALE models for metal cutting was explained by Movahhedy [32], where an Eularian region was assigned to the workpiece area near the tool cutting edge, while other areas are Lagrangian regions. Figure 2-8 shows initial and final geometries when using ALE formulations. ALE technique in FE cutting model has been further improved by Nasr et al. [33]. An example of a similar, but better portioning scheme is shown in Figure 2-8. The Eulerian region is located around the same area (region B), however initial chip shape and the feed rate were assigned as Lagrangian region. The main purpose of the Eulerian region assigned is for the workpiece material to flow towards the chip and the machined surface, preventing excess element distortion and eliminating chip separation criterion. By assigning the initial chip shape area as Lagrangian region, the final shape of the chip will be absolutely formed based on the material deformation. ALE technique has been used for a long time for temperature prediction [34], and for residual prediction [33].

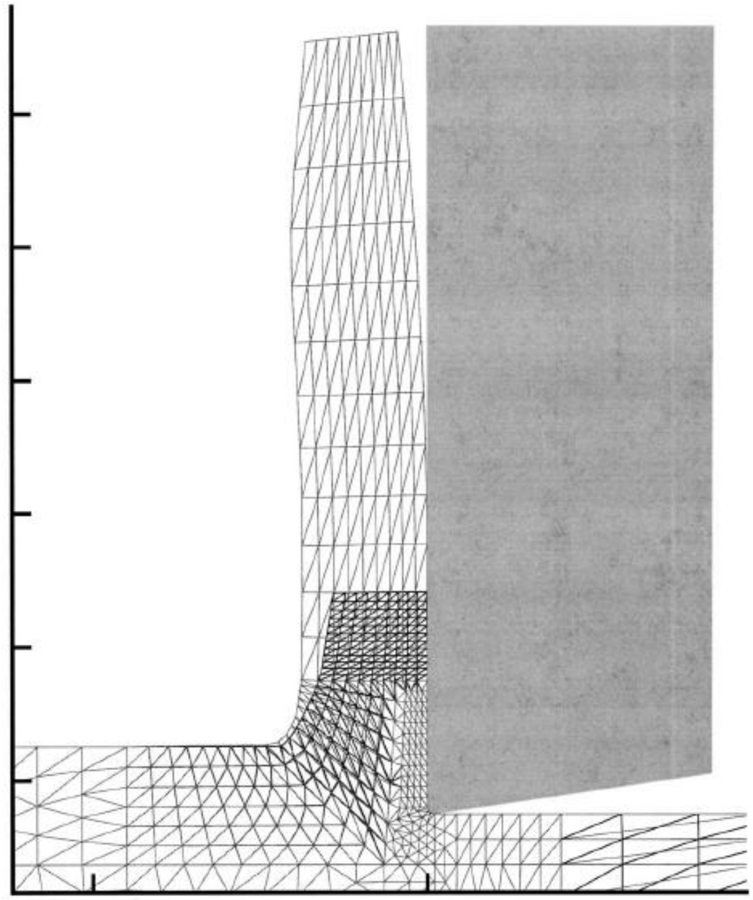

Figure 2-7: Initial and final chip shape in a typical ALE [35]

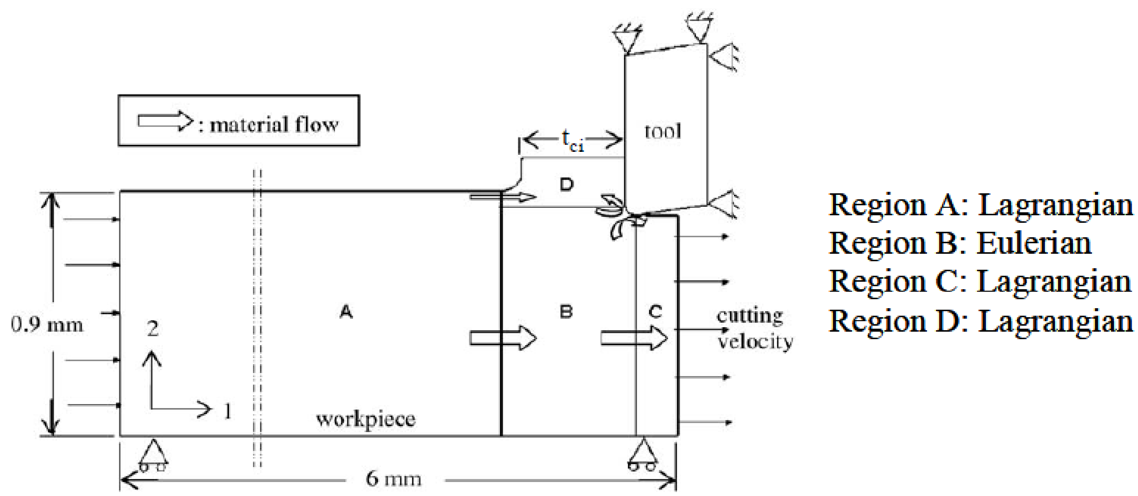

Figure 2-8: Boundary conditions, partitioning scheme and material flow when employing ALE [33]

2.2 Effect of Cutting Parameters on Cutting Coefficients

Various cutting parameters could have an effect cutting coefficients, such as feed rates f, cutting speeds v, cutting edge radius ρ_e, rake angle α, and other parameters. It is important to study the effect of these parameters so that we can choose the optimum parameters that guarantee the least possible cutting coefficient values while considering quality and time efficient cutting processes.

2.2.1 Effect of Feed Rate (*f*) on Cutting Coeffecients

It was reported by many researchers that the size effect in metal cutting is characterised by a non-linear increase in cutting coefficients for decreased undeformed chip thickness t [36], which is the feed rate in case of orthogonal metal cutting. Other researchers have also noted that the ratio of undeformed chip thickness to cutting edge radius plays a significant role on cutting coefficients especially when the undeformed chip thickness is less than the cutting edge radius [37]. Arsecularatne [38] found out that ploughing has a great effect on the size effect phenomenon. However, since it is difficult to measure ploughing accurately, it was stated that the best way is to observe the change in the cutting coefficients as feed rate is changed. Aramcharoen and Mativenga [39] made that observation, where they studied three cases; the first case Figure 2-9 (a) is when the undeformed chip thickness t is less than the minimum chip thickness t_m (referred to as h and h_m respectively), in this case the material will undergo an elastic deformation as it is compressed by the tool, and then recovers after the tool passes, in this case no chip is actually formed.

The second case Figure 2-9 (b) is when the undeformed chip thickness is equal to the minimum chip thickness; in this case the material will start to form a chip through shearing; however there would still be a portion of elastic deformation and recovery. Thus, the removed material is less than the desired value undeformed chip thickness *t*. Finally when the chip thickness is larger than the minimum chip thickness as shown in Figure 2-9 (c), material is removed and formed as a chip with no elastic deformation or recovery.

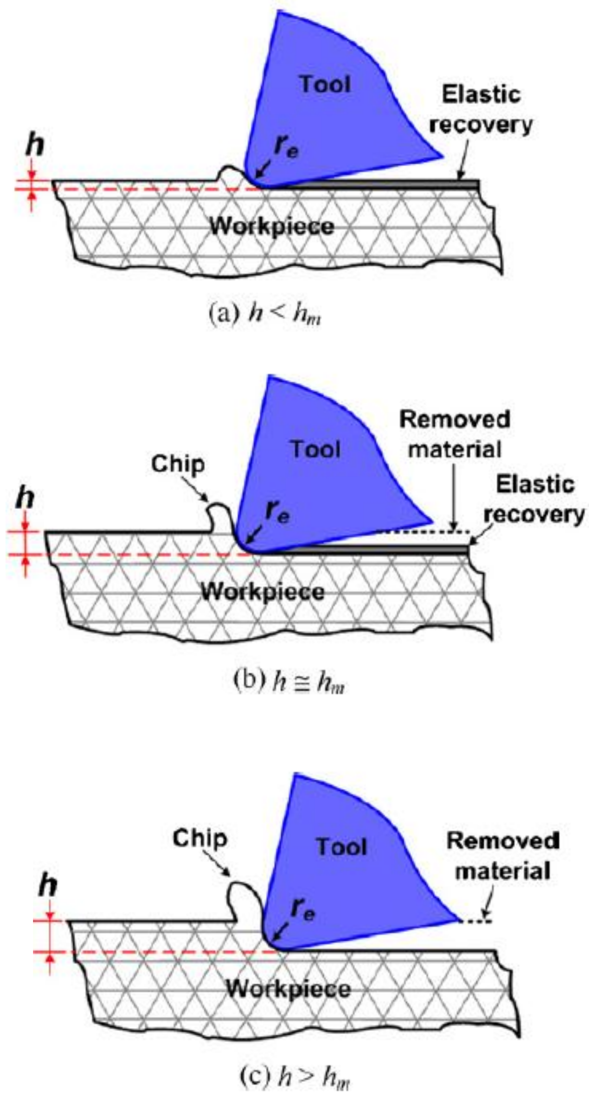

Figure 2-9: Chip formation relative to the minimum chip thickness in micro-scale machining [39]

Therefore it is essential to determine the ratio of the minimum uncut chip thickness or feed rate in case of orthogonal cutting to the cutting edge radius in order to eliminate ploughing. It is important to state that in case this ratio is less or equal 1 the effective rake angle will be negative which requires more energy to cut [39].

Figure 2-10 shows the experimental results and the theoretical curve for the cutting coefficients (referred to as specific cutting force) and the ratio of the uncut chip thickness to the cutting edge radius. A non-linear increase of the cutting coefficients is seen at lower ratios due to the ploughing effect, especially when the ratio is less than or equal 1. As the ratio starts to increase the cutting coefficients decrease and reach almost a fixed value resulting from the disappearance of ploughing.

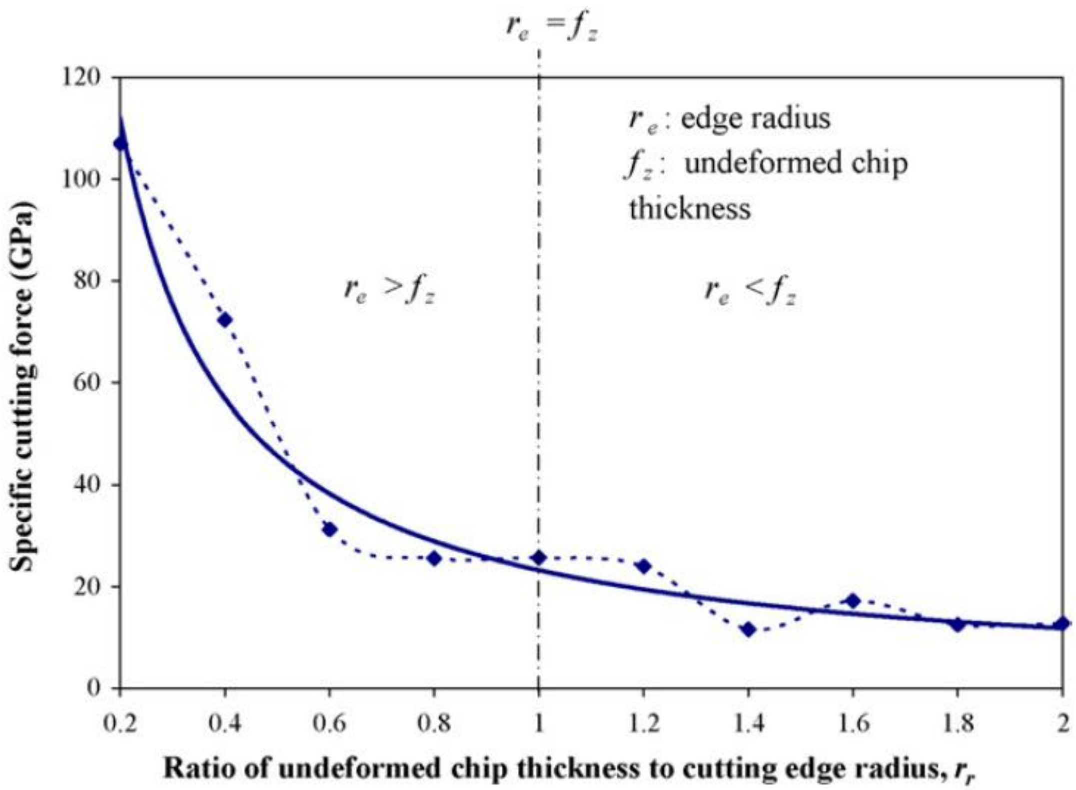

Figure 2-10: Specific cutting force in feed direction [39]

Lai et al. [5] built a FEA model to study the effect of feed rate on cutting coefficients for micro-scale milling; a modified Johnson–Cook constitutive equation was formulated to model the material strengthening. It can be seen from Figure 2-11 that maximum effective stress increase as the uncut chip thickness is decreased, which is 1009, 888 and 704MPa when uncut chip thickness t was 1, 4 and 20 μm.

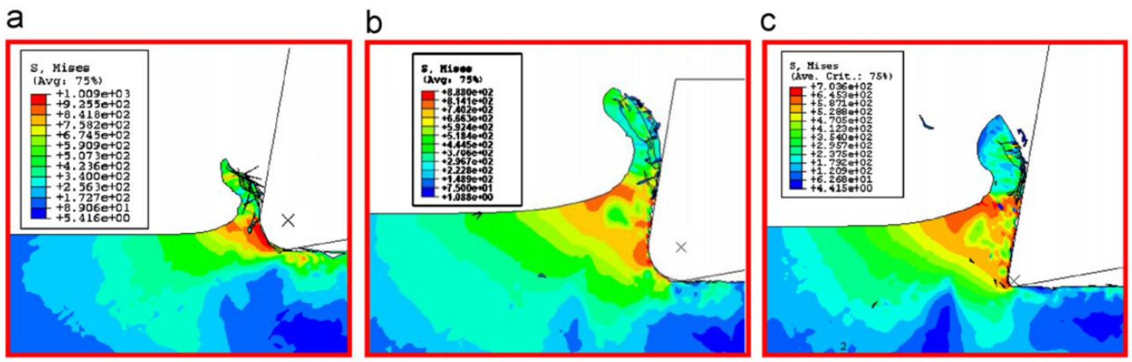

Figure 2-11: Size effect at different uncut chip thickness. (a) h =1 μm; (b) h = 4 μm (c) h = 20 μm. [5]

Figure 2-12 shows the specific shear energy (which is directly proportional to the cutting coffecients) and the feed per tooth for milling operations. And as expected the FEA simulation agrees with the experimental results that lower feeds results in higher specific shear energy.

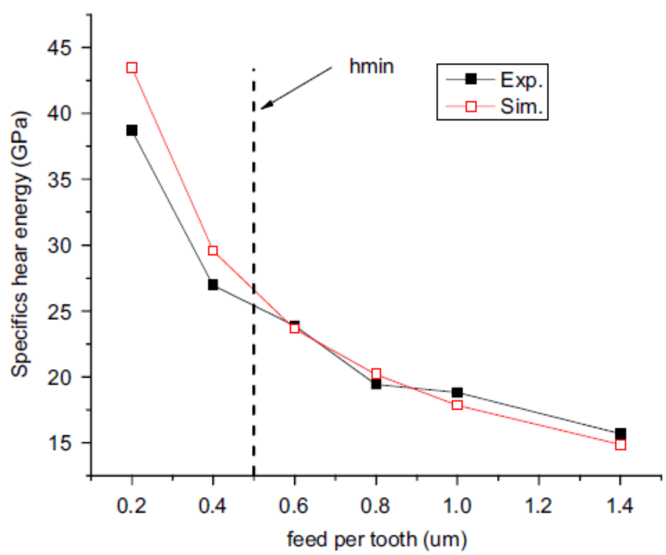

Figure 2-12: Size effect in specific shear energy at different feed rates [5]

2.2.2 Effect of Cutting Speed (*v*) on Cutting Coefficients

It has been well documented in the literature that cutting speed *v* has little effect on cutting coefficients. Usually increasing cutting speed is accompanied by decreasing cutting forces. Yan et al. [40] presented a coupled thermo-mechanical model of plane-strain orthogonal turning of hardened steel H13 taking into account the effect of large strain, strain-rate, temperature and initial workpiece hardness. From their simulation it was shown that as cutting speeds increase, cutting and feed forces decrease. Ng et al. [41] built an FEA model to study the effect of cutting speed on cutting forces during cutting AISI H13 (52HRC), with polycrystalline cubic boron nitride (PCBN) tooling. The results shows an agreement between simulation and experimental results that increasing cutting speeds results in decreasing cutting forces, as detailed in Figure 2-13.

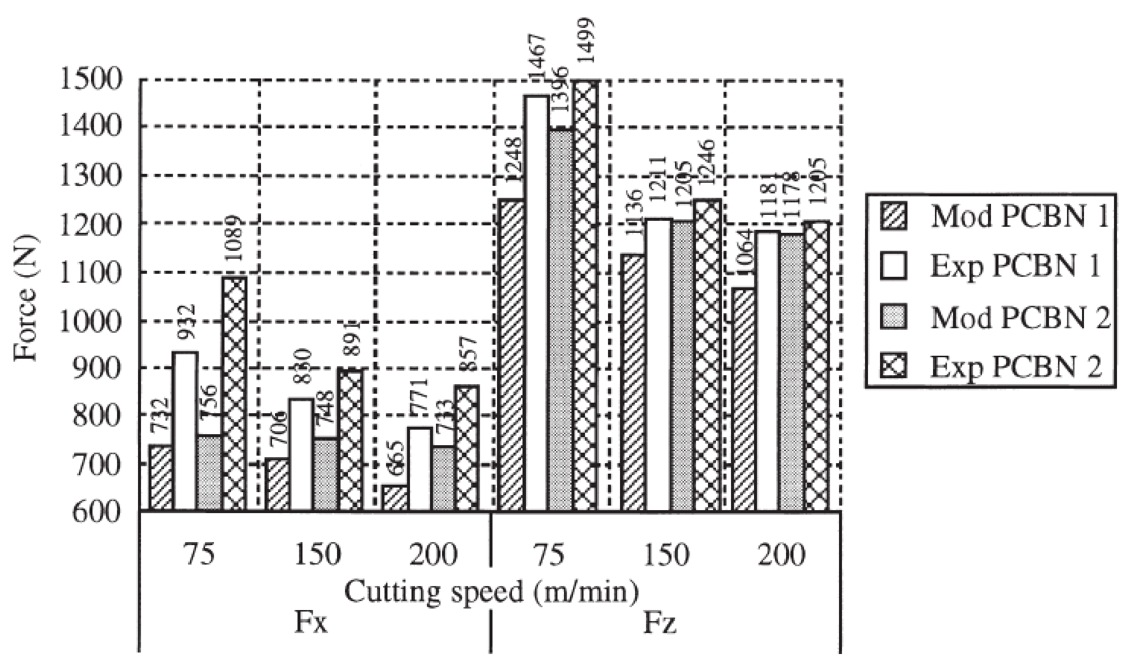

Figure 2-13: Comparison between model and experimental data on the effect of cutting speed on the feed force F_f and tangential force Fc (referred to as Fx and Fz) [41]

Qian and Hossan [42] built a Lagrangian FEA model to study the effect of cutting speed on cutting forces during cutting various workpiece materials. The effect of cutting speed on cutting forces and feed forces are shown in Figure 2-14 (a) and (b) respectively. The two forces do not change much with increasing cutting speeds from 140 to 240 m/min. However, cutting hardened steel H13 which was then annealed resulted in a slight decrease of forces as speed increased.

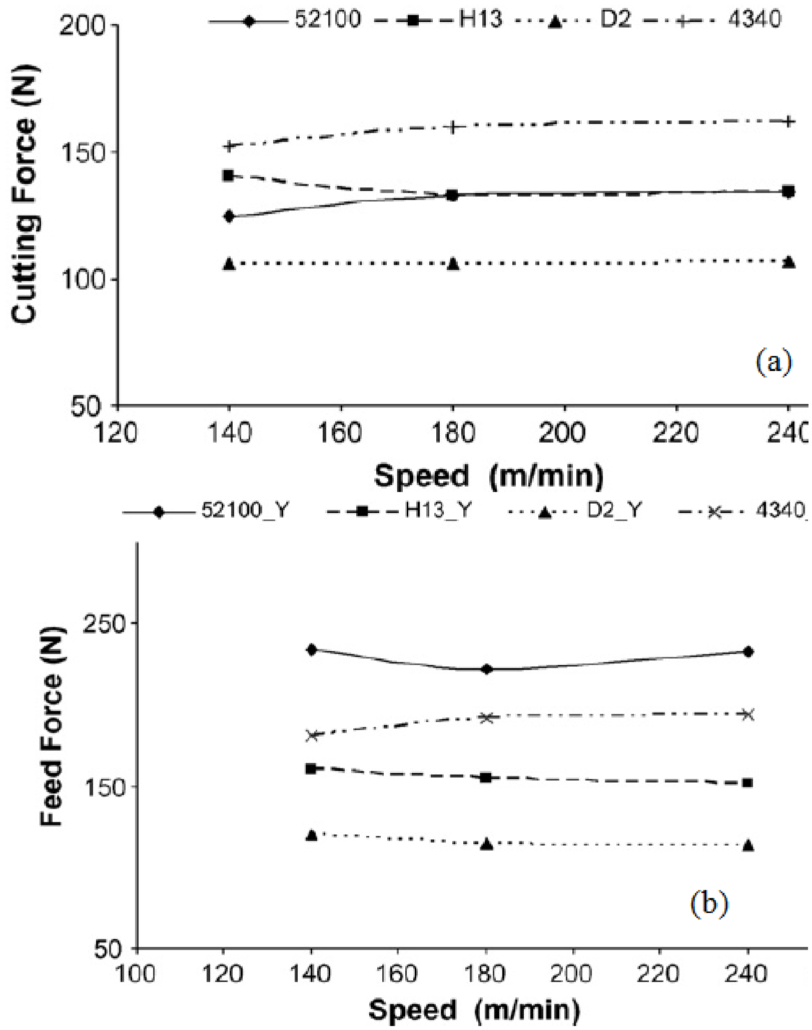

Figure 2-14: (a) Effect of cutting speed and workpiece material on cutting force (b) Effect of cutting speed and workpiece material on feed force [42]

Huang and Liang built an analytical model in order to study the effect of tool thermal properties on cutting forces by modelling thermal behaviors of the primary and the secondary heat sources [43]. The predicted cutting forces are shown in Figure 2-15.

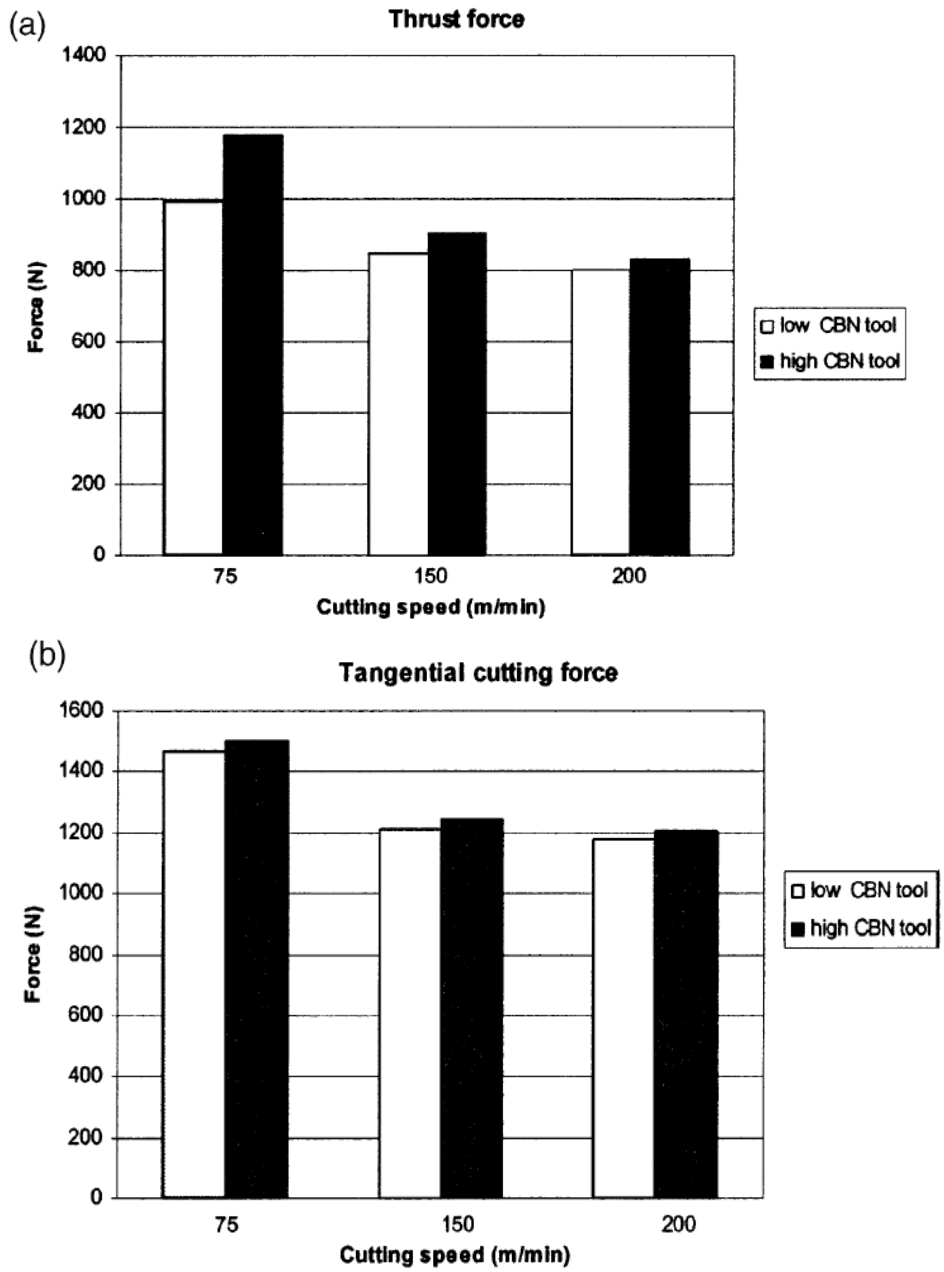

Figure 2-15: The predicted cutting forces when using different CBN content tools: (a) thrust force with cutting speed 75, 150, and 200 m/min;(b) tangential cutting force with cutting speed 75, 150, and 200 m/min. [43]

Marusich [44] built an FEA model through which he discovered that the effect of cutting is more dominant at higher chip loads (feed rate for instance), the reason for that is at lower chip loads the secondary shear zone cannot fully develop, thus the full reduction in interfacial strength due to thermal softening is not realized. At higher chip the tool-chip interface is enough to afford full reduction in interfacial strength and consequently, cutting force. The same result was found by Liu and Melkote [45]; that the size effect in machining at high cutting speeds and large uncut chip thickness is primarily caused by an increase in the shear strength of the workpiece material due to a decrease in the tool-chip interface temperature. The maximum temperatures in the primary and secondary shear zones versus uncut chip thickness are shown in Figure 2-16. The temperature in the secondary shear zone drops by nearly 200°C while the maximum temperature in the primary shear zone remains almost unchanged with a decrease in uncut chip thickness from 200 to 20 µm.

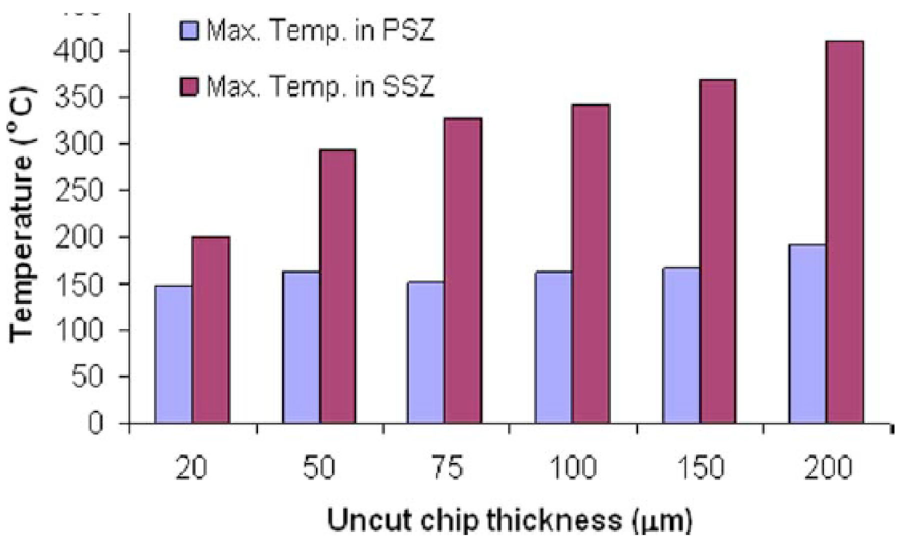

Figure 2-16: Variation of maximum temperature in the primary and secondary shear zones at 200 m/min cutting speed, PSZ: primary shear zone, SSZ: secondary shear zone [45]

2.2.3 Effect of Cutting Edge Radius (ρ_e) on Cutting Coffecients

Cutting edge radius of tool inserts plays a role similar to the feed rate, as the ratio of the uncut chip thickness to the cutting edge radius reduces; a lot of energy is dissipated in ploughing process, and thus increasing the cutting constants. Generally, when the cutting edge is perfectly sharp $\rho_{e=}$ 0^o, there would be no contact between the cutting tool and workpiece material along the clearance face, and thus there would be no ploughing on the surface of the workpiece and the chip will be formed by the mechanical shear force resulting from interaction between the sharp tool and workpiece, as shown in Figure 2-17 (a). In case of relatively large edge radius compared to the undeformed chip thickness, a negative effective rake angle prevails and chip separation becomes difficult, as shown in Figure 2-17 (b) [39]. Waldorf provided experimental data in support of a modified theoretical model for quantifying the effect of cutting tool edge geometry on machining forces [46]. Aramcharoen and Mativenga [39] studied the of the size effect in micro-milling of H13 hardened tool steel. The size effect in micro-milling hardened tool steel was observed by studying the effect of the ratio of undeformed chip thickness to the cutting edge radius on process performance. Afazov [47] investigated the effects of the cutting tool edge radius on the cutting forces during micro-milling using (FEA).

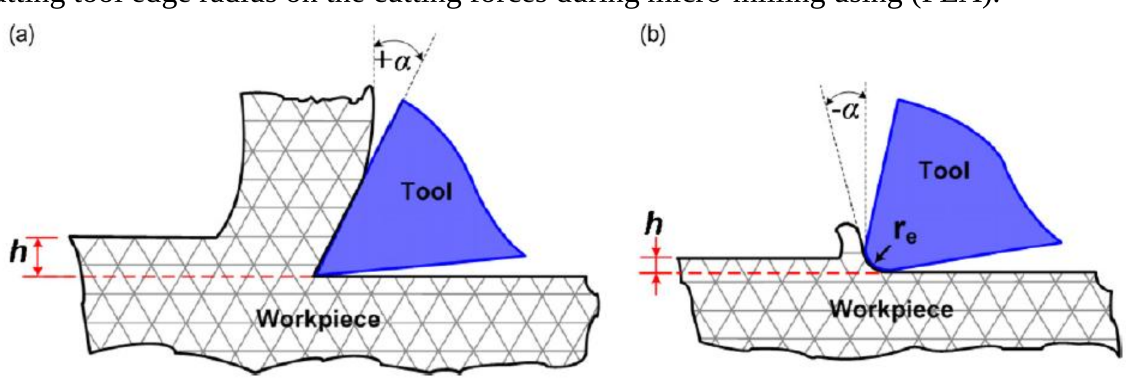

Figure 2-17: cutting edge in (a) macro-scale and (b) micro-scale cutting. [39]

Figure 2-18 shows different stress distribution and chip formation using different cutting edge radii at 3 µm uncut chip thickness. Figure 2-19 (a) and (b) show the cutting forces in the cutting and feed directions at different edge radii. It can be seen that the cutting forces in both directions increase by increasing the edge radius.

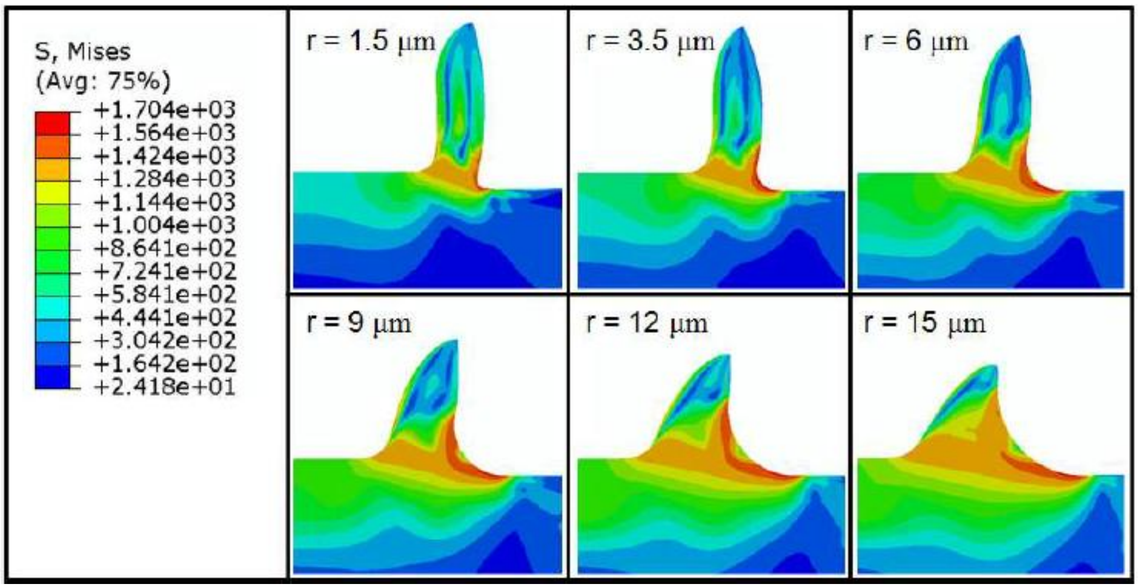

Figure 2-18: Chip morphology and von Mises stresses in MPa for different edge radii obtained at 1571 mm/s cutting velocity, 3 µm uncut chip thickness [47]

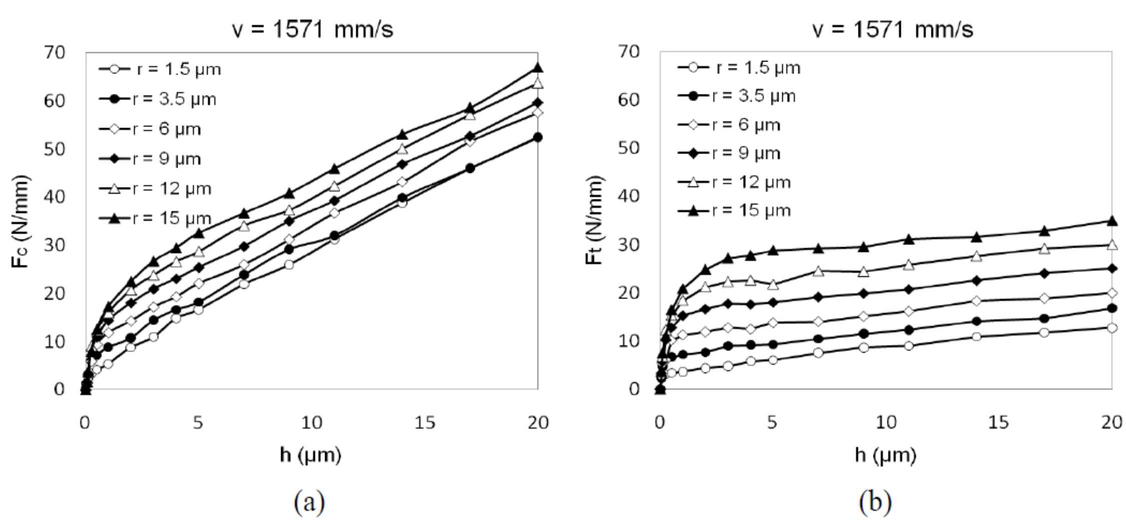

Figure 2-19: FE predicted cutting forces at 1571 mm/s cutting velocity and 3 µm uncut chip thickness in the : (a) cutting direction; (b) feed direction [47]

Chapter 3 Modelling of Orthogonal Metal Cutting

3.1 Finite Element Simulation

Finite element has been widely used for simulation of metal cutting process. Metal cutting is classified as a large deformation material removal process that involves severe plastic deformation of the material at a large strain rate and high temperature. Such conditions make the simulation of this process a challenging task. In order to properly capture the high strain rates and high temperatures, it's very usual to use Johnson-Cook material model [1], equation (3.1)

$$\sigma = (A + B\varepsilon^{n})(1 + C\ln(\frac{\dot{\varepsilon}}{\dot{\varepsilon_0}}))(1 - (\frac{T-T_r}{T_m-T_r})^{m}) \ldots\ldots\ldots \quad (3.1)$$

where σ is the plastic plastic flow stress, A is the initial plastic flow stress at zero plastic strain, B is the strain hardening coefficient, *n* is the strain-hardening index , *C* is the strain rate index, ε is the plastic strain, $\dot{\varepsilon}$ is the plastic strain rate, $\dot{\varepsilon_0}$ is the reference plastic strain rate, *T* is the current temperature, T_r is the reference temperature, T_m is the melting temperature, and *m* is the thermal softening index.

3.2 Model Mesh

3.2.1 Meshing Approach

The approach used to build the model is Arbitrary Lagrangian Eulerian (ALE) shown in Figure 3-1, where certain area of the workpiece will have fixed nodal position in which the material flow through it, this area is called Eulerian region which is surrounded by the red boundary. Applying this approach insures that high mesh distortion is avoided. The major advantage of ALE is that no fracture criteria are required and cutting edge radius can be simulated. Plane strain assumption was used in the simulation.

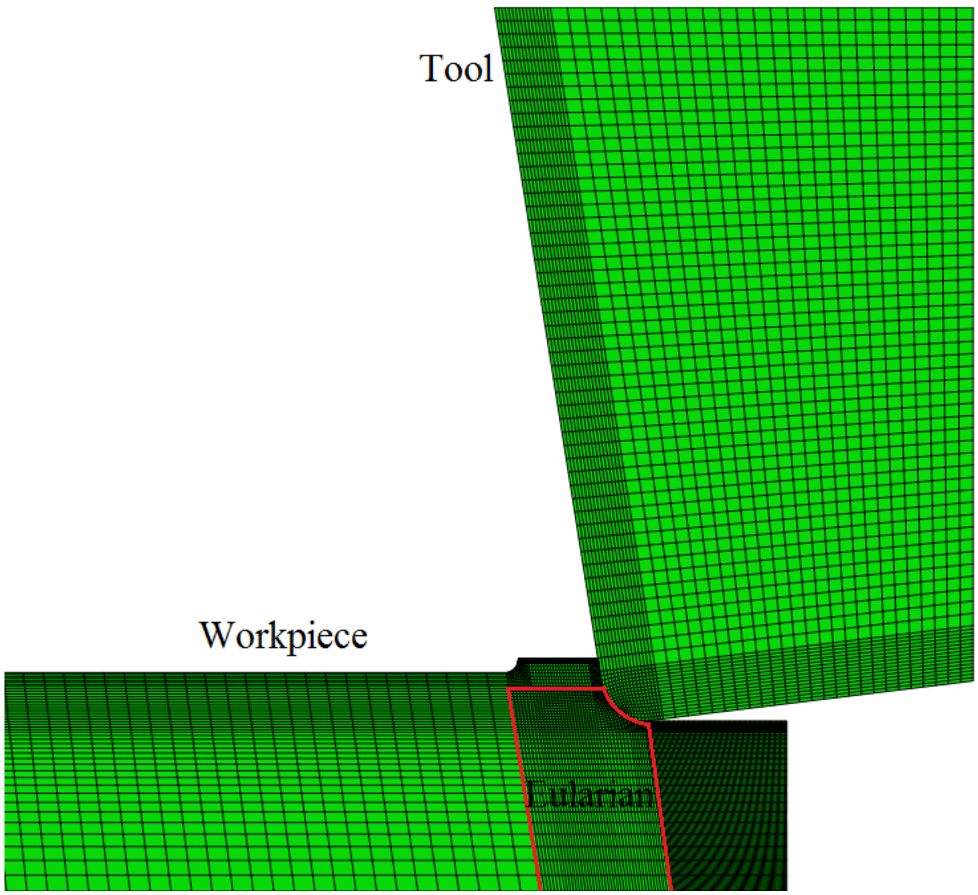

Figure 3-1: ALE approach for FEM model

3.2.2 Mesh Generation Technique

The mesh is created to conform exactly to the geometry of a region and works down to the element and node positions. ABAQUS follows these basic steps to generate a mesh:

1. Generate a mesh on each top-down region using the meshing technique currently assigned to that region. By default, ABAQUS generates meshes with first-order line, quadrilateral, or hexahedral elements throughout.

2. Merge the meshes of all regions into a single mesh. Typically, ABAQUS merges the nodes along the common boundaries of neighboring regions into a single set of nodes.

There are mainly three major techniques for the generation of mesh:

1. Structured Mesh: The structured meshing technique generates structured meshes using simple predefined mesh topologies Figure 3-2.
2. Swept Mesh: Swept mesh is used to mesh complex solid and surface regions. It creates a mesh on one side of the region, known as the source side. And then copies the nodes of that mesh, one element layer at a time, until the final side, known as the target side, is reached. ABAQUS copies the nodes along an edge, and this edge is called the sweep path. The sweep paths can be straight or circular Figure 3-3.
3. Free Mesh: Unlike structured meshing, free meshing uses no pre-established mesh patterns. In contrast, it is impossible to predict a free mesh pattern before creating the mesh.

For a complex model that simulates metal cutting the most convenient technique from above is the swept mesh. However free mesh was used in some areas of the model, where swept mesh cannot be used, as the tool edge.

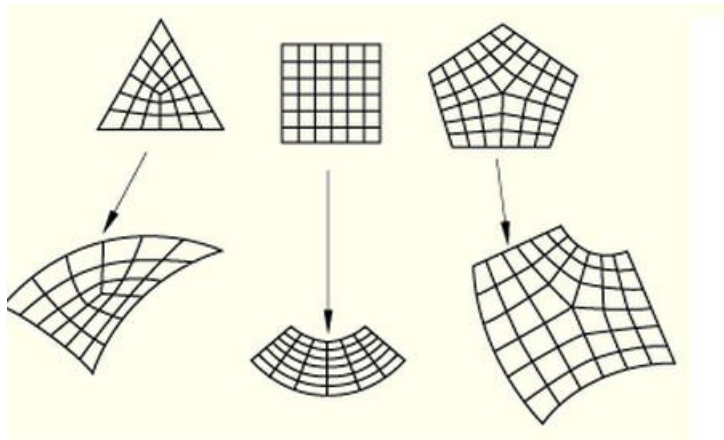

Figure 3-2: Structured Mesh [48]

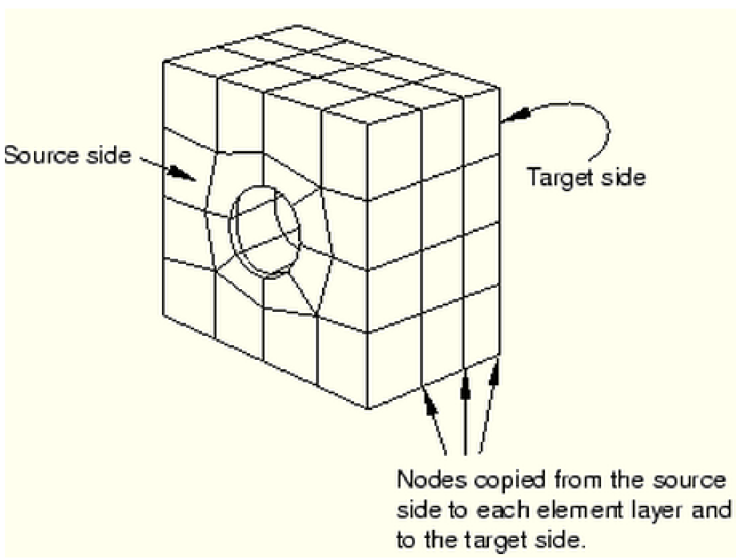

Figure 3-3: Swept Mesh [48]

3.2.3 Element Type

The element type in this model is CPE4RT, which is a 4-node plane strain thermally coupled quadrilateral, bilinear displacement and temperature. And the reason for choosing it is that orthogonal metal cutting process is a plain strain process that generates a huge amount of temperature, and this element is the best to model such a process.

3.2.4 Mesh Refinement

Mesh is refined around some areas of interest -where studying temperature and stress distribution is of an essence- such as tool-chip interface and primary and secondary shear zones in order to get more accurate results Figure 3-4. However refinement of mesh means increasing elements number, and so there is a trade between the mesh refinement and the processing time, and that should be taken in consideration.

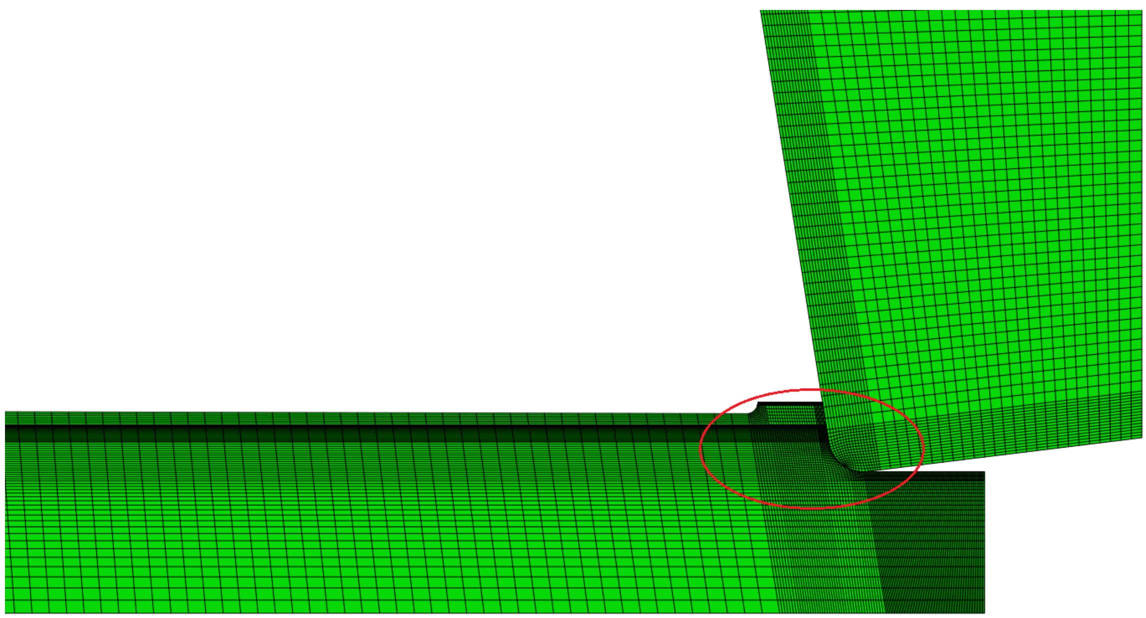

Figure 3-4: Mesh refinement around tool-chip interface and primary and secondary shear zones

3.3 Material Properties

The workpiece material is AISI 1045 with (85 ± 2 HRB) The J-C material constant for this material is shown in Table 3-1 and was obtained by using split Hopkinson pressure bar (SHPB) [49]

The cutting tools are Sandvik Coromant carbide tools of ANSI: N123J2-0500-0004-GM 4225 carbide. The assumed coefficient of friction between the tool and the workpiece is μ=0.15.

Table 3-2 shows the thermal and the mechanical properties of the workpiece and carbide tool materials in which thermal expansion, specific heat capacity and thermal conductivity are function of temperature.

Table 3-1: Johnson- Cook Material constants values

A (MPa)	**B (MPa)**	**n (-)**	**C (-)**	$\dot{\varepsilon}$ **(s^{-1})**	**m (-)**	**T_m (°C)**	**T_r (°C)**
550.0	600.8	0.234	0.0134	1	1	1500	25

Table 3-2: Thermal and the mechanical properties of the material

	Workpiece [50] [49]	**Carbide Tool [50]**
Young's Modulus E (GPa)	205	560
Poisson's ratio υ	0.30	0.22
Density ρ (kg/m^3)	7850	14500
Thermal expansion α (°C^{-1} x 10^6)	10.1 (20 °C) 12.0 (200 °C) 13.0 (400 °C) 14.0 (600 °C)	5.2 (20 °C) 5.3 (200 °C) 5.4 (400 °C) 5.6 (600 °C)
Specific heat capacity c_p (J/Kg °C)	470 (20 °C) 535 (200 °C) 635 (400 °C) 800 (600 °C)	220 (20 °C-600 °C)
Thermal Conductivity k (W/m°C)	46 (20 °C) 40 (250 °C) 34 (500 °C) 27 (750 °C) 26 (1000 °C)	20 (20 °C) 13 (250 °C) 10 (500 °C) 8 (750 °C) 7 (1000 °C)

3.4 Geometry and Boundary Conditions

The cutting tool being simulated is designed for orthogonal cutting, mainly grooving and plunging. Two different types of tool were simulated one is CVD coated with cutting edge radius ρ_e= 60 μ, and the other is PVD coated with cutting edge radius ρ_e= 30 μ. Both have edge width=5 mm, it has a clearance angle $\beta=7^o$ and rake angle was α= -9^o. These parameters were measured accurately as will be shown in the next chapter. They also have as a chip breaker; however, for simplicity the chip breaker is not simulated in the FEM model. Figure 3-5 Shows an isometric view of the tool, whereas Figure 3-6, shows a top and front view of the cutting tool. The model is only simulating the cutting tool and the workpiece but not the tool holder.

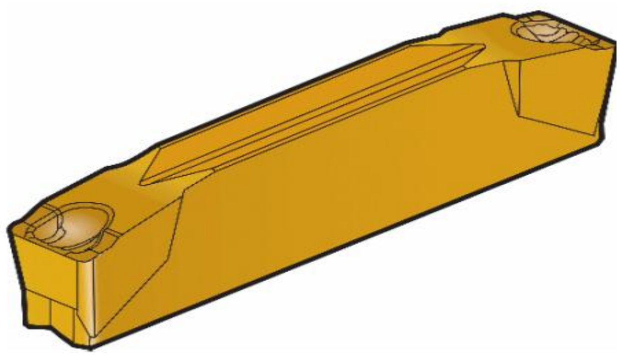

Figure 3-5: Isometric view for the cutting tool (Sandvik Coromant)

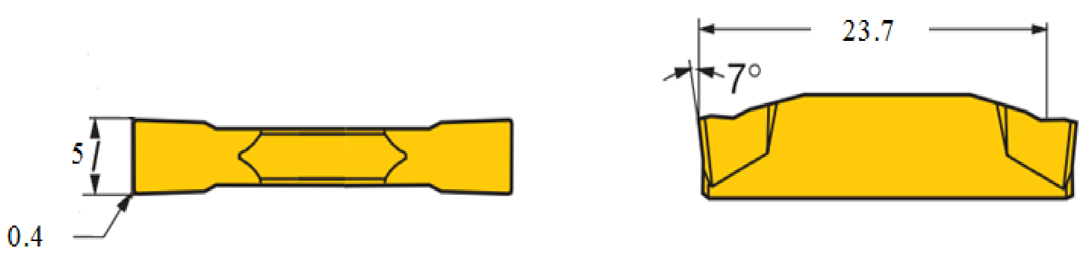

Figure 3-6: A top and front view for the cutting tool- dimensions in mm-(Sandvik Coromant)

Figure 3-7 (a) and (b) shows the experiment set up for plunging process on the front view and side view respectively. Orthogonal cutting was carried out in the experiment. For all cutting processes, the width of cut was fixed at w= 3 mm. The workpiece plunging depth will be kept constant at 7.5 mm.

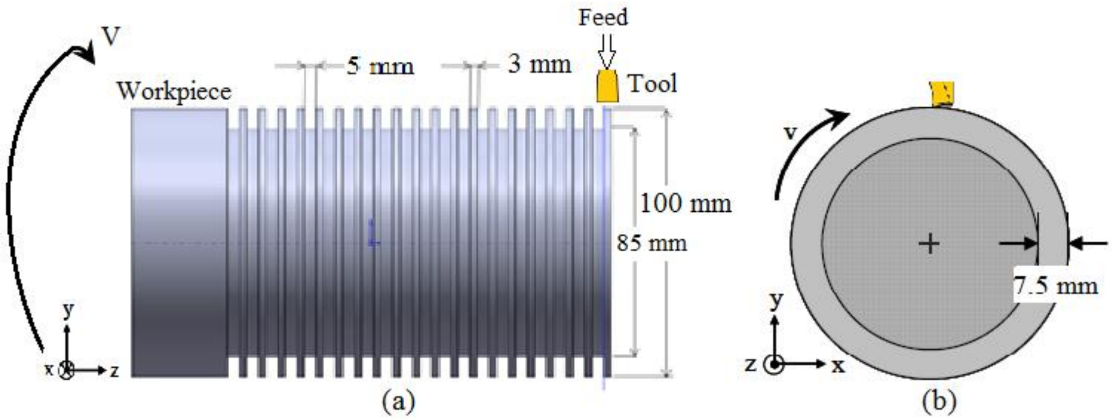

Figure 3-7: The experiment set up for plunging process. (a) Front view (b) Side view

The circle drawn on Figure 3-8 (a) shows the portion of the experiment set up being taken into consideration in the FEM model; only a small portion of the insert and the workpiece is being taken into consider, and the tool holder is not included into the model. Figure 3-7 (b) shows the geometry and boundry conditions used by conventional FE cutting model With ALE formulation, the moving object will be the workpiece material, and the tool will be fixed. For orthogonal plunging process, only the region on the top of the tool has to be defined as encastre. The bottom of the workpiece will be constrained in the y-direction; however, it is free to move in the x-direction.

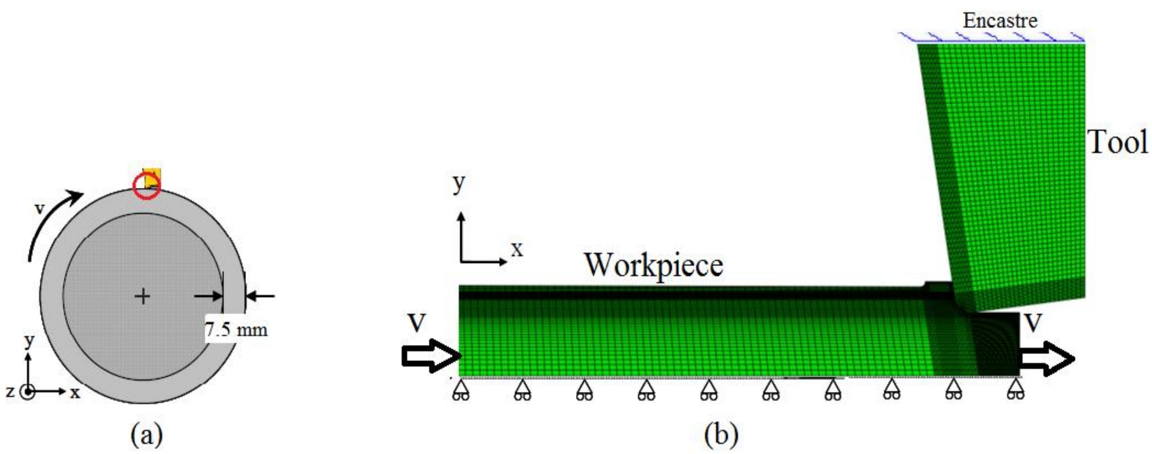

Figure 3-8: (a) Portion of experiment set up being modeled. (b) B.C. for FE cutting model

3.5 Modelling Matrix

Twelve simulations were carried out at two different cutting speeds and three different feed rates with two different cutting edge radii. Table 3-3: details the models that were carried in this research. A width of cut of *w*= 3 mm was used in all the simulation. These simulations will then be calibrated experimentally.

Table 3-3: Modeling Matrix

	Cutting Edge Radius (μm)			
	30		60	
Cutting speeds (m/min)	100	150	100	150
Feed rates (mm/rev)	0.05, 0.07, 0.10	0.05, 0.07, 0.10	0.05, 0.07, 0.10	0.05, 0.07, 0.10

3.6 Sample Simulation Result

The following is a sample simulation result for the ALE model at cutting parameters *f*= 0.05 mm/rev, *v*= 100 m/min and ρ_e= 60 µm. Figure 3-9 shows the deformed mesh while also showing the stress distribution along the tool and workpiece. Figure 3-10 shows the cutting and feed forces *Fc* and F_f at the same cutting parameters.

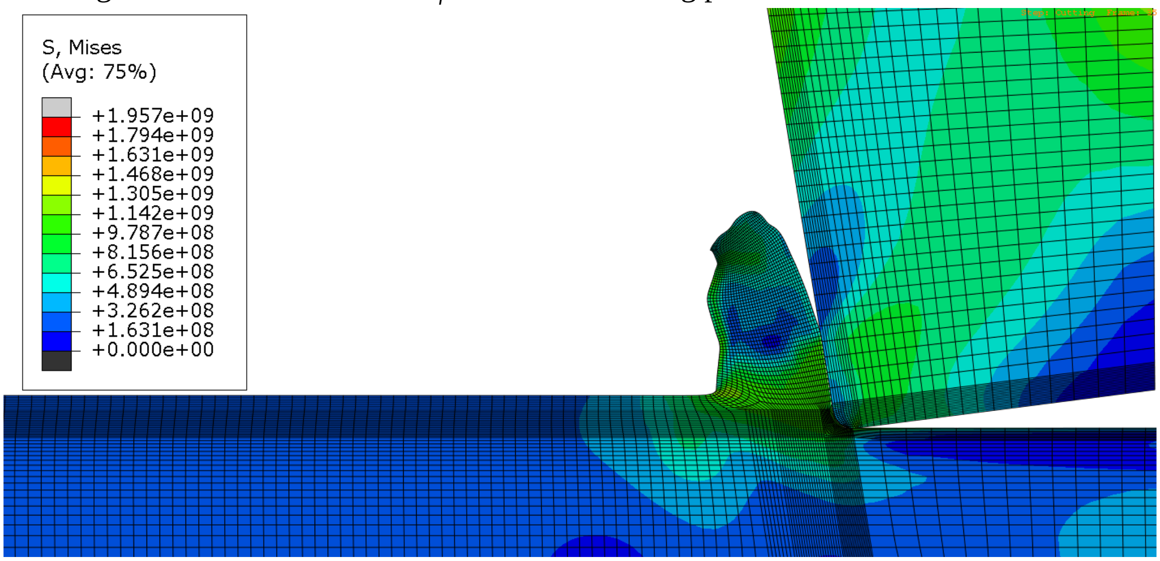

Figure 3-9: Chip formation *f*= 0.05 mm/rev, *v*= 100 m/min and ρ_e= 60 µm

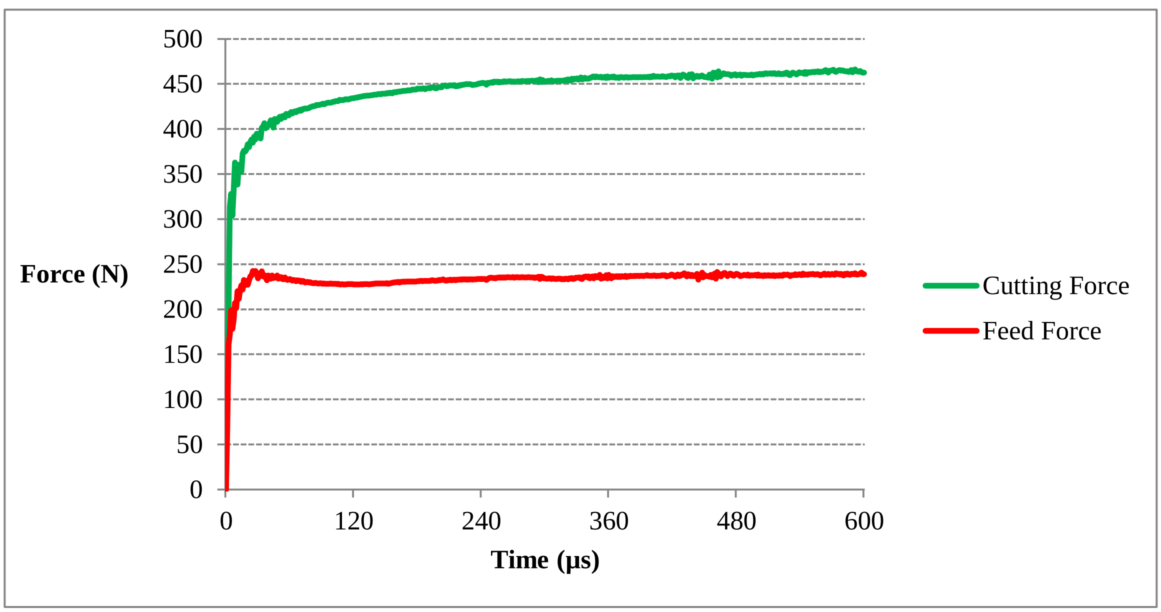

Figure 3-10: Cutting and Feed forces *Fc* and F_f *f*= 0.05 mm/rev, *v*= 100 m/min and ρ_e= 60 µm

Chapter 4 Experimental Work

4.1 Experimental Set Up for Orthogonal Cutting

Experimental work was carried out to validate the FEM cutting models as well as to perform the parametric study of the model; this will be discussed in details in the results and discussion chapter. Orthogonal cutting tests were carried out on a Boehringer VDF 180CM (CNC) lathe Figure 4-1. The experimental set up is shown in Figure 4-2; it shows the workpiece and the cutting tool attached to the dynamometer ready for cutting.

Figure 4-1: Boehringer VDF 180CM (CNC) lathe

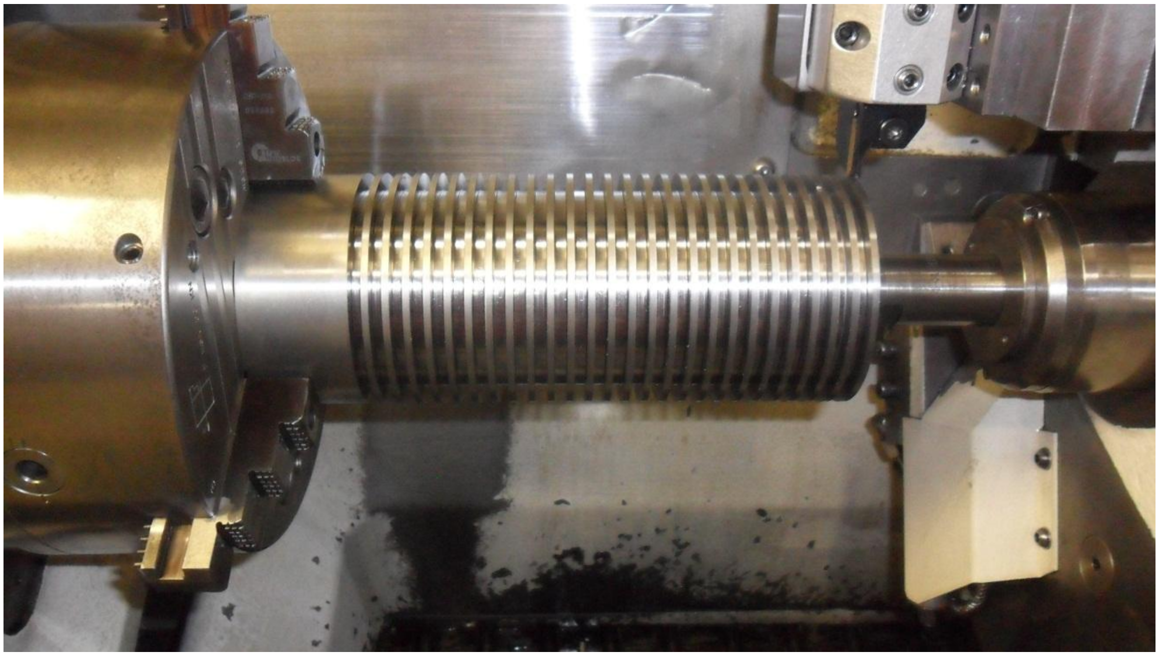

Figure 4-2: Experimental set up (a) Front view (b) Side view

4.2 Workpiece and Cutting Insert Geometry and Design

The workpiece is AISI 1045 (85 ± 2 HRB) fully annealed. The cutting tools used were Sandvik Coromant carbide tool of ANSI: N123J2-0500-0004-GM 4225. One of them is CVD coated, while the other is PVD coated. Figure 4-3 shows the geometry of the workpice.

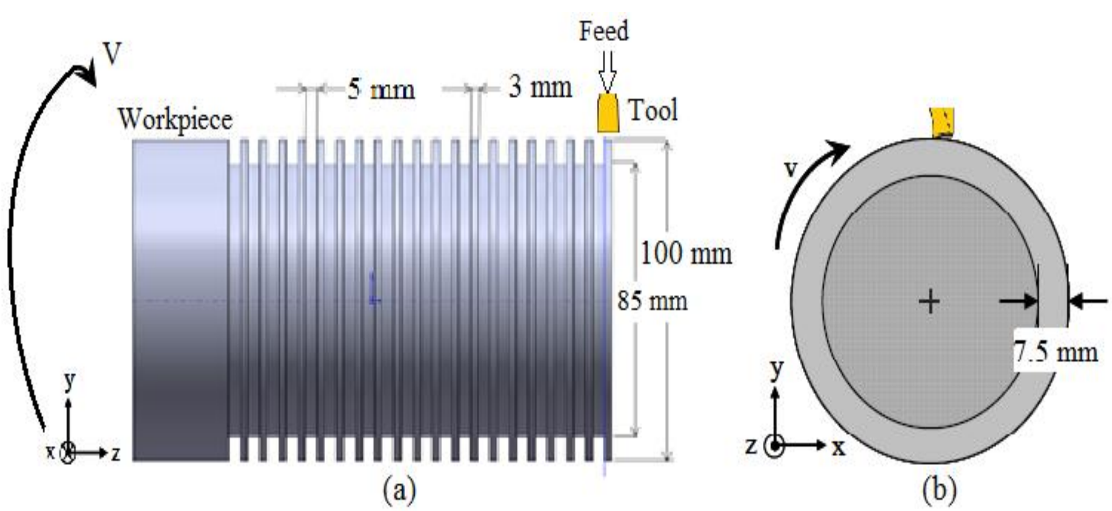

Figure 4-3: Workpiece Geometry

Figure 4-4 shows an isometric view of the tool, whereas Figure 4-5 shows a top and front view of the cutting tool.

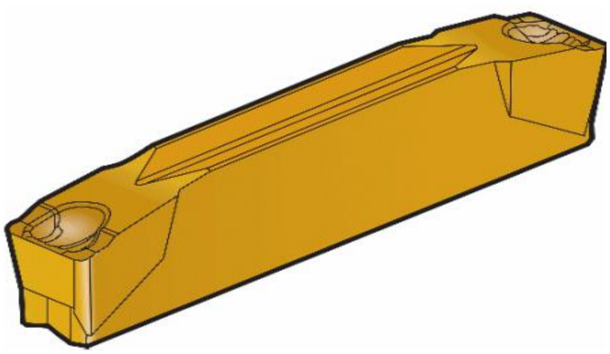

Figure 4-4: Isometric view for the cutting tool (Sandvik Coromant)

Figure 4-5: A top and front view for the cutting tool-dimensions in mm (Sandvik Coromant)

The geometry of the cutting tool is of a great influence on the cutting forces and accordingly the cutting coefficients. Two important geometries are the cutting edge radius *ρe*, and the rake angle. The cutting edge radius has an influence on the cutting forces. As the cutting edge increases the cutting forces increased due to ploughing as shown in the work done by Afazov et al. [47]. Also the rake angle has a remarkable effect on the cutting forces, particularly negative rake angle that causes larger contact area and also higher chip volume, which both resulted in increased cutting forces and heat generation [51].

In order to accurately predict the cutting forces using FEM the tool cutting edge radius was measured using a Mitutoyo Formtracer CS-5000 (Figure 4-6), where the formtracer is able to draw the profile for the tool cutting edge as the stylus moves along the tool cutting edge. And then using data output software, the X-Y co-ordinates are measured for a chosen number of points on the surface of the tool, the drawn profile is then transferred into a text file containing the X-Y co-ordinates values for these points, which is then fed into a MATLAB code to calculate the cutting edge radius, as shown in Figure 4-7. The previous steps were carried two times for each of the two cutting tools, for total of four measurements.

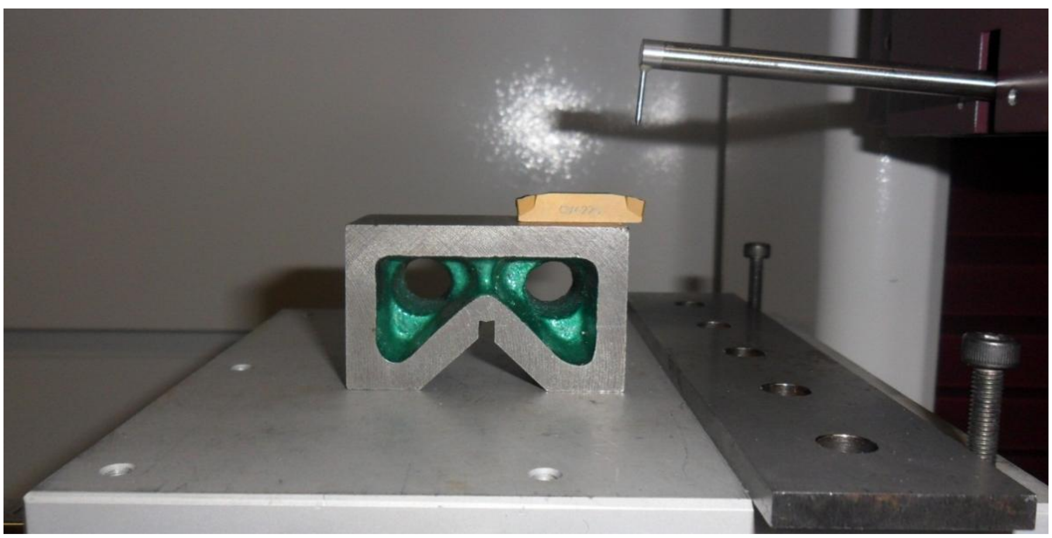

Figure 4-6: Mitutoyo Formtracer for measuring the tool cutting edge radius

The values for the measurements for the CVD coated insert are shown in Table 4-1. Whereas the values for the measurements for the PVD coated insert are shown in Table 4-2. The average value for the CVD tool cutting edge radius is ρe= 60.4 µm. And for the PVD is ρe= 30 µm.

Table 4-1: Cutting edge radius measurements for CVD insert

Measurment	Value (μm)
1	62.5
2	58.2
Average Value	60.4

Table 4-2: Cutting edge radius measurements for PVD insert

Measurment	Value (μm)
1	30.6
2	29.4
Average Value	30

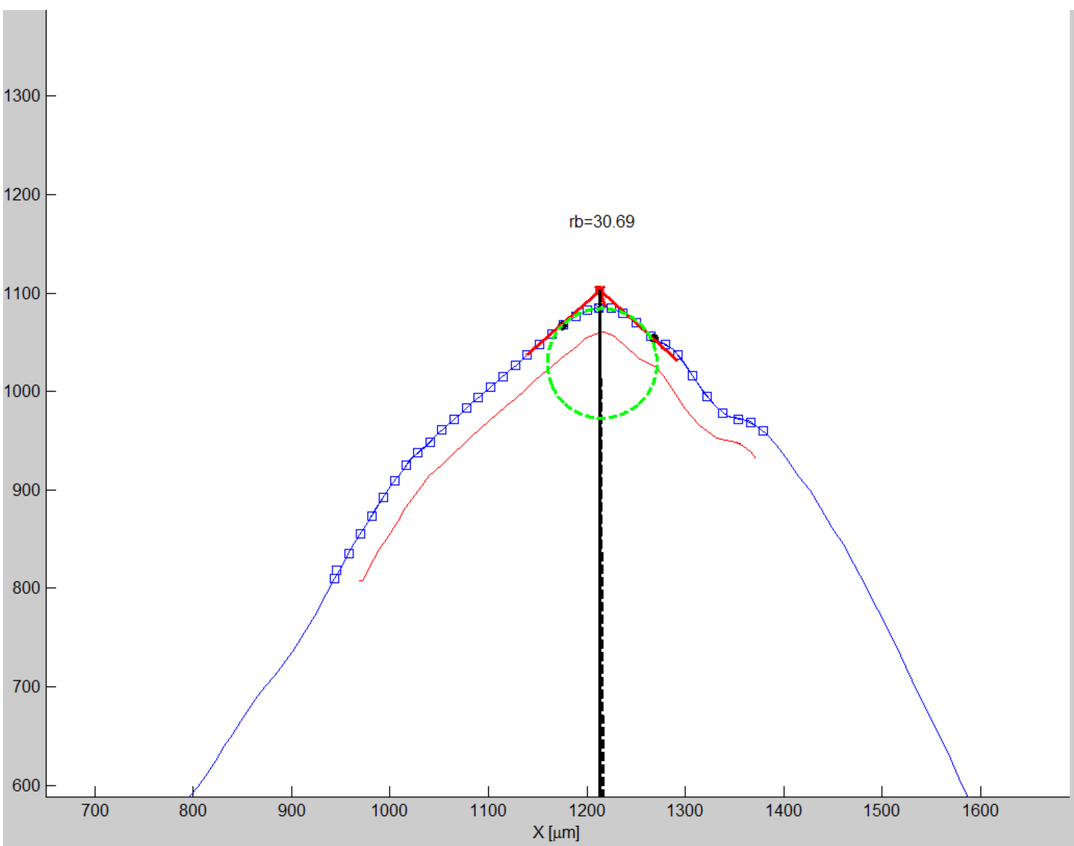

Figure 4-7: MATLAB graph for calculating the cutting edge radius

The rake angle of the cutting tool is also of a great importance in terms of its great influence on the cutting forces, as mentioned previously. The tool rake angle was measured using a Nikon AZ100 microscope shown in Figure 4-8, where a magnified photo for the front view of the cutting insert was taken as shown in Figure 4-9 in order to accurately measure the rake angle. The measured rake angle was α= -9^{o} which means the rake angle is a negative rake angle which usually contributes to higher cutting forces.

Figure 4-8: Nikon AZ100 microscope for measuring the tool rake angle

Figure 4-9: Magnified photo for the cutting tool front view

4.3 Cutting Conditions

The Cutting conditions for the experimental work are shown Table 4-3.

Table 4-3: Cutting conditions for the experimental work

Cutting Conditions	
Tool	
Cutting edge radius (μm)	60, 30
Tool rake angle	-9
Tool clearance angle	7
Workpiece	
Disk diameter (mm)	100
Disk width (mm)	3
Plunging depth (mm)	7.5
Cutting fluids	Dry

4.4 Force Measurement

A three axis Kistler type tool-post piezoelectric dynamometer Figure 4-10 was used to measure the cutting force Fc, feed force F_f and axial force Fz. Sampling rate was fixed at 20 kHz. Orthogonal cutting tests were carried out with width of cut w= 3 mm. LabVIEW software programme was used for data acquisition.

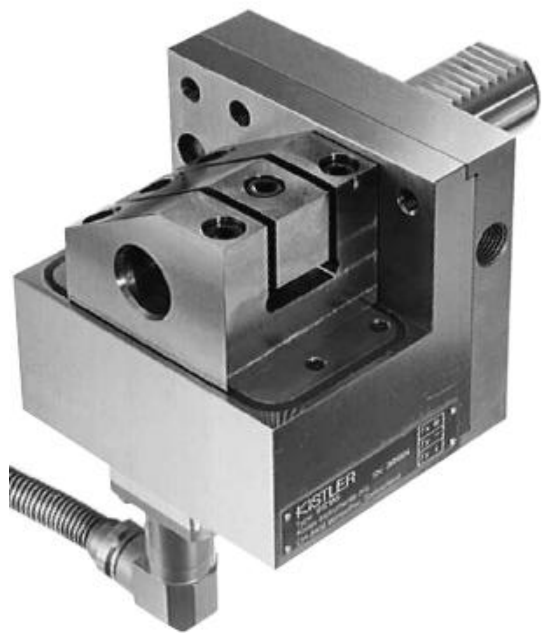

Figure 4-10: Kistler type tool-post piezoelectric dynamometer

The lower and upper range limits of the dynamometer are -3 kN and 3 kN respectively for X-direction and Y-direction, while they are -6 kN and 6 kN for Z-direction. The sensitivity for the dynamometer is -7.9 pC/N for X-direction and Y-direction, while it is –3.8 pC/N for Z-direction.

4.5 Experiment Matrix

All the cutting tests were carried out orthogonally in a dry environment. Table 4-4 shows the experimental test matrix carried out for phase I which is the validation phase, whereas Table 4-5 shows the experimental test matrix carried for phase II which is the parametric study phase.

Table 4-4: Experimental test matrix out for phase I

	Cutting Edge Radius (μm)			
	30		60	
Cutting speeds (m/min)	100	150	100	150
Feed rates (mm/rev)	0.05, 0.07, 0.10	0.05, 0.07, 0.10	0.05, 0.07, 0.10	0.05, 0.07, 0.10

Table 4-5: Experimental test matrix carried out for phase II

	Cutting Edge Radius (μm)							
	30				60			
Cutting speeds (m/min)	100	150	200	250	100	150	200	250
Feed rates (mm/rev)	0.14	0.14	0.05, 0.07, 0.10, 0.14	0.05, 0.07, 0.10, 0.14	0.14	0.14	0.05, 0.07, 0.10, 0.14	0.05, 0.07, 0.10, 0.14

Figure 4-11 shows an example of forces obtained experimentally. The obtained F_z was approximately 0 N, thus plane strain assumption is acceptable for modeling.

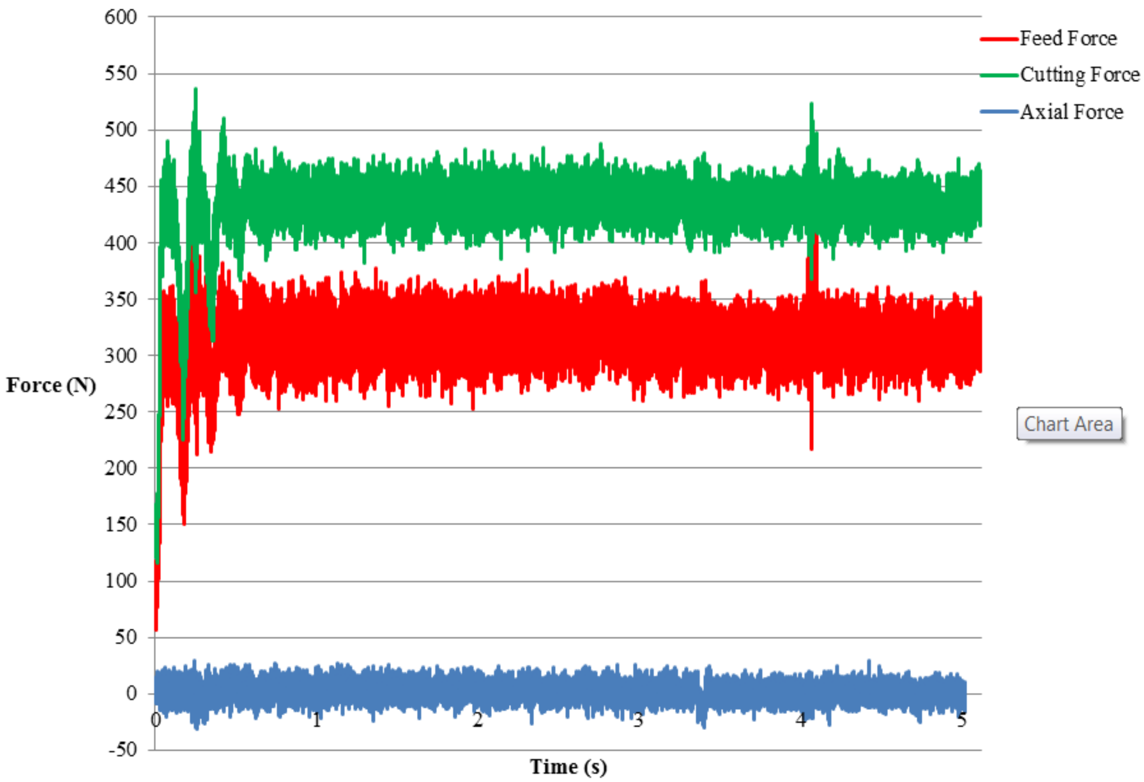

Figure 4-11: Example of forces obtained experimentally at *f*=0.05 mm/rev, *v*=100 m/min

Chapter 5 Results and Discussion

5.1 Cutting Edge I

5.1.1 Phase I: Validation

The main objective for Phase I is to validate the FEA model by comparing the cutting force *Fc* and feed force F_f with the experimental results. Six simulations were carried out at two different cutting speed *v* and three different feed rates *f* as shown in Table 5-1. The cutting edge radius is ρ_e= 60 µm. The tool has a CVD coating.

Table 5-1: Modeling Matrix experimentally validated

Cutting speeds (m/min)	100	150
Feed rates (mm/rev)	0.05, 0.07, 0.10	0.05, 0.07, 0.10

In order to investigate the validation of FEM model before the experimental validation, a stress and thermal analysis was first carried out. Figure 5-1 Shows the stress distribution

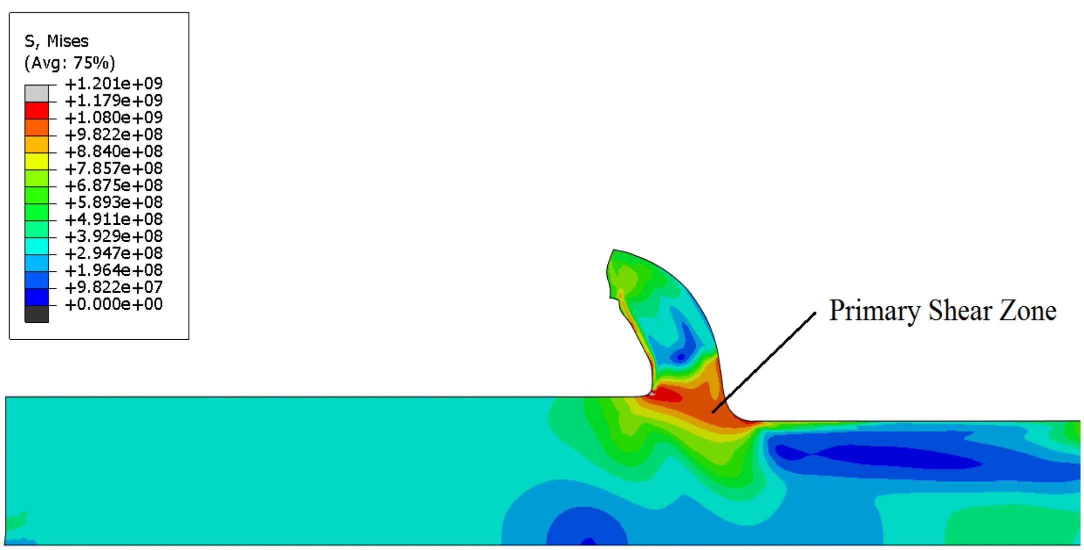

Figure 5-1: Stress distribution for workpiece at *f*= 0.05 mm/rev and *v*= 100 m/min

for the workpiece during cutting at *f*= 0.05 mm/rev and *v*= 100 m/min, the distribution shows that the maximum stress is at the primary shear zone, which is always the case during metal cutting due to the low temperature at this zone [52]. Figure 5-2 Shows the thermal distribution for the workpiece during cutting at *f*= 0.05 mm/rev and *v*= 100 m/min, the distribution shows that the maximum temperature is at the secondary shear zone, which is the case during metal cutting due to the heat generated from both plastic deformation, and to overcome friction along the tool/chip interface. [52].

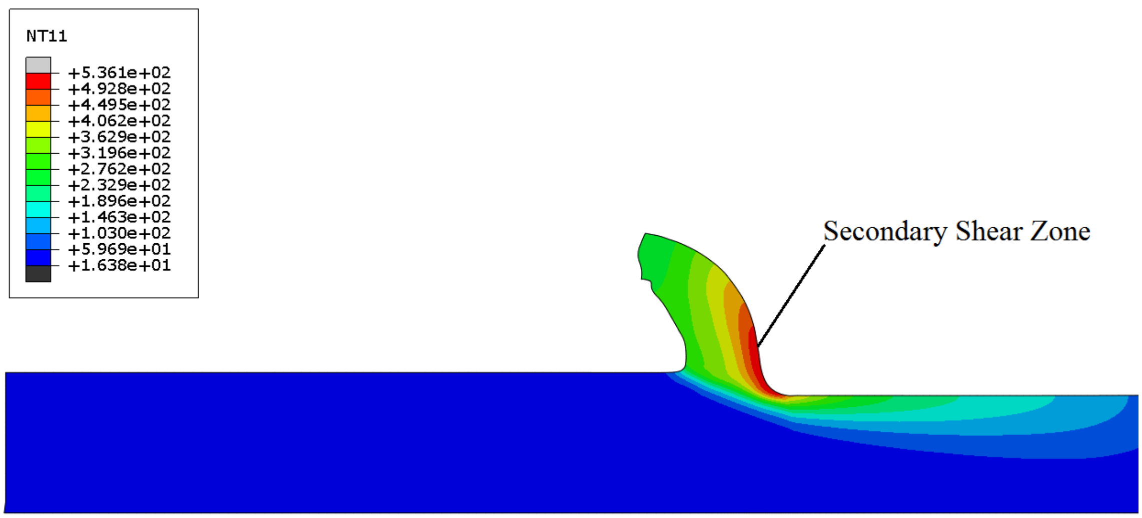

Figure 5-2: Thermal distribution for workpiece at *f*= 0.05 mm/rev and *v*= 100 m/min

Figure 5-3 (a) and (b) show the effect of varying feed rate *f* on the cutting force *Fc* and feed force F_f respectively at fixed cutting speed of *v*=100 m/min, where Figure 5-4 (a) and (b) is at *v*=150 m/min. The results show a good agreement between the simulation and the experimental results on how the cutting force *Fc* and feed force F_f increase by increasing the feed rate due to the increase of chip load. This showed that the Johnson-Cook used in this research and the COF were valid.

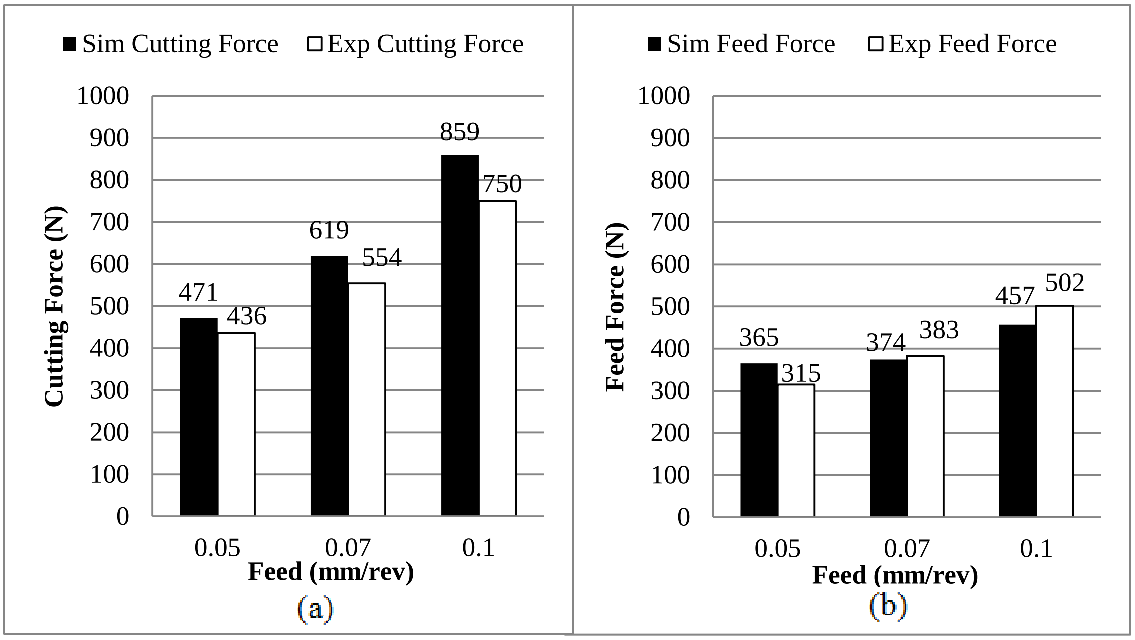

Figure 5-3: Simulation and Experimental results (a) Cutting force *Fc* (b) feed force F_f. Cutting speed *v*=100 m/min

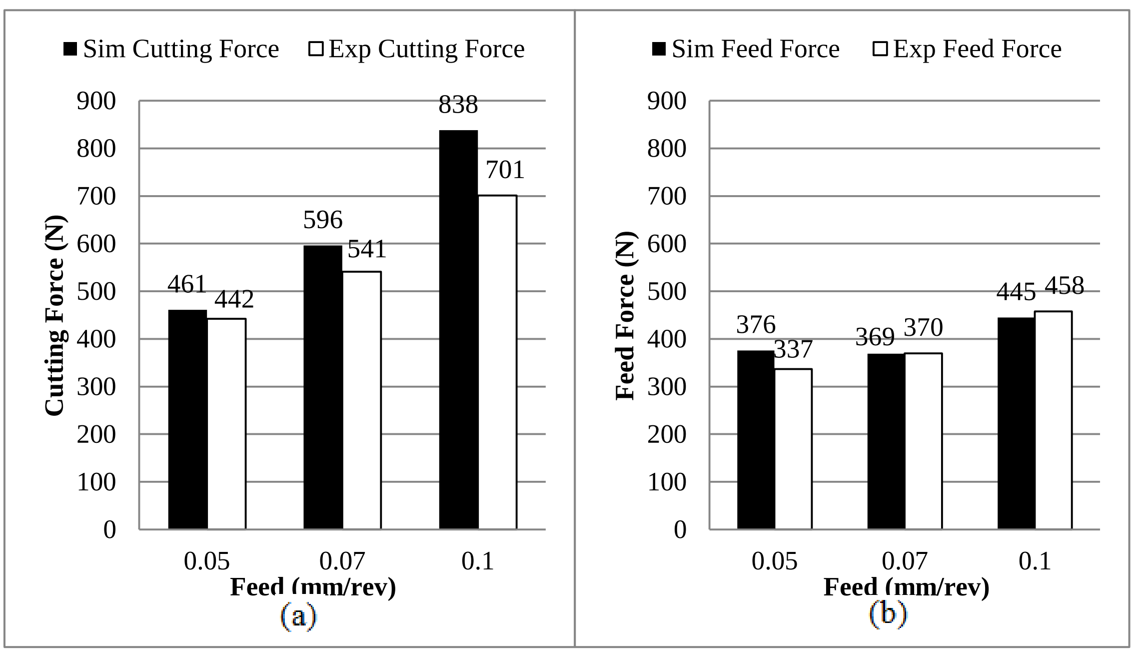

Figure 5-4: Simulation and Experimental results (a) Cutting force *Fc* (b) feed force F_f.

Cutting speed *v*=150 m/min

The cutting coefficients are then found by using the cutting force Fc and feed force F_f and knowing the chip area according to the following equations (5.1), (5.2), and (5.3).

$$Kc = Fc/Ac \quad \text{……….} \ (5.1)$$

$$K_f = F_f/Ac \quad \text{………...} \ (5.2)$$

$$Ac = f.w \quad \text{…………} \ (5.3)$$

where Kc and K_f are the cutting coefficients in the cutting and feed direction respectively and Ac is the chip area and w is the depth of cut that is constant throughout all the simulation and experimental work w=3 mm.

Table 5-2 shows the values of the cutting forces Fc and feed forces F_f and Table 5-3 shows the corresponding cutting coefficients Kc and K_f.

Table 5-2: Values of the cutting forces Fc and feed forces F_f

	v (m/min)	f (mm/rev)	Sim Fc (N)	Sim Ff (N)	Exp Fc (N)	Exp Ff (N)
Simulation 1	100	0.05	471	365	436	315
Simulation 2	100	0.07	619	374	554	383
Simulation 3	100	0.10	859	457	750	502
Simulation 4	150	0.05	461	376	442	337
Simulation 5	150	0.07	596	369	541	370
Simulation 6	150	0.10	838	445	701	458

Table 5-3: Values of cutting coefficients *Kc* and K_f

	Sim *Kc*	Sim *Kf*	Exp *Kc*	Exp *Kf*	*Kc* error%	*Kf* error%
Simulation 1	3140	2433	2907	2100	8	16
Simulation 2	2948	1781	2638	1824	12	2
Simulation 3	2863	1523	2500	1673	15	9
Simulation 4	3073	2507	2947	2247	4	12
Simulation 5	2838	1757	2576	1762	10	0
Simulation 6	2793	1483	2337	1527	20	3
	Units for *Kc* and *Kf* are (N/mm^2)				**Avg= 11.4%**	**Avg= 7%**

The average errors for *Kc* and K_f are 11.4% and 7% respectively which indicates that the model could be useful for the parametric study phase.

5.1.2 Phase II: Parametric Study

After the FEM model has been validated, the next step is to study the effect of cutting parameters on the cutting coefficients. In this research the effect of feed rate *f* and cutting speed *v* on the cutting coefficients are considered. The objective is to be able to predict the effect of these parameters on cutting coefficients at cutting parameters that hasn't been simulated or lay outside the simulation matrix. Table 5-4 shows the range of FEM simulation and prediction at every cutting speed *v* and feed *f*.

The methodology used to find the predicted values at the cutting speeds 100 m/min and 150 m/min with different feed rates is the best curve to fit using the least squares error method, then the predicted values at 200 m/min and 250 m/min are found using this curve.

Table 5-4: The range of Validation and prediction at every cutting speed *v* and feed *f*

Feed/Speed	100 (m/min)	150 (m/min)	200 (m/min)	250 (m/min)
0.05 (mm/rev)	Validated in Phase I	Validated in Phase I	Predicted	Predicted
0.07 (mm/rev)	Validated in Phase I	Validated in Phase I	Predicted	Predicted
0.10 (mm/rev)	Validated in Phase I	Validated in Phase I	Predicted	Predicted
0.14 (mm/rev)	Predicted	Predicted	Predicted	Predicted

According to equation (5.4), that was pointed out by Shaw [52], the equation describes the effect of feed rates on cutting coefficient; it describes a phenomenon known as the size effect phenomenon, where at lower feed rates (especially when lower than the cutting edge radius) the cutting coefficients increase significantly and instead of cutting only, the tool is also ploughing the surface of the workpiece, which contribute to increased cutting coefficients.

$$K = \frac{U}{f\ \hat{}\ e} \quad \ldots\ldots\ldots\ (5.4)$$

In which (U) and (e) are constants that depend on the material and the cutting parameters. These constants were found using least squares error method as mentioned before. Table 5-5 shows the (U) and (e) values.

Table 5-5: (U) and (e) values for speed *v*=100 m/min and speed *v*=150 m/min

	Kc		*Kf*	
Cutting Speed (m/min)	U	e	U	e
100	2089	0.14	283	0.71
150	2000	0.14	220	0.81

Figure 5-5 (a) and (b) shows the effect of changing feed rates f on cutting coefficients Kc and K_f at constant cutting speed v=100 m/min. The simulated Kc and K_f are calculated from equation (5.4) with values shown in Table 5-5. Figure 5-6 (a) and (b) shows the same at cutting speed v=150 m/min. There is a good agreement between the simulation and the experimental values especially for the K_f. It is clear that the cutting coefficients decrease as feed rates increase due to the size effect phenomenon explained previously in the literature review section, and the FEM model is able of capturing this effect. The difference between simulated and experimental K_f values increases with higher feed rates. This was likely due to the fact that the chip breaker was not considered in the FE model. The curve for K_f has larger gradient than that for Kc, which shows that the feed has bigger effect on the cutting coefficient in the feed direction rather than the cutting direction.

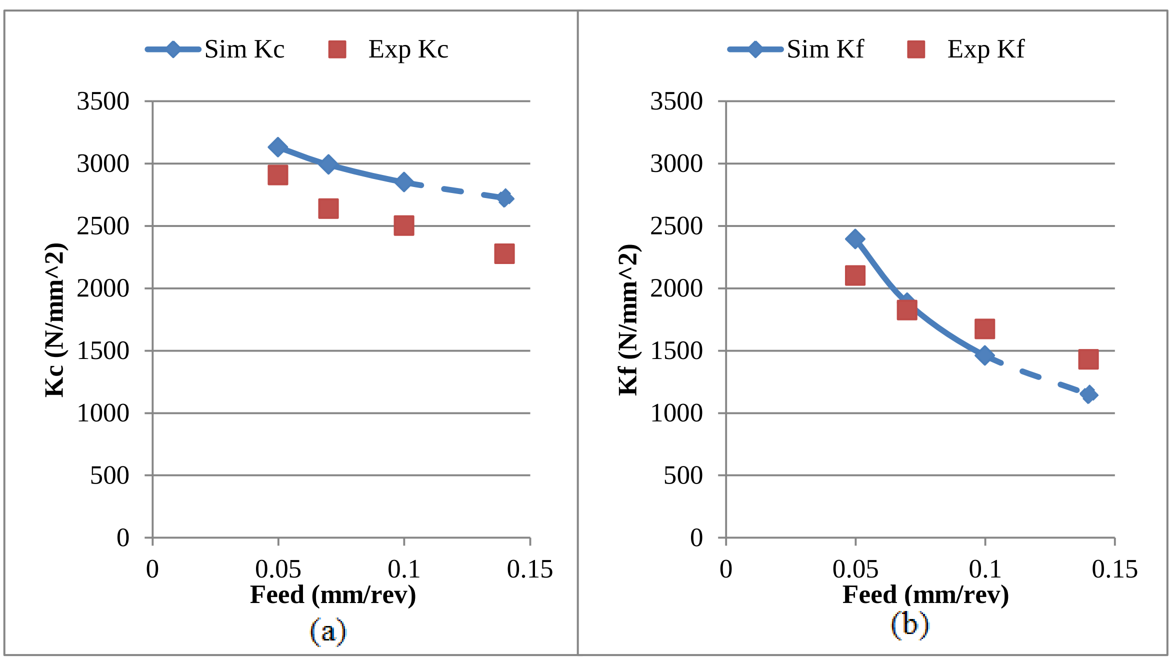

Figure 5-5: Simulation and Experimental results (a) cutting coefficient Kc (b) cutting coefficient K_f. Cutting speed v=100 m/min

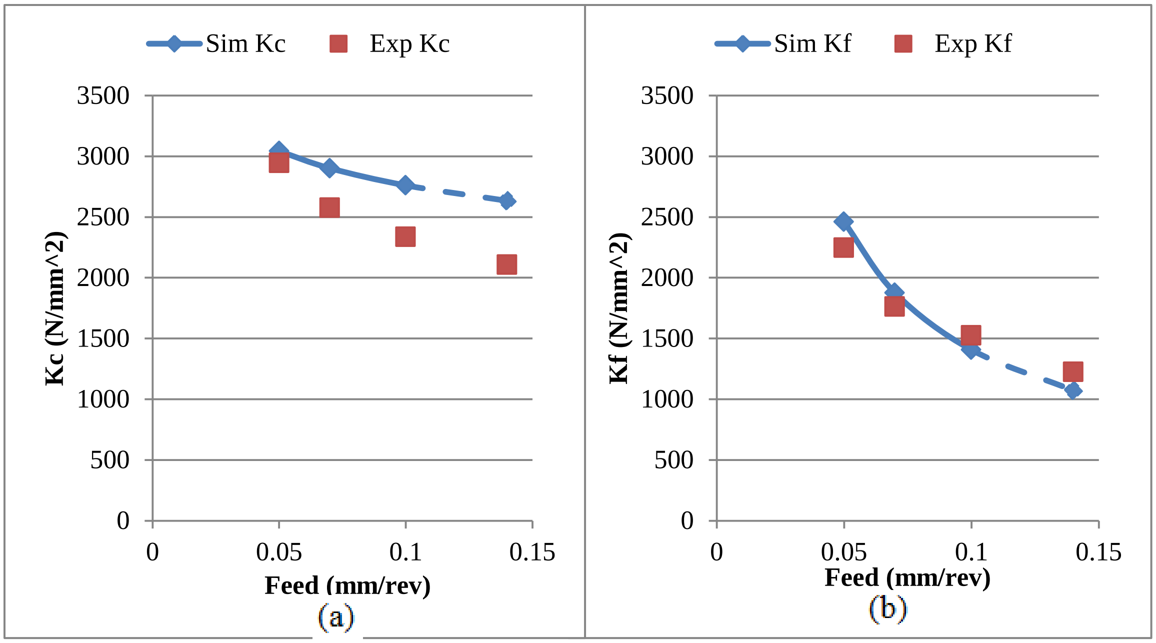

Figure 5-6: Simulation and Experimental results (a) cutting coefficient *Kc* (b) cutting coefficient K_f. Cutting speed *v*=150 m/min

In order to find the predicted values at the feed rates (0.07, 0.10 and 0.10 mm/rev) with different cutting speed, linear regression equations were used to find a trend line, in which the two calibrated values are used to find the slope and the intercept of the line, and then the predicted values are found using this trend line. Figure 5-7 (a) and (b) shows the effect of changing cutting speed *v* on cutting coefficients *Kc* and K_f at constant feed rate *f*= 0.05 mm/rev. Figure 5-8 (a) and (b) and Figure 5-9 (a) and (b) is at feed rate *f*= 0.07 mm/rev and *f*= 0.10 mm/rev. There is agreement between the simulation and the experimental values. The trend for *Kc* and K_f is usually downwards as the speed increases, this is due to the high thermal softening. That agrees with Huang and Liang results when cutting steel [43] shown in Figure 2-14. However Figure 5-7 (b) shows that K_f trend is increasing, this is due to the small contact length between the tool and the chip at this low feed rate; therefore, the temperature will have little effect as opposed to strain rate effect as the speed increases. This agrees with Liu and Melkote conclusion [45].

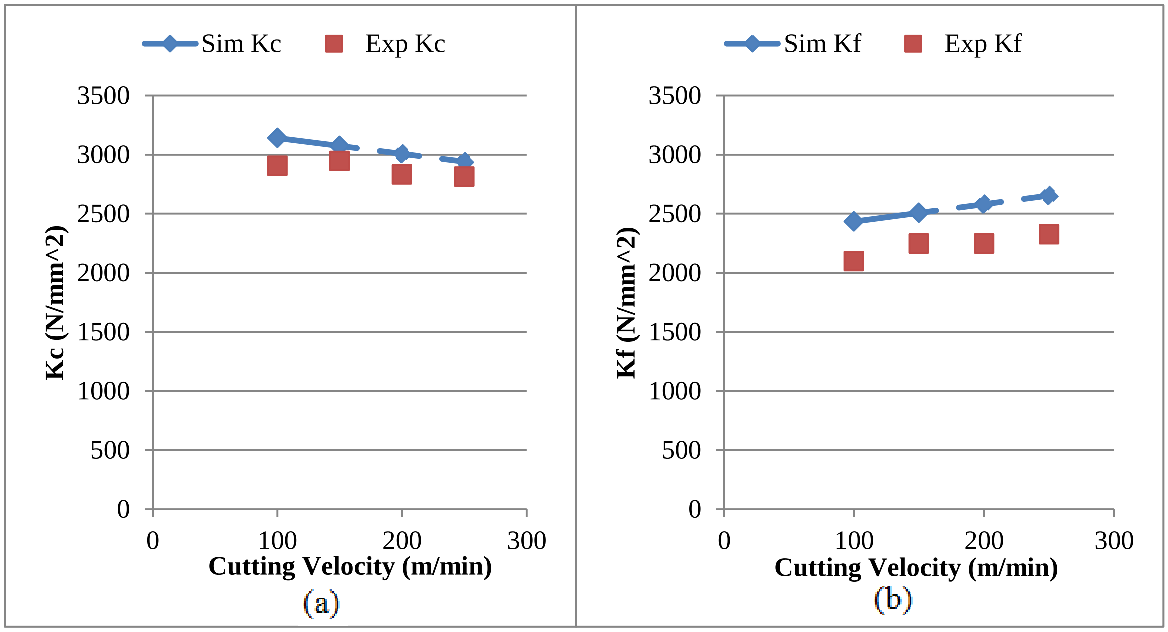

Figure 5-7: Simulation and Experimental results (a) cutting coefficient *Kc* (b) cutting coefficient K_f. Feed rate *f*= 0.05 mm/rev

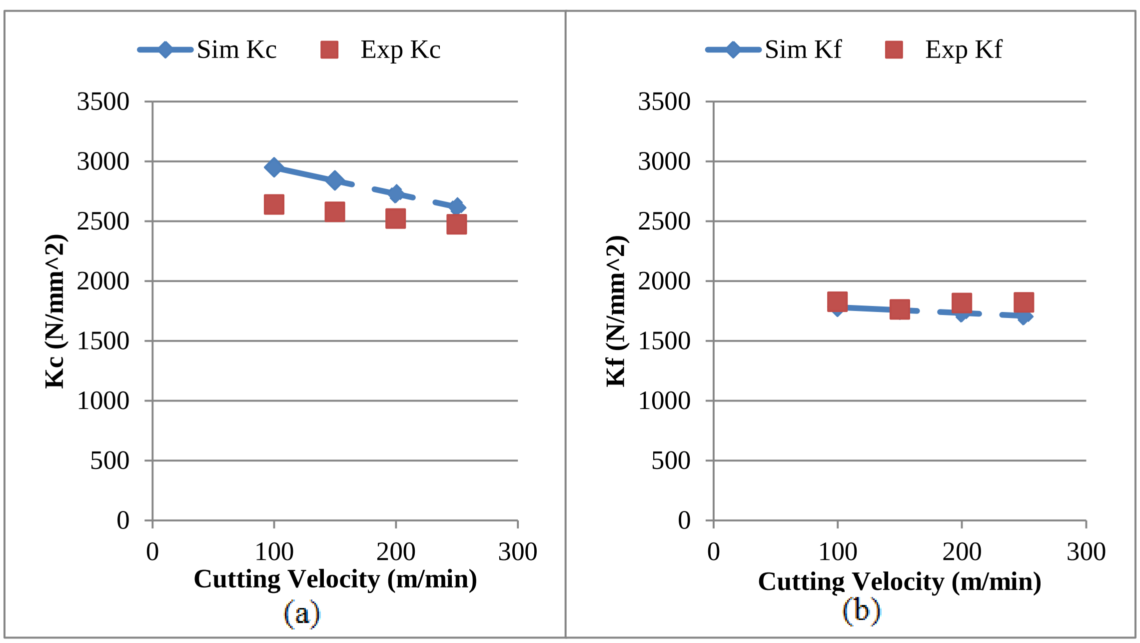

Figure 5-8: Simulation and Experimental results (a) cutting coefficient *Kc* (b) cutting coefficient K_f. Feed rate *f*= 0.07 mm/rev

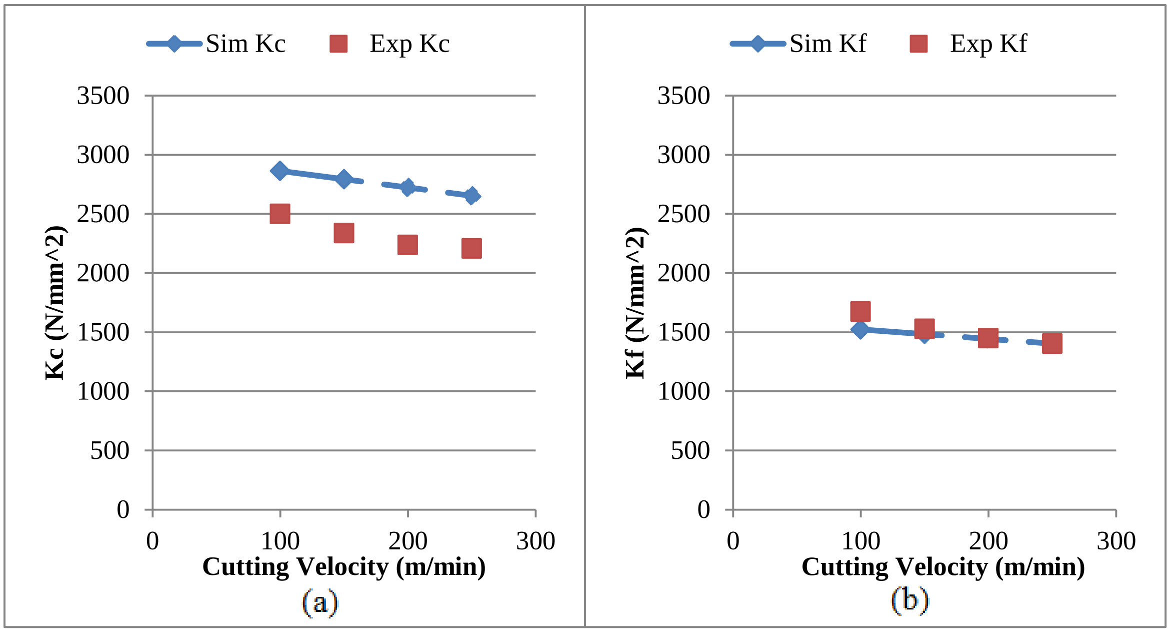

Figure 5-9: Simulation and Experimental results (a) cutting coefficient *Kc* (b) cutting coefficient K_f. Feed rate f= 0.10 mm/rev

All the predicted values have been validated except for at feed rate f=0.14 mm with speed v= 200 m/min and v= 250 m/min. These two values are easily estimated using the regression method after the predicted values at rate f=0.14 mm with speed v= 100 m/min and v= 150 m/min have been calculated. The slope and the intercept for all the trend lines are show in Appendix A.

Figure 5-10 (a) and (b) and Figure 5-11 (a) and (b) show the effect of changing feed rates f on cutting coefficients *Kc* and K_f at constant cutting speed v=200 m/min and v=250 m/min repectively. It is again clear that the cutting coefficients decrease as feed rates increase due to the ploughing, this is clearer in the case of K_f. Figure 5-12 (a) and (b) shows effect of changing cutting speed v on cutting coefficients *Kc* and K_f at constant feed rate f= 0.14 mm/rev, the trend for the simulation and experimental values agreed well, the trend is downwards due to the sensitivity of the work material to the increasing temperature rather than strain rate.

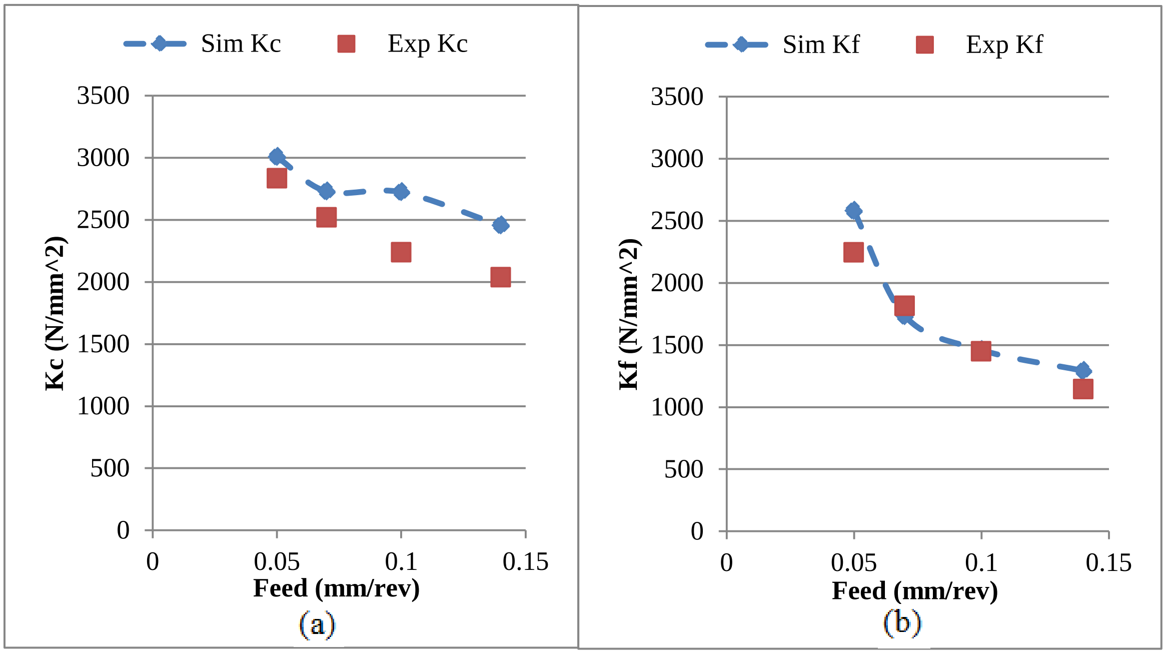

Figure 5-10: Simulation and Experimental results (a) cutting coefficient *Kc* (b) cutting coefficient K_f. Cutting speed *v*=200 m/min m/min

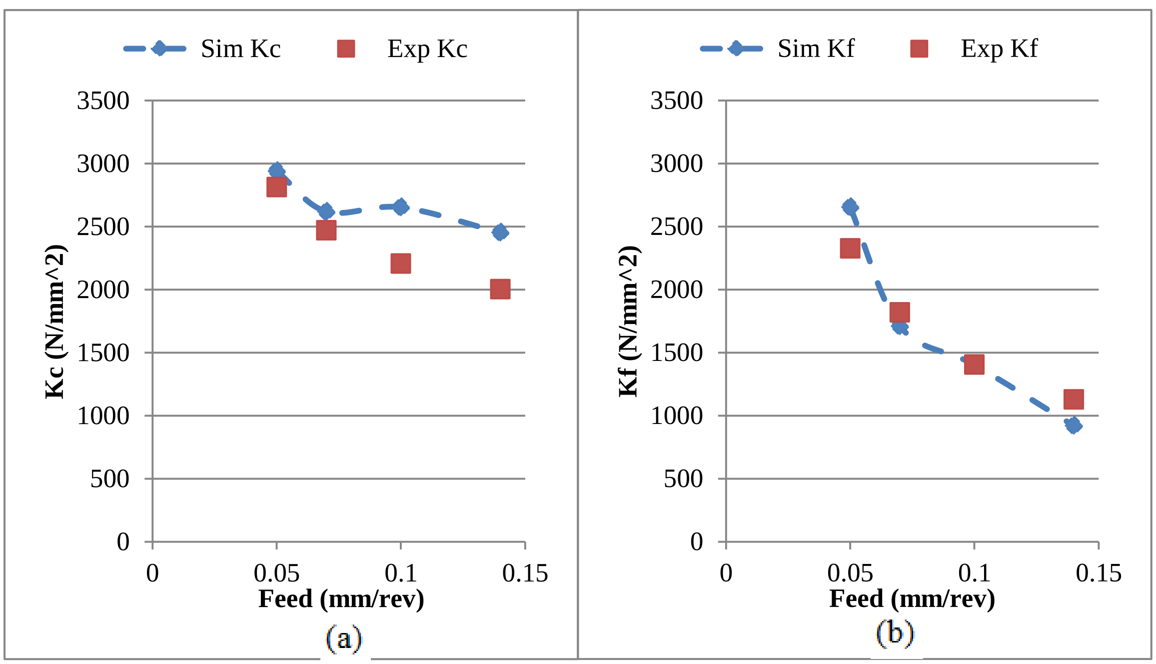

Figure 5-11: Simulation and Experimental results (a) cutting coefficient *Kc* (b) cutting coefficient K_f. Cutting speed *v*=250 m/min

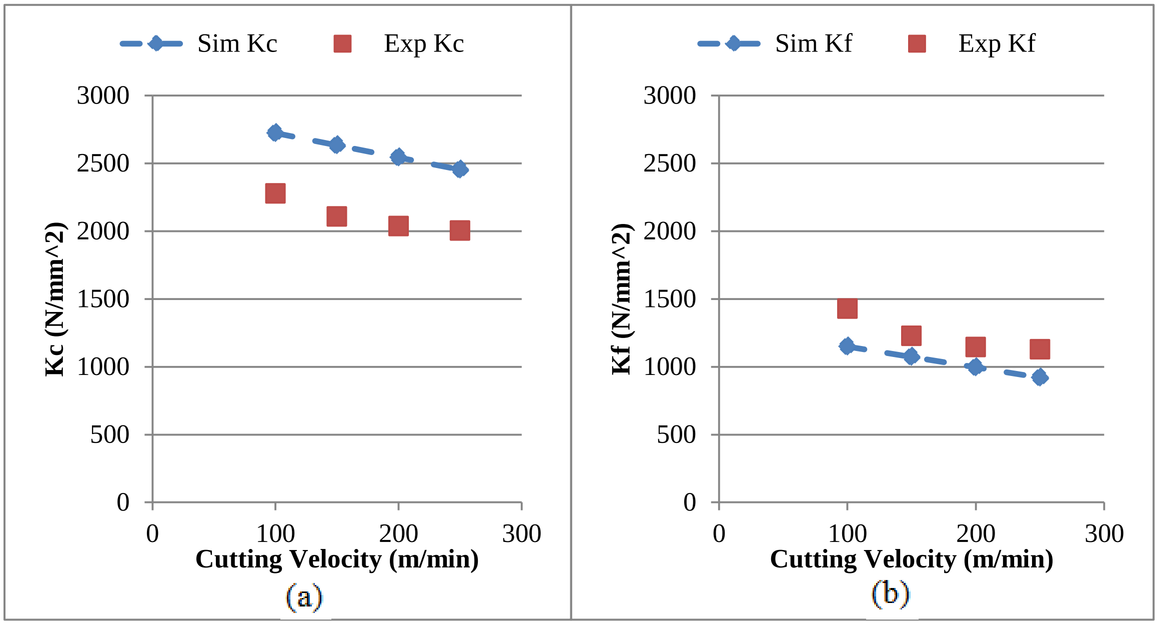

Figure 5-12: Simulation and Experimental results (a) cutting coefficient *Kc* (b) cutting coefficient K_f. Feed rate *f*= 0.14 mm/rev

As the feed rate gets higher, the contact length between the tool and the chip increases, as a result, the temperature at the secondary shear zone (SSZ) increases. Figure 5-13 (a) (b) and (c) shows how different contact length at different feed rates affect the temperature of the SSZ.

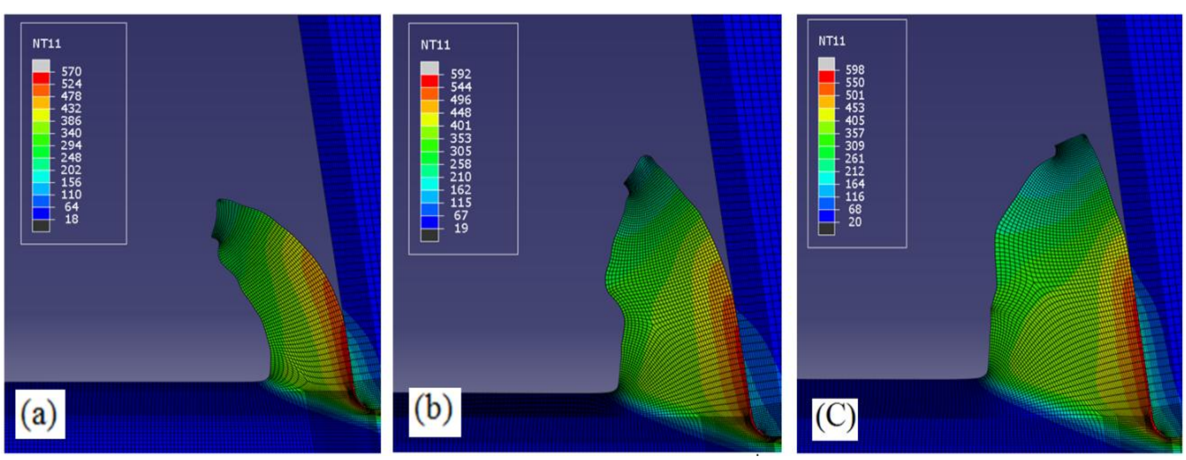

Figure 5-13: Temperature of SSZ at *v*= 150 m/min (a) *f*= 0.05 mm/rev (b) *f*= 0.07 mm/rev (c) rate *f*= 0.10 mm/rev

Figure 5-14 shows the maximum temperature at the SSZ at different feed rates and speeds found by simulation. The results show an agreement with the results of Liu and Melkote [45] Figure 2-15.

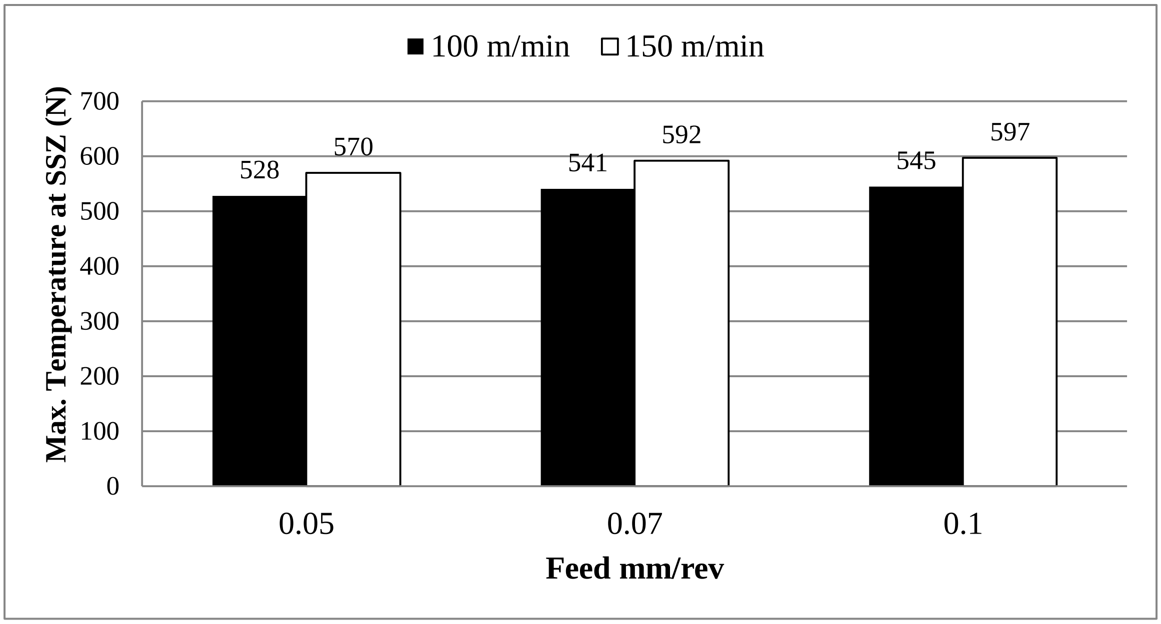

Figure 5-14: Maximum temperature at the SSZ at *v*= 100 m/min and *v*= 150 m/min at different feed rates (simulation results only)

As a result for increasing the SSZ temperature, the flow stress is lowered as the tool cuts through the workpiece. Figure 5-15 shows the results obtained by the FEA simulation, where it shows the effect of the temperature drop in the SSZ due the change in feed rate on the flow stress at *v*= 100 m/min, while Figure 5-16 shows the same effect at at *v*= 150 m/min. It can be seen that at higher speed the effect of temperature on the flow stress is more evident, this also agrees with claim made by Liu and Melkote [45].

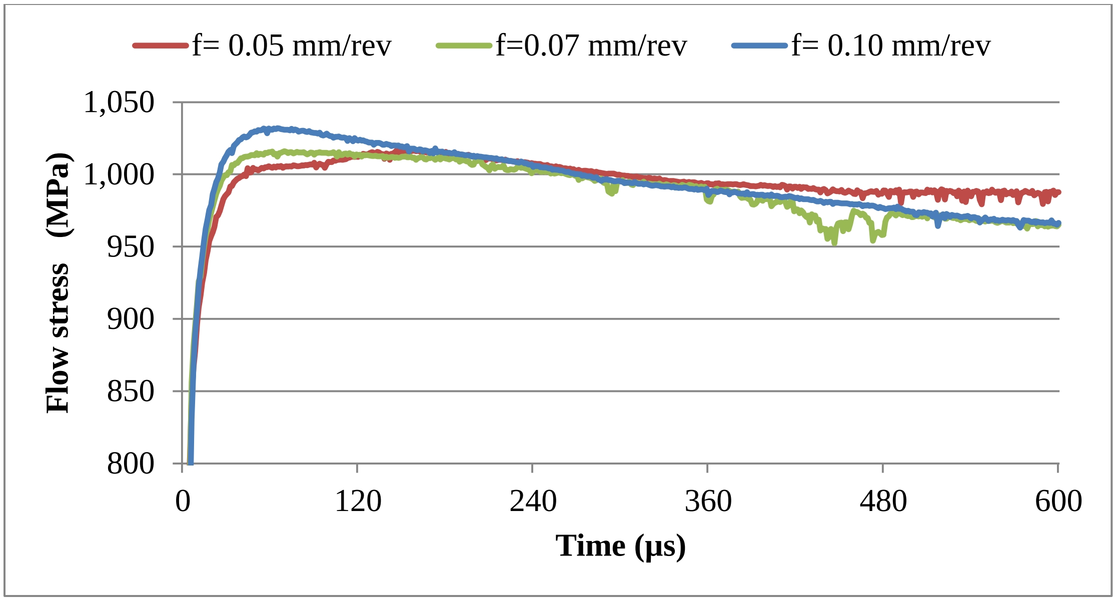

Figure 5-15: flow stress at feed rates *f* = 0.05, *f*= 0.07 and *f*= 0.10 mm/rev. *v*= 100 m/min

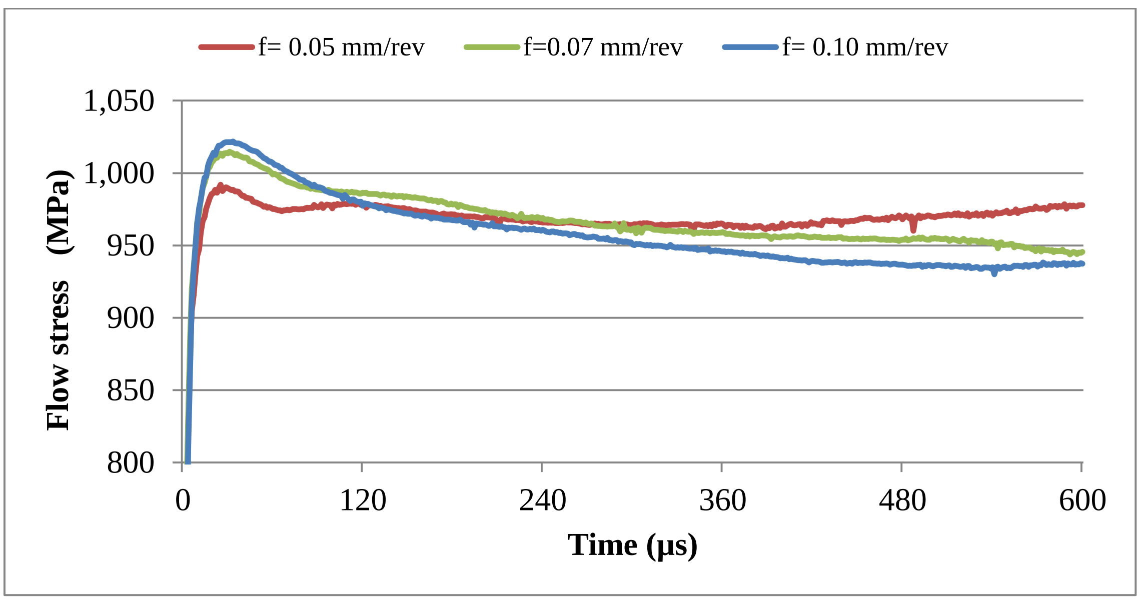

Figure 5-16: flow stress at feed rates *f* = 0.05, *f*= 0.07 and *f*= 0.10 mm/rev. *v*= 150 m/min

Table 5-6 show the values for the predicted and experimental cutting coffecients Kc and K_f and their error at each. It also shows the average error for each of them which was 15.5% and 10.4% for Kc and K_f respectively.

Table 5-6: Predicted and experimental cutting coffecients *Kc* and K_f and their error

	v (m/min)	*f* (mm/rev)	Pre *Kc*	Pre *Kf*	Exp *Kc*	Exp *Kf*	*Kc* error%	*Kf* error%
Predicted 1	100	0.14	2723	1148	2276	1429	19.6	19.7
Predicted 2	150	0.14	2634	1072	2107	1226	25	12.6
Predicted 3	200	0.05	3007	2580	2833	2246	6.1	14.9
Predicted 4	200	0.07	2729	1733	2519	1814	8.3	4.5
Predicted 5	200	0.1	2723	1459	2236	1450	21.8	0.6
Predicted 6	200	0.14	2455	1292	2035	1145	20.6	12.8
Predicted 7	250	0.05	2940	2653	2813	2326	4.5	14.1
Predicted 8	250	0.07	2619	1710	2471	1819	6	6
Predicted 9	250	0.1	2653	1403	2206	1403	20.3	0
Predicted 10	250	0.14	2453	919	2002	1128	22.5	18.5
			Units for Kc and K_f are (N/mm^2)				**Avg= 15.5%**	**Avg= 10.4%**

5.2 Cutting Edge II

5.2.1 Phase I: Validation

Phase I is again repeated to validate the FEM model by comparing the cutting force *Fc* and feed force F_f with the experimental results. Six simulations were carried out at two different cutting speed *v* and three different feed rates *f* as shown in Table 5-7. The cutting edge radius is ρ_e= 30 µm. The tool has a PVD coating.

Table 5-7: Modeling Matrix experimentally validated

Cutting speeds (m/min)	100	150
Feed rates (mm/rev)	0.05, 0.07, 0.10	0.05, 0.07, 0.10

Figure 5-17 (a) and (b) show the effect of varying feed rate f on the cutting force Fc and feed force F_f respectively at fixed cutting speed v=100 m/min, where Figure 5-18 (a) and (b) shows the same but at v=150 m/min.

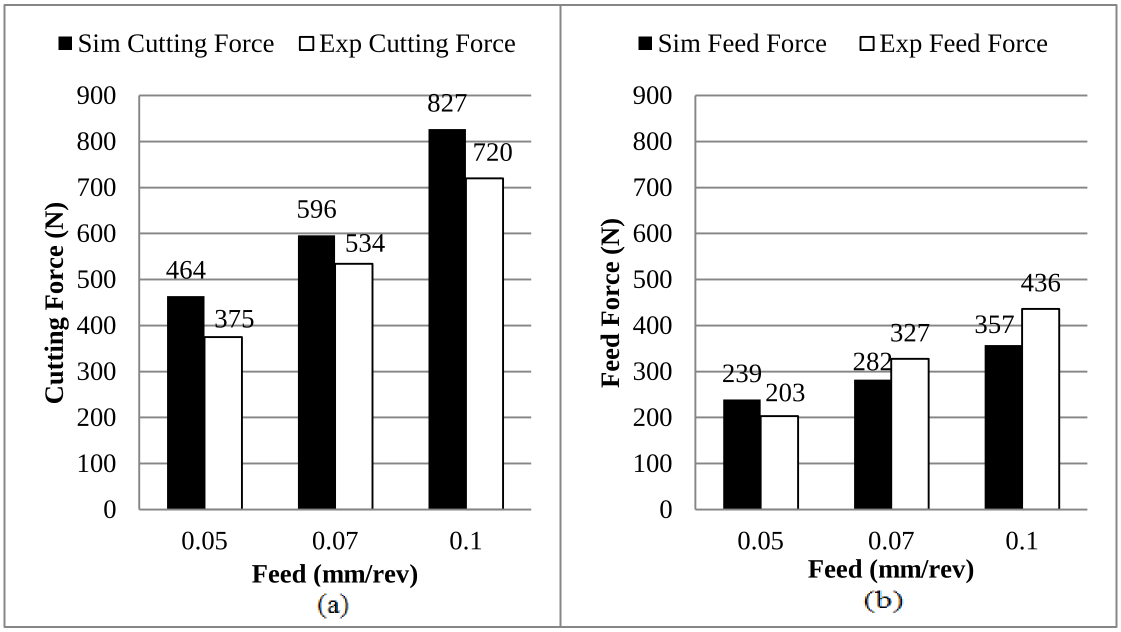

Figure 5-17: Simulation and Experimental results (a) Cutting force Fc (b) feed force F_f. Cutting speed v=100 m/min

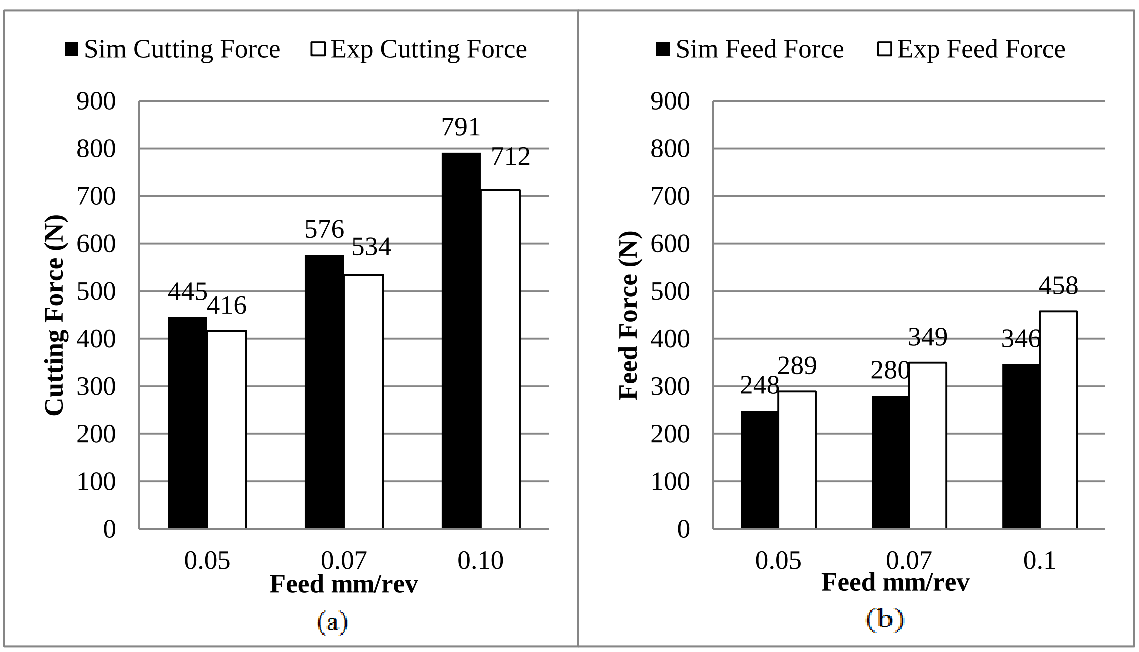

Figure 5-18: Simulation and Experimental results (a) Cutting force Fc (b) feed force F_f. Cutting speed v=150 m/min

Simulation and the experimental results on how the cutting force *Fc* and feed force F_f increase by increasing the feed rate due to the increase of chip load. Table 5-8 shows the values of the cutting forces *Fc* and feed forces F_f and Table 5-9 shows the corresponding cutting coefficients *Kc* and K_f.

Table 5-8: Values of the cutting forces *Fc* and feed forces F_f

	v (m/min)	*f* (mm/rev)	Sim *Fc* (N)	Sim *Ff* (N)	Exp *Fc* (N)	Exp *Ff* (N)
Simulation 1	100	0.05	464	239	375	203
Simulation 2	100	0.07	596	282	534	327
Simulation 3	100	0.10	827	357	720	436
Simulation 4	150	0.05	445	248	416	289
Simulation 5	150	0.07	577	281	533	349
Simulation 6	150	0.10	791	347	712	457

Table 5-9: Values of cutting coefficients *Kc* and K_f

	Sim *Kc*	Sim *Kf*	Exp *Kc*	Exp *Kf*	*Kc* error%	*Kf* error%
Simulation 1	3094	1593	2501	1355	24	18
Simulation 2	2839	1344	2543	1559	12	14
Simulation 3	2757	1191	2400	1454	15	18
Simulation 4	2972	1656	2773	1927	7	14
Simulation 5	2746	1338	2538	1664	8	20
Simulation 6	2637	1155	2374	1523	11	24
	Units for *Kc* and *Kf* are (N/mm^2)				**Avg= 13%**	**Avg= 18%**

The average errors for *Kc* and K_f are 13% and 18% respectively which indicates that the model could be useful for the parametric study phase.

5.2.2 Phase II: Parametric Study

Phase II is repeated for cutting edge II using the same methodologies used for cutting edge I. The aim is to study the effect of some parameters on the cutting coefficients. Table 5-10 shows the range of validation and prediction at every cutting speed and feed.

Table 5-10: The range of Validation and prediction at every cutting speed *v* and feed *f*

Feed/Speed	100 (m/min)	150 (m/min)	200 (m/min)	250 (m/min)
0.05 (mm/rev)	Validated in Phase I	Validated in Phase I	Predicted	Predicted
0.07 (mm/rev)	Validated in Phase I	Validated in Phase I	Predicted	Predicted
0.10 (mm/rev)	Validated in Phase I	Validated in Phase I	Predicted	Predicted
0.14 (mm/rev)	Predicted	Predicted	Predicted	Predicted

Figure 5-19 (a) and (b) shows the effect of changing feed rates *f* on cutting coefficients *Kc* and K_f at constant cutting speed *v*=100 m/min. Figure 5-20 (a) and (b) shows the same at cutting speed *v*=150 m/min. Table 5-11 shows the constants (U) and (e) values.

Table 5-11: (U) and (e) values for speed *v*=100 m/min and speed *v*=150 m/min

	Kc		*Kf*	
Cutting Speed (m/min)	U	e	U	e
100	1854	0.17	439	0.42
150	1750	0.17	333	0.53

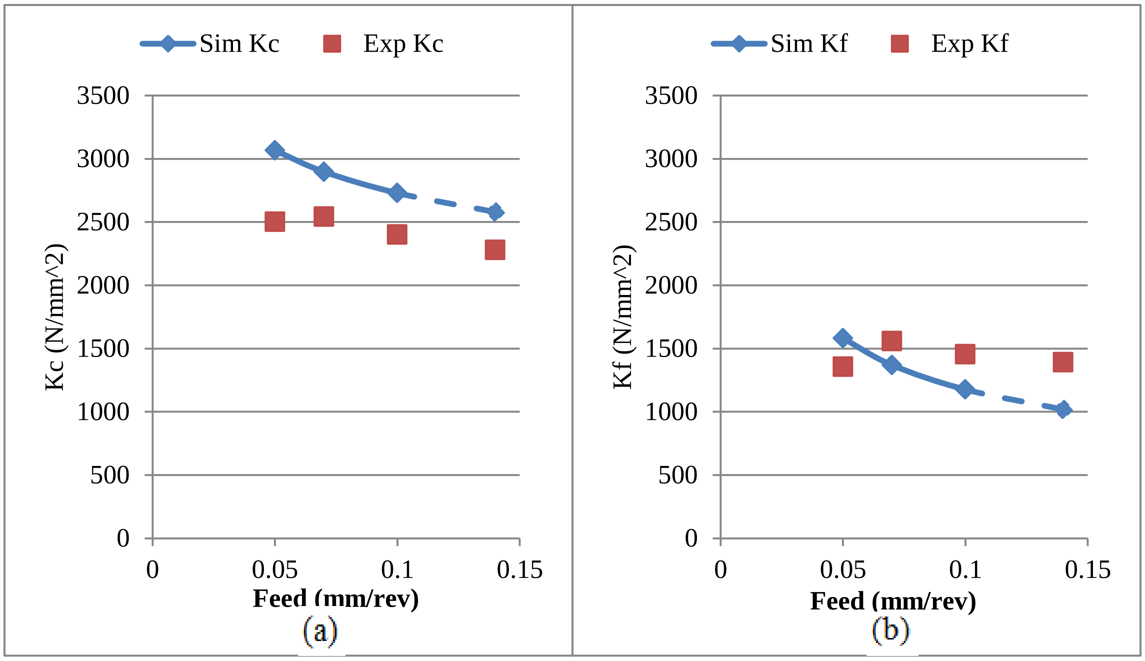

Figure 5-19: Simulation and Experimental results (a) cutting coefficient *Kc* (b) cutting coefficient K_f. cutting speed v=100 m/min

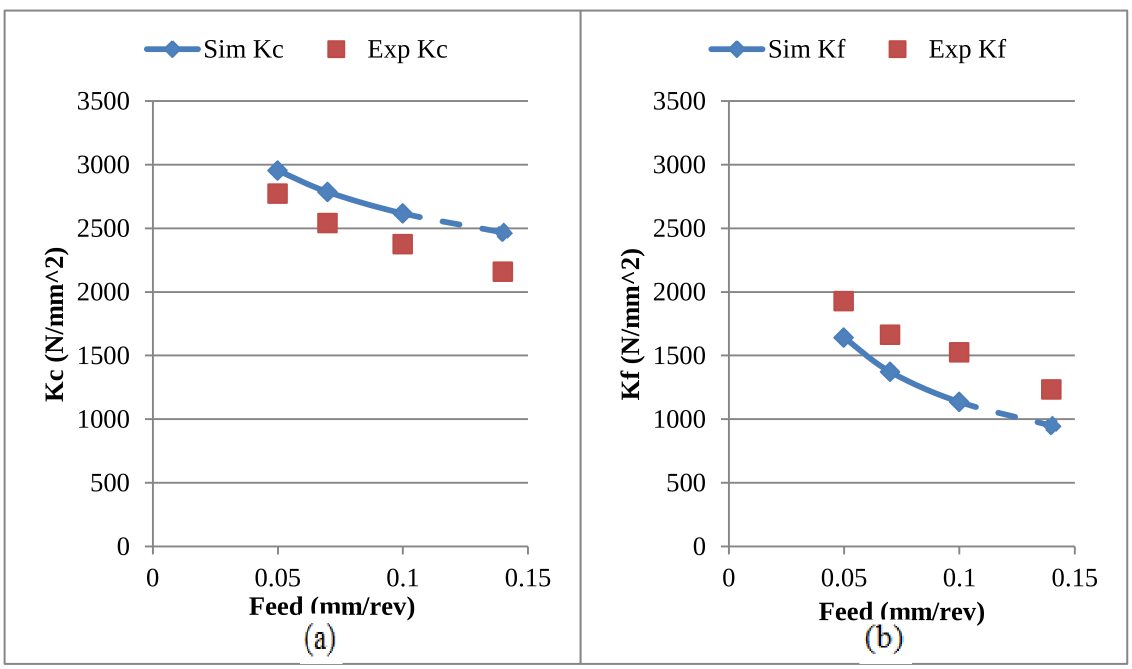

Figure 5-20: Simulation and Experimental results (a) cutting coefficient *Kc* (b) cutting coefficient K_f. cutting speed v=150 m/min

The methodology used to find these curves is least square method, which was explained earlier in this chapter The curve for K_f has larger slope than that for Kc, which means that the feed has bigger effect on the cutting coefficient in the feed direction rather than the cutting direction. This is similar to those observed with larger cutting edge radius. Figure 5-21 (a) and (b) shows the effect of changing cutting speed v on cutting coefficients Kc and K_f at constant feed rate f= 0.05 mm/rev. Figure 5-22 (a) and (b) and Figure 5-23 (a) and (b) show the same at feed rate f= 0.07 mm/rev and f= 0.10 mm/rev. Again there is a good agreement between the simulation and the experimental values. The trend for Kc and K_f is usually downwards; this is due to the sensitivity of the work material to the increasing temperature as the speed increases due to thermal softening of the material at the tool-chip interface. These curves are found using linear regression. Figure 5-21 (b) shows that K_f trend is increasing, this is due to the small contact length between the tool and the chip at this low feed rate rate (f= 0.05) mm/rev, which does not allow high heat generation in the chip; thus more energy is required to cut.

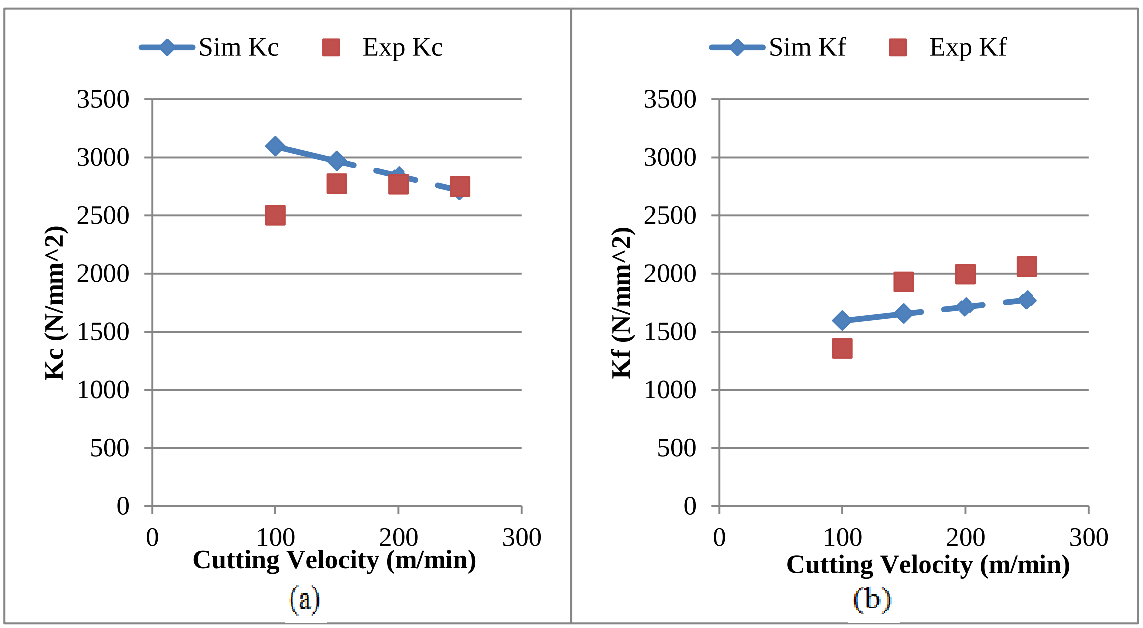

Figure 5-21: Simulation and Experimental results (a) cutting coefficient Kc (b) cutting coefficient K_f. Feed rate f= 0.05 mm/rev

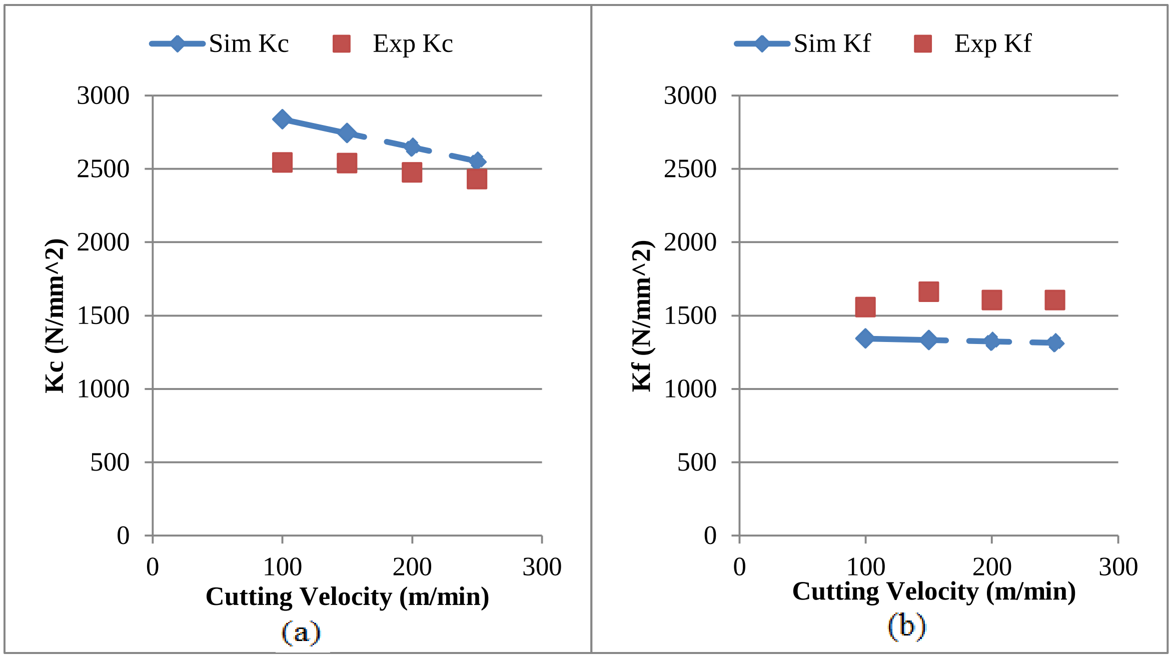

Figure 5-22: Simulation and Experimental results (a) cutting coefficient *Kc* (b) cutting coefficient K_f. Feed rate f= 0.07 mm/rev

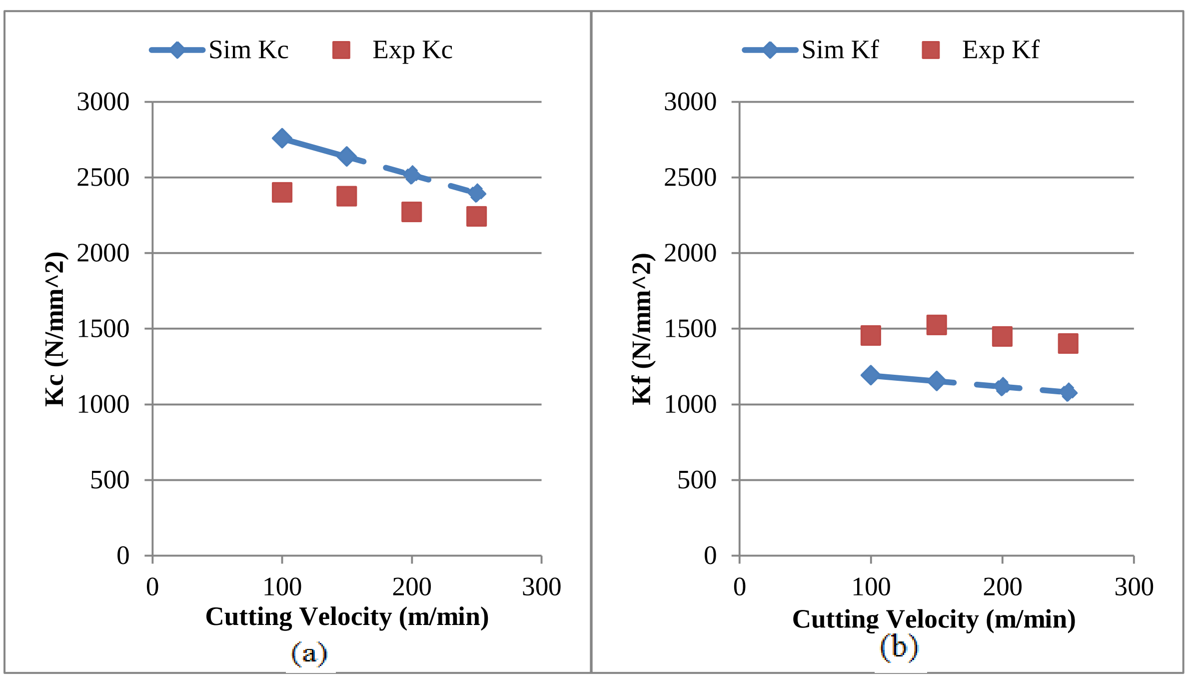

Figure 5-23: Simulation and Experimental results (a) cutting coefficient *Kc* (b) cutting coefficient K_f. Feed rate f= 0.10 mm/rev

All the predicted values have been estimated except for at feed rate f=0.14 mm with speed v= 200 m/min and v= 250 m/min. These two values are easily estimated using the same method of regression after the predicted values at rate f=0.14 mm with speed v= 100 m/min and v= 150 m/min have been estimated. The slope and the intercept for all the trend lines are show in Appendix A. Figure 5-24 (a) and (b) and Figure 5-25 (a) and (b) show the effect of changing feed rates f on cutting coefficients Kc and K_f at constant cutting speed v=200 m/min and v=250 m/min repectively. It is again clear that the cutting coefficients decrease as feed rates increase due to the ploughing, this is clearer in the case of K_f. Figure 5-26 (a) and (b) shows the effect of changing cutting speed v on cutting coefficients Kc and K_f at constant feed rate f= 0.14 mm/rev, the trend for the simulation and experimental value is again agreeing together, the trend is downwards due to the sensitivity of the work material to the increasing temperature rather than strain rate.

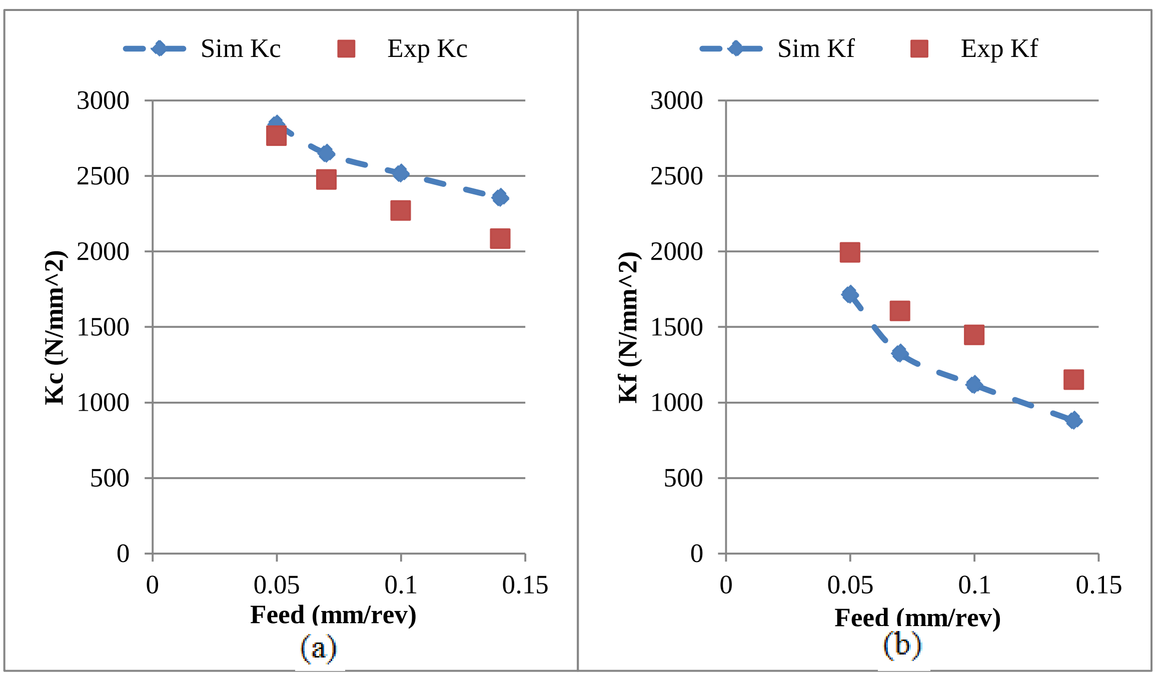

Figure 5-24: Simulation and Experimental results (a) cutting coefficient Kc (b) cutting coefficient K_f. cutting speed v=200 m/min

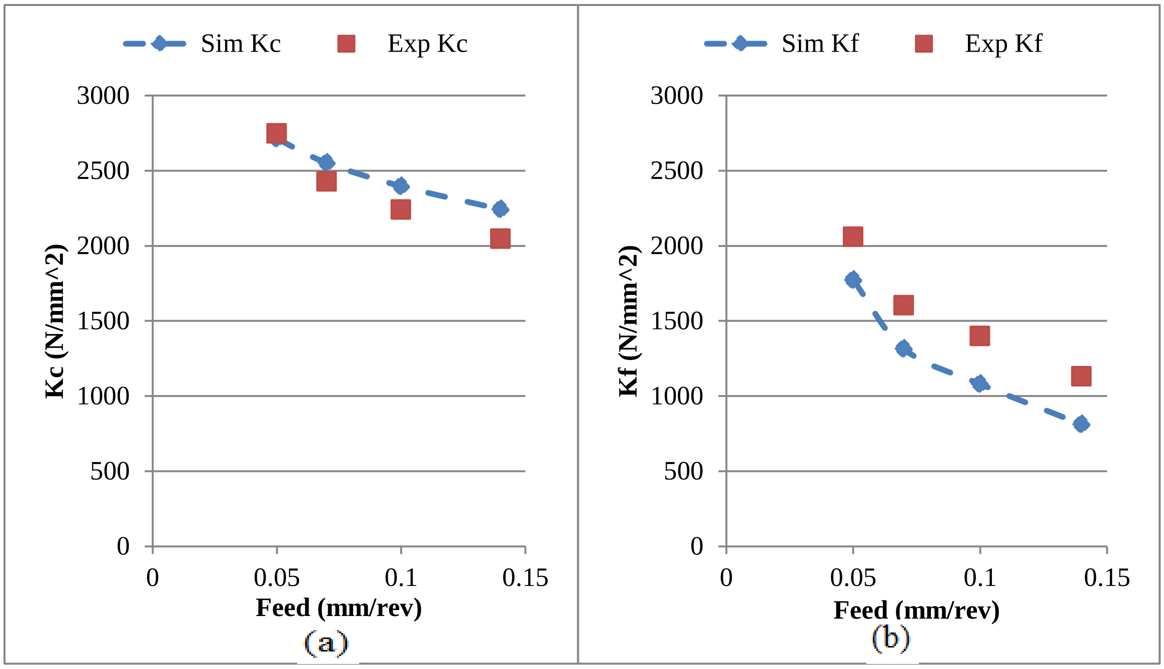

Figure 5-25: Simulation and Experimental results (a) cutting coefficient *Kc* (b) cutting coefficient K_f. cutting speed v=250 m/min

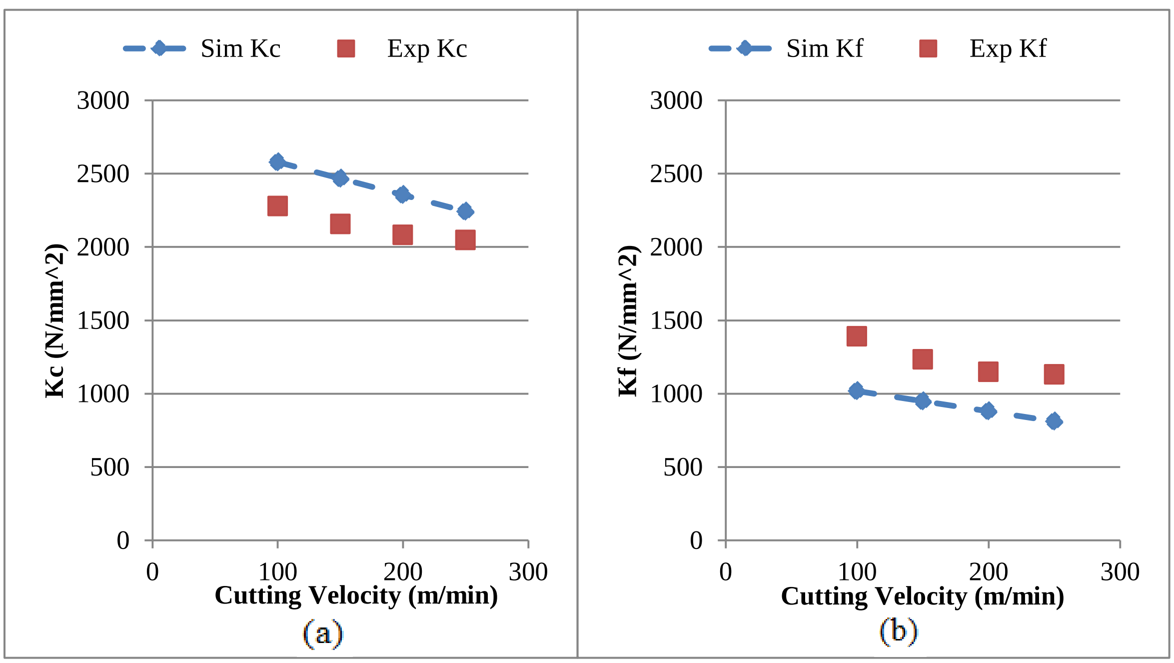

Figure 5-26: Simulation and Experimental results (a) cutting coefficient *Kc* (b) cutting coefficient K_f. Feed rate f= 0.14 mm/rev

It is important to say that the size effect phenomenon is mainly due to the decrease in the flow stress of the workpiece as result of increasing temperature of the secondary shear zone. And as mentioned before this happens due to the increase in the tool-chip contact length as the feed rates gets higher.

Table 5-12 show the values for the predicted and experimental cutting coffecients *Kc* and K_f and their error at each. It also shows the average error for each of them which were 8.4% and 21.1% for *Kc* and K_f respectively, these error values is very promising and reasonable and could be further improved by improving the FEM model.

Table 5-12: Predicted and experimental cutting coffecients *Kc* and K_f and their error

	v (m/min)	*f* (mm/rev)	Pre *Kc*	Pre *Kf*	Exp *Kc*	Exp *Kf*	*Kc* error%	*Kf* error%
Predicted 1	100	0.14	2579	1018	2280	1392	13.1	26.9
Predicted 2	150	0.14	2467	949	2157	1234	14.4	23.1
Predicted 3	200	0.05	2840	1713	2767	1993	2.6	14.0
Predicted 4	200	0.07	2648	1324	2476	1605	6.9	17.5
Predicted 5	200	0.1	2517	1116	2270	1447	10.9	22.9
Predicted 6	200	0.14	2355	880	2083	1150	13.1	23.5
Predicted 7	250	0.05	2713	1773	2747	2060	1.2	13.9
Predicted 8	250	0.07	2552	1314	2429	1604	5.1	18.1
Predicted 9	250	0.1	2397	1080	2240	1400	7.0	22.9
Predicted 10	250	0.14	2243	811	2048	1130	9.5	28.2
			Units for Kc and K_f are (N/mm^2)				**Avg= 8.4%**	**Avg= 21.1%**

5.3Effect of Cutting Edge Radius

This section discusses the effect of cutting edge radius on the cutting coefficients. When using relatively large edge radius compared to feed rate; a considerable amount of material around the cutting edge will have almost zero velocity vector. This area is called stagnation zone. The stagnation zone increases with larger edge radius [53]. Figure 5-27 and Figure 5-28 show the stagnation zones at cutting radii ρ_e= 60 μm and ρ_e= 30 μm respectively and at cutting speed v= 100 m/min and feed rate f= 0.05 mm/rev for both cases.

Figure 5-29 to Figure 5-36 compare the simulation and experimental values for Kc and K_f at cutting edge radii ρ_e= 60 μ and ρ_e= 30 μ at different cutting feed rates and cutting speeds. From the results it's clear that the cutting coefficients Kc and K_f values differs when using different cutting edge radius. The experimental and the simulation results agrees that in all the cases the cutting coefficients at the larger cutting edge radius ρ_e= 60 μm is always higher than those at cutting edge radius ρ_e= 30 μm at the same cutting parameters, which also means that cutting forces also increase by increasing the cutting edge radius. The reason for that is that when the ratio between the feed rate and the cutting edge radius f/ρ_e is relatively low, large amount of machining energy is consumed in the plastic deformation of the surface of the workpiece or what is known as ploughing. These results agree with Afazov et al. [47] as shown in Figure 2-17 and in Figure 2-18. It is observable that the effect of ploughing more evident in the feed force direction.

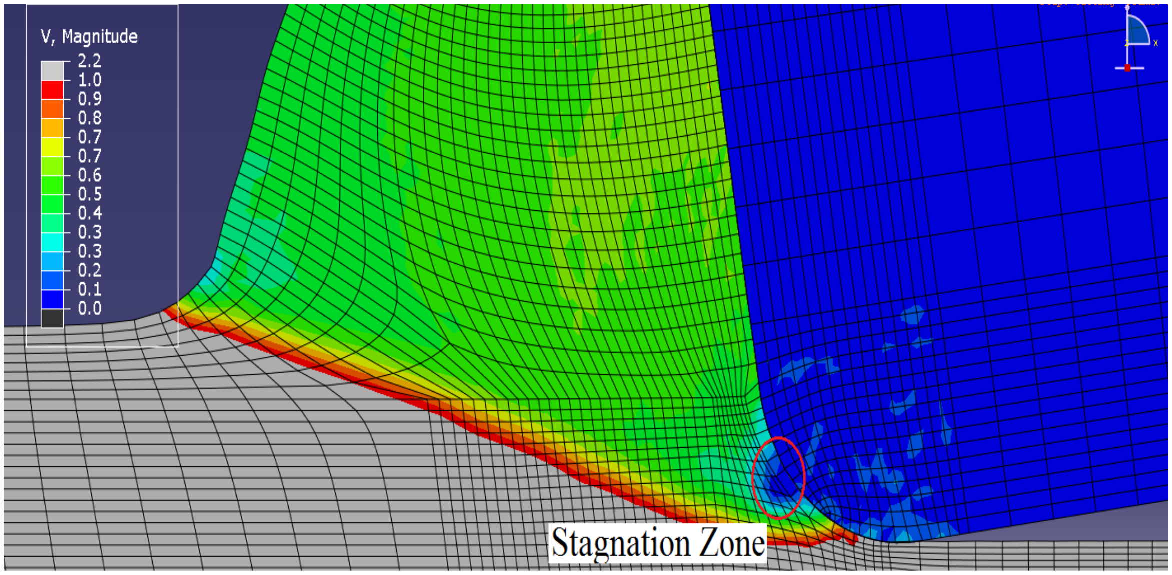

Figure 5-27: stagnation zone at cutting radii ρ_e= 60 µm cutting speed v= 100 m/min feed rate f= 0.05 mm/rev

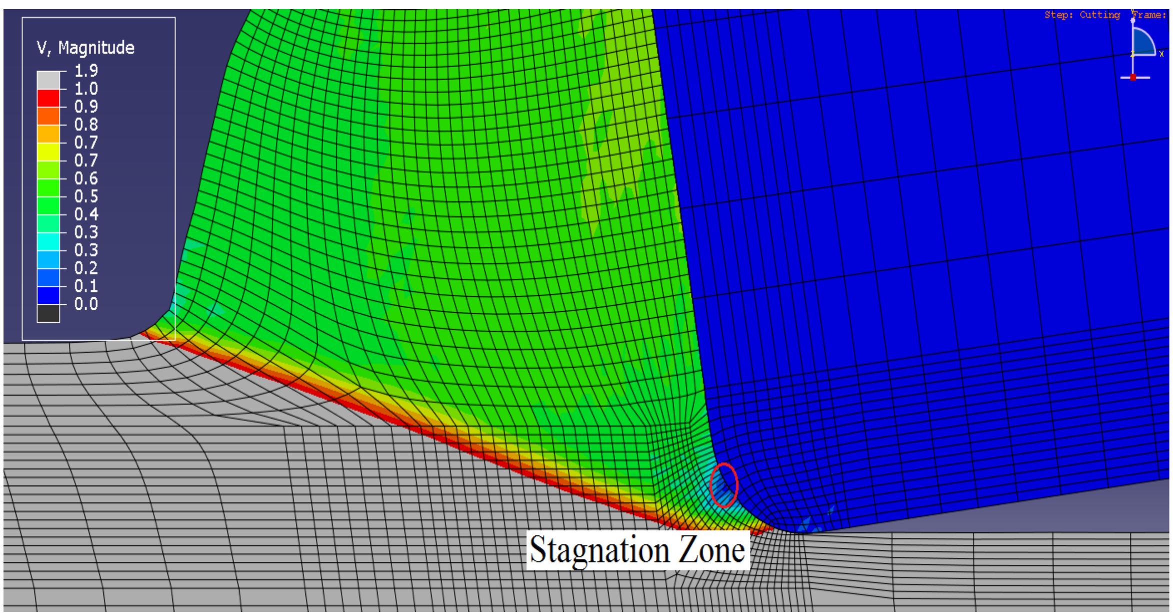

Figure 5-28: stagnation zone at cutting radii ρ_e= 30 µm cutting speed v= 100 m/min feed rate f= 0.05 mm/rev

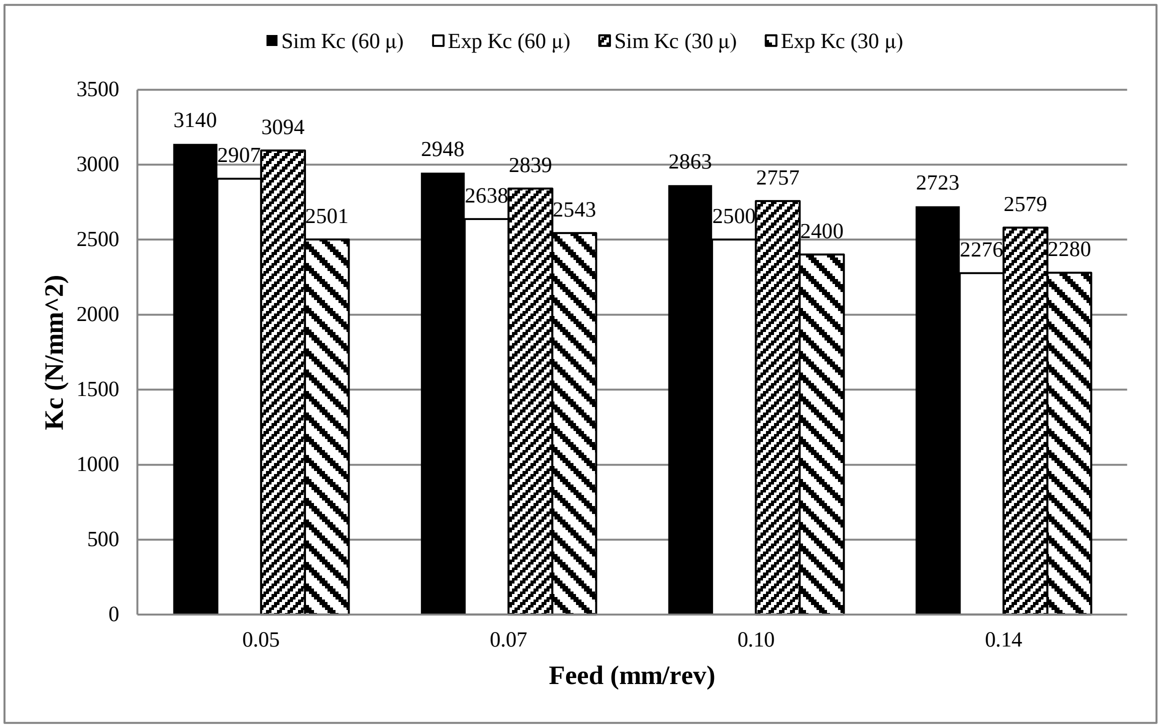

Figure 5-29: Effect of cutting edge radius on K_f at v= 100 m/min

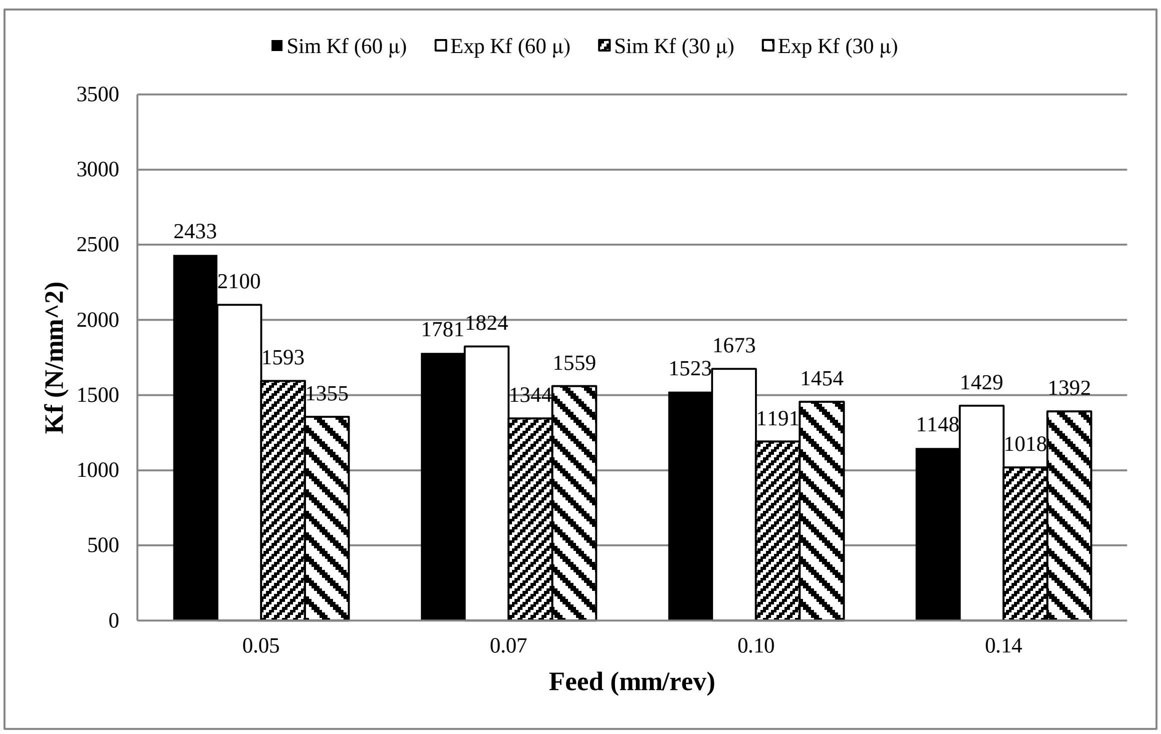

Figure 5-30: Effect of cutting edge radius on K_c at v= 100 m/min

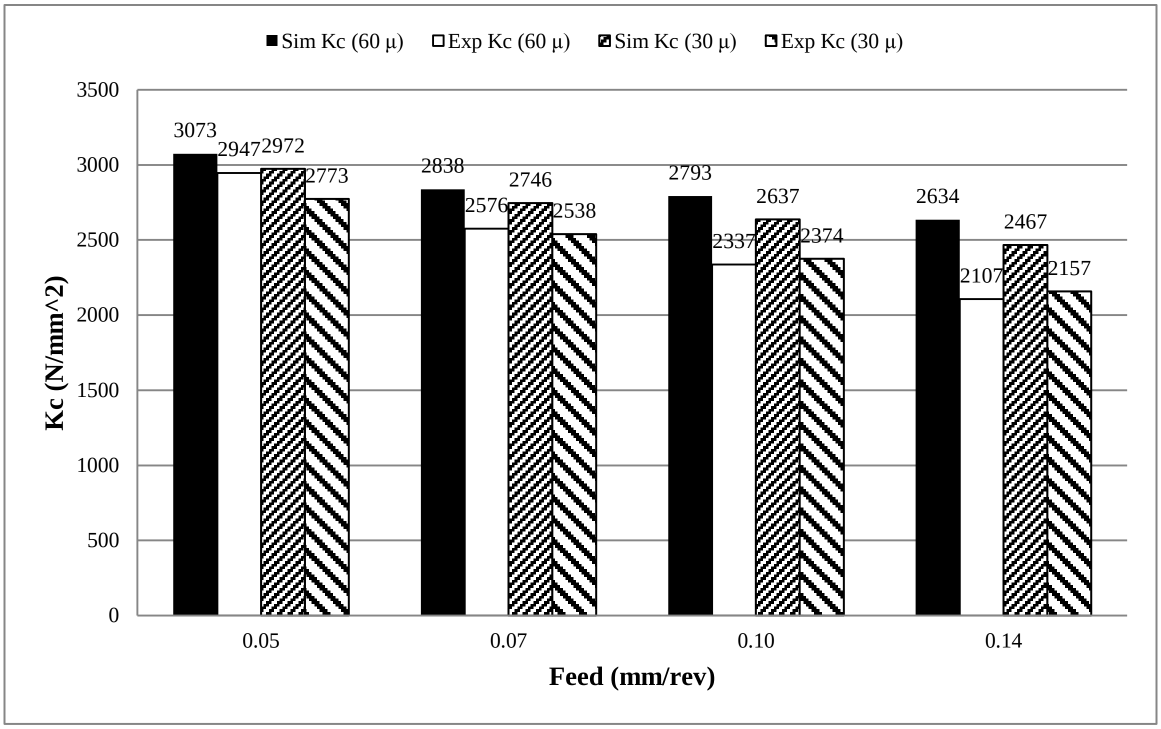

Figure 5-31: Effect of cutting edge radius on K_c at v= 150 m/min

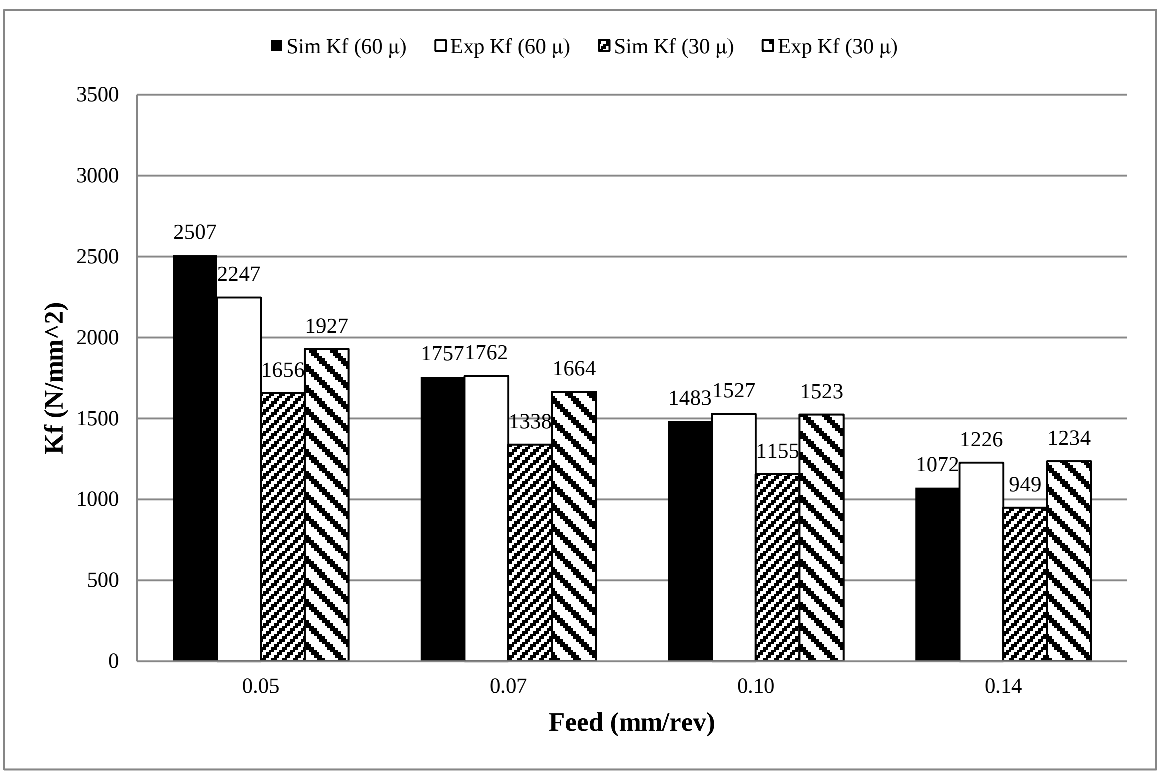

Figure 5-32: Effect of cutting edge radius on K_f at v= 150 m/min

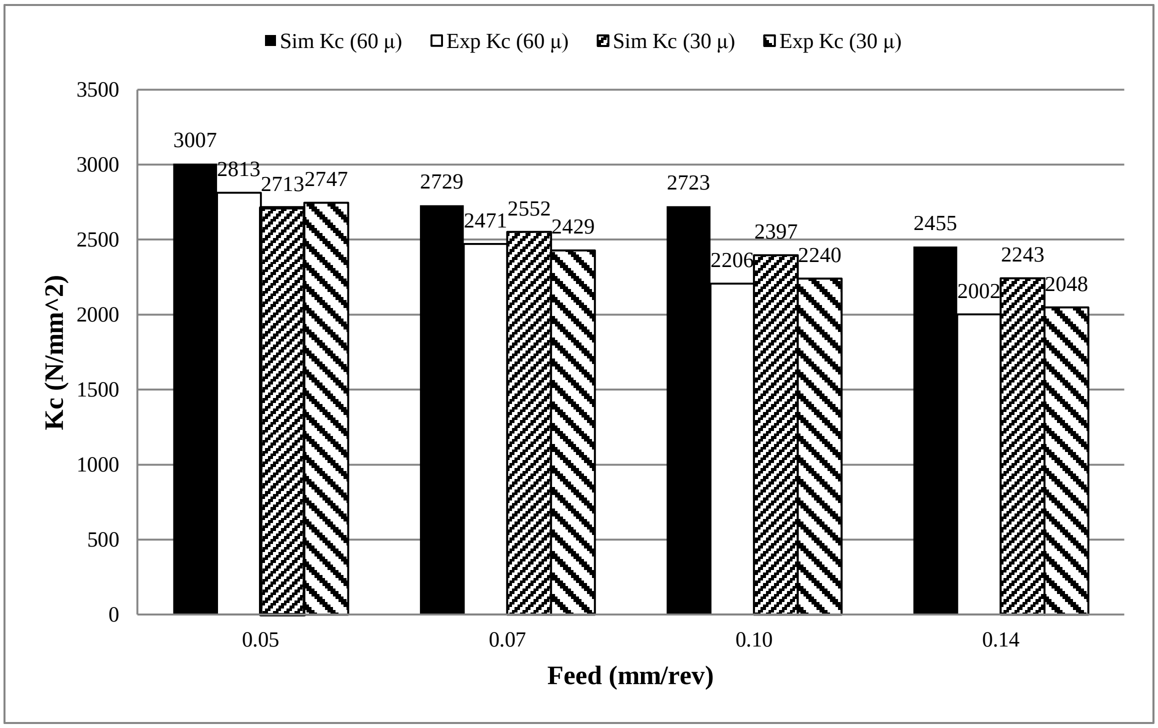

Figure 5-33: Effect of cutting edge radius on K_c at v=200 m/min

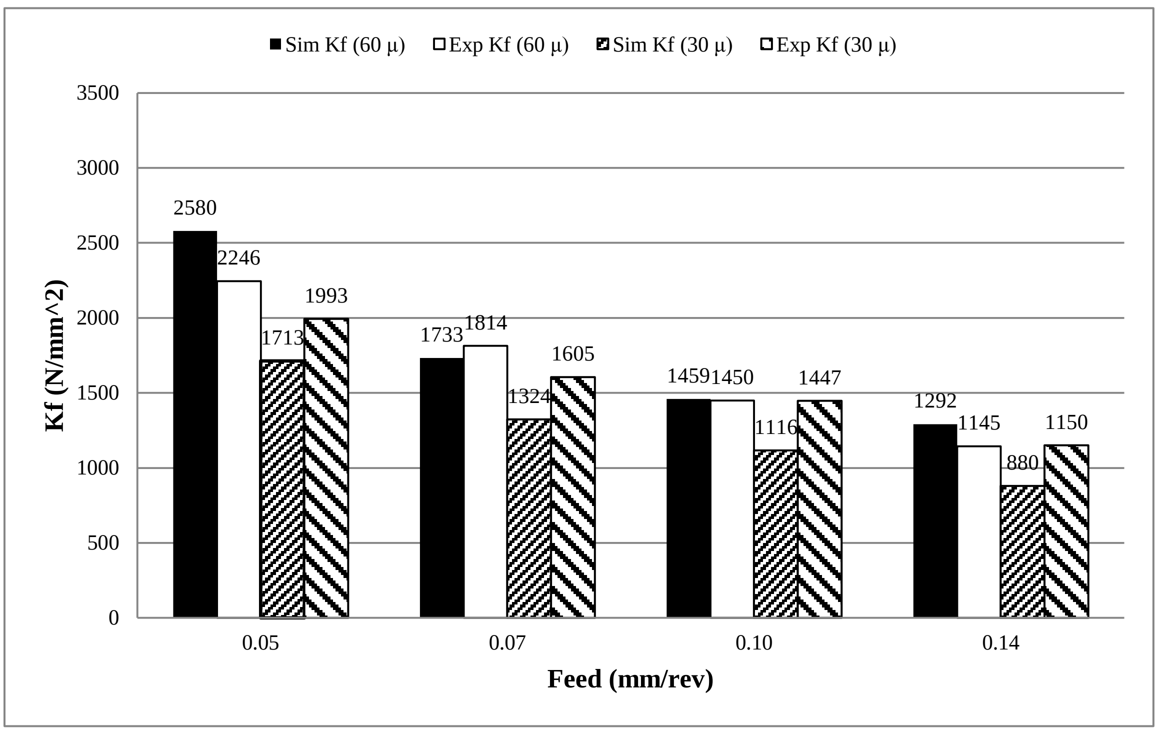

Figure 5-34: Effect of cutting edge radius on K_f at v= 200 m/min

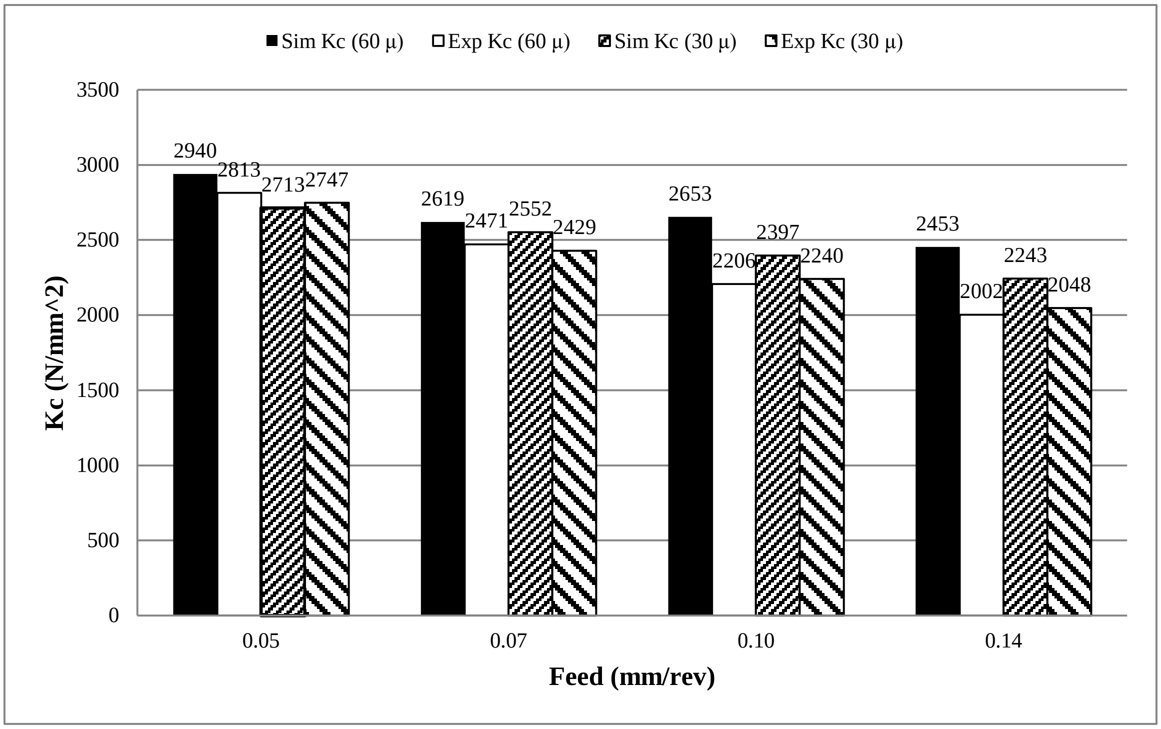

Figure 5-35: Effect of cutting edge radius on K_c at v= 250 m/min

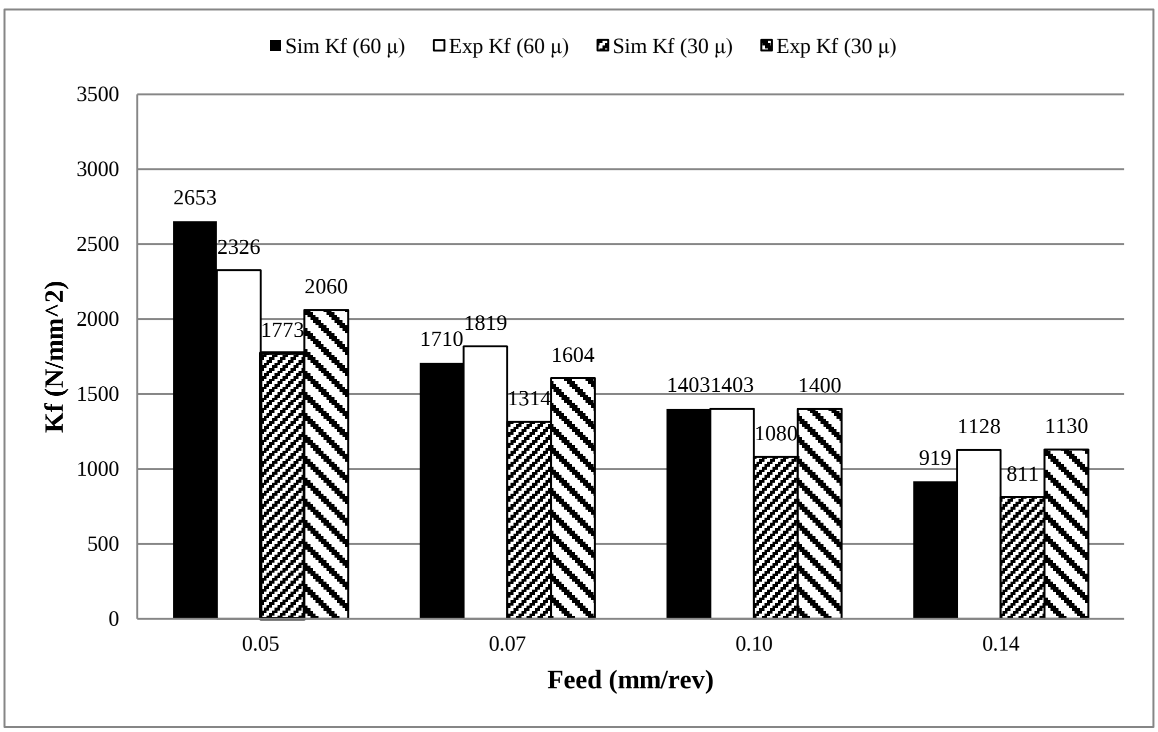

Figure 5-36: Effect of cutting edge radius on K_f at v= 250 m/min

Chapter 6 Conclusion

- Detailed literature search on studying the effect of feed rate *f*, cutting speed *v*, and cutting edge radius ρ_e on the cutting coefficients. The research shows that as the ratio of feed rate and cutting edge radius f/ρ_e is relatively low (less than or equal 1) the cutting coefficients increase due to ploughing. Cutting speed has little effect on cutting coefficients. Usually at higher speeds cutting coefficients tends to decrease slightly due to thermal softening.
- Results obtained from Phase I shows that FE models and experimental results has a good agreement for both cutting and feed directions. The average error for cutting coefficients in cutting and feed directions Kc and K_f are 11.4% and 7% respectively for cutting edge I prepared by CVD method. While the error is 13% and 18% for edge II prepared by PVD method.
- Because the chip breaker was not simulated, there is relatively high error in Kc especially at higher feed rates as it become more difficult for the chip to curl and break in without chip breaker.
- The parametric study shows that cutting coefficients increase at lower feed rates due to ploughing of the workpiece surface. While it decrease at higher cutting speeds due to thermal softening. This applies to the two cutting edges simulated.
- The size effect at high cutting speeds is more evident; this is primarily caused by a decrease in the shear strength of the workpiece material due to an increase in the tool-chip interface temperature as feed rates gets higher. However, this is more evident at relatively large cutting speeds (v >200 m/min) and large feed rates (f >50 μm). This was captured by FEA models at v= 100 m/min and v= 150 m/min.

- Results obtained from phase II also shows a good agreement between FE models and experimental results for both cutting and feed directions. The average error for cutting coefficients in cutting and feed directions *Kc* and K_f are 15.5% and 10.4% respectively for cutting edge I prepared by CVD method. While the error is 8.4% and 21.1% for edge II prepared by PVD method.
- Cutting coefficients *Kc* and K_f values differs when using different cutting edge radius. The experimental and the simulation results agrees that in all the cases the cutting coefficients at the larger cutting edge radius ρ_e= 60 μm is always higher than those at cutting edge radius ρ_e= 30 μm at the same cutting parameters, the reason for that is that when the ratio between the feed rate and the cutting edge radius f/ρ_e is relatively low, large amount of machining energy is consumed in the plastic deformation of the surface of the workpiece or what is known as ploughing.

Chapter 7 Future Work

- Simulating the complex shape of the chip breaker will help reduce the error at higher feed rates. As this will force the chip to curl at high feed rates.
- Simulating other parameters that could affect the cutting coefficients. One of the important parameters is the rake angle, which has a significant impact on the cutting forces. The cutting force is affected by the rake angle; it increases with the rake angle's decreasing [23].
- Simulating the effect of workpiece hardness, and how it could affect the cutting coefficients. There is a direct relation between increased workpiece hardness and high cutting coefficients. This could be easily noticed from Johnson-Cook material model [1].
- Simulating the effect of tool wear on cutting coefficients, especially flank wear.
- Investigating the effect of COF is also of great importance. It was arbitrary chosen in the current work. It is recommended that COF should be changed as a function of temperature.
- Studying the effect of damping on cutting coefficients. This could be done using a wiper insert that usually involves a lot of friction between the flank face and the workpiece.
- Using the cutting coefficients in a Multi-Scale model that study the dynamics of the machine tools including vibrations and chatter [6] [7].

References

[1] G. R. Johnson and W. H. Cook, "A Constitutive Model and Data for Metals," in *Seventh International Symposium on Ballistics*, Hague, Netherlands, 1983.

[2] O. Kienzel, "Die Bestimmung von Kraften und Leistungen an Spanenden Werkzeugen und Werkzeugmaschinen," *Z-VDI,* vol. 94, pp. 299-302, 1952.

[3] M. E. Merchant, "Basic Mechanics of the Metal Cutting Process," *Journal of Applied Mechanics,* vol. 11, pp. 168-175, 1944.

[4] Y. Huang and S. Y. Liang, "Modeling of Cutting Forces Under Hard Turning Conditions Considering Tool Wear Effect," *Journal of Manufacturing Science and Engineering,* vol. 127, pp. 262-270, 2005.

[5] X. Lai, H. Li, C. Li, Z. Lina and J. Nib, "Modelling and Analysis of Micro Scale Milling Monsidering Size Effect, Micro Cutter Edge Radius and Minimum Chip Thickness," *International Journal of Machine Tools & Manufacture,* vol. 48, p. 1–14, 2008.

[6] M. Eynian and Y. Altintas, "Chatter Stability of General Turning Operations With Process Damping," *Journal of Manufacturing Science and Engineering,* vol. 131, pp. 1-10, 2009.

[7] Y. Altintas and M. Weck, "Chatter Stability of Metal Cutting and Grinding," *CIRP Annals- Manufacturing Technology,* vol. 53, pp. 619-642, 2004.

[8] F. Villumsen and T. G. Fauerholdt, "Prediction of Cutting Forces in Metal Cutting, Using a Finite Element Methode, A lagrangian Approach," in *LS-DYNA Anwenderforum*, Bamberg, 2008.

[9] S. M. T. Halim, "Finite Element Modeling of the Orthogonal Metal Cutting Process: Modeling the Effects of Coefficient of Friction and Tool Holding Structure on Cutting Forces and Chip Thickness," *M.A.Sc. Thesis, McMaster Univeristy, Hamilton, Ontario,* 2008.

[10] S. G. Kapoor, R. E. Devor, R. Zhu, R. Gajjela, G. Parakkal and D. Smithey, "Develompent of Mechanistic Models for the Prediction of Machining Performance: Model Building Methodolgy," *Machining Science and Technology: An International Journal*, vol. 2:2, pp. 213-238, 1998.

[11] M. K. Das and S. A. Tobias, "The Relation between the Static and the Dynamic

Cutting of Metals," *Int. Journal of MTDR*, vol. 7, pp. 63-89, 1967.

[12] P. W. Wallace and C. Andrew, "Machining Forces: Some Effects of Removing a Wavy Surface," *Journal of Mechanical Engineering Science*, vol. 7, pp. 129-139, 1966.

[13] S. M. Pandit, T. L. Subramanian and S. M. Wu, "Modeling Machine Tool Chatter by Time-Series," *Journal of Engineering for Industry*, vol. 97, pp. 211-215, 1975.

[14] E. H. Lee and B. W. Shaffer, "The Theory of Plasticity Applied to a Problem of Machining," *Journal ofApplied Mechanics*, vol. 18, pp. 405-413, 1951.

[15] P. L. B. Oxley and A. P. Hatton, "Shear Angle Solution Based on Experimental Shear Zone and Tool-Chip Interface Stress Distribution," *International Journal of Mechanics*, vol. 5, p. 41, 1963.

[16] F. Koenigsberger and A. J. P. Sabberwal, "An Investigation into the Cutting Force Pulsations During Milling Operations," *International Jornal of MTDR*, vol. 1, pp. 15-33, 1961.

[17] H. J. Fu, R. E. Devor and S. G. Kapoor, "A Mechanistic Model for Prediction of the Force System in Face Milling Operations," *Journal of Engineering for Industry*, vol.

106, pp. 81-88, 1984.

[18] V. Chandrasekharan, S. G. Kapoor and R. E. Devor, "A Mechanistic Approach to Predicting the Cutting Forces in Drilling: With Application to Fiber-Reinforced Composite Materials," *Jornal of Engineering for Industry,* vol. 117, pp. 559-570, 1995.

[19] V. Chandrasekharan, "A Model to Predict the Three-Dimensional Cutting Force System for Drilling with Arbitrary Point Geometry," *Ph.D. Thesis, University of Illinois at Urbana-Champaign, Urbana, Illinois,* 1996.

[20] B. E. Klamecki, "Incipient Chip Formation in Metal Cutting—a Three Dimension Finite Element Analysis," *Ph.D. Thesis, University of Illinois at Urbana-Champaign, Urbana, Illinois,* 1973.

[21] E.-G. Ng and D. K. Aspinwall, "Modelling of Hard Part Machining," *Journal of Materials Processing Technology,* vol. 127, pp. 222-229, 2002.

[22] J. M. Huang and J. T. Black, "An Evaluation of Chip Separation Criteria the FEM Simulation of Machining," *Journal of Manufacturing Science Engineering,* vol. 118, pp. 545-554, 1996.

[23] G. Fang and P. Zeng, "Effects of Tool Geometrical Parameters on the Chip Formation and Cutting Force in Orthogonal Cutting," *Material Science Forum*, Vols. 471-472, pp. 16-20, 2004.

[24] K. W. Kim, W. Y. Lee and H. C. Sin, "A Finite Element Analysis Of Machining With The Tool Edge Considered," *Journal Of Materials Processing Technology*, vol. 86, pp. 45-55, 1999.

[25] E. Usui, A. Hirota and M. Masuko, "Analytical Prediction of Three Dimensional Cutting Process," *ASME Journal Engineering Ind*, vol. 100, p. 222–228, 1978.

[26] A. Raczy, M. Elmadagli, W. J. Altenhof and A. T. Alpas, "An Eulerian Finite-Element Model for Determination of Deformation State of a Copper Subjected to Orthogonal Cutting," *Metallurgical and Materials Transactions*, vol. 35A, pp. 2393-2400, 2004.

[27] T. H. C. Childs and K. Maekawa, "Computer Aided Simulation and Experimental Studies of Chip Flow and Tool Wear in the Turning of Low Alloy Steels by Cemented Carbide Tools," *Wear*, vol. 139, pp. 235-250, 1990.

[28] M. R. Movahhedy and M. A. Y. Gadala, "Simulation of Orthogonal Metal Cutting Process using an Arbitrary Lagrangian-Eulerian Finite Element Method," *Journal of*

Materials Processing Technology, vol. 103, pp. 267-275, 2000.

[29] H. Miguelez, R. Zaera, A. Rusinek, A. Moufki and A. Molinari, "Numerical Modelling of Orthogonal Cutting: Influence of Cutting Conditions and Separation criterion," *Journal of Physics IV France,* vol. 134, pp. 417-422, 2006.

[30] P. J. Arrazola, D. Ugarte and X. Dominguez, "A New Approach for the Friction Identification during Machining Through the use of Finite Element Modeling," *International Journal of Machine Tools & Manufacture,* vol. 48, pp. 173-183, 2008.

[31] T. Ozel and Z. Erol, "Finite Element Modeling the Influence of Edge Roundness on the Stress and Temperature Fields Induced by High-Speed Machining," *International Journal of Advance Manufacturing Technology,* vol. 35, pp. 255-267, 2007.

[32] M. R. Movahhedy and M. A. Y. Gadala, "Simulation of Chip Formation in Orthogonal Metal Cutting Process: an ALE Finite Element Approach," *Machining Science and Technology,* vol. 4, pp. 15-42, 2000.

[33] M. N. A. Nasr, E.-G. Ng and M. A. Elbestawi, "Modelling the Effects of Tool-Edge Radius on Residual Stresses when Orthogonal Cutting AISI 316L," *International Journal of Machine Tools & Manufacture,* vol. 47, pp. 401-411, 2007.

[34] R. T. Coelho, E.-G. Ng and M. A. Elbestawi, "Tool Wear When Turning Hardened AISI 4340 with Coated PCBN tools using Finishing Cutting Conditions," *International Journal of Machine Tools & Manufacture,* vol. 47, pp. 263-272, 2007.

[35] M. R. Movahhedy, Y. Altintas and M. S. Gadala, "Numerical Analysis of Metal Cutting With Chamfered and Blunt Tools," *Journal of Manufacturing Science and Engineering,* vol. 124, pp. 178-188, 2002.

[36] C. K. Ng, S. N. Melkote, M. Rahman and A. S. Kumar, "Experimental Study of Micro and Nano-Scale Cutting of Aluminum 7075-T6," *International Journal Machining Tool Manufuring,* vol. 46, p. 929–936, 2006.

[37] X. Liu, R. E. Devor, S. G. Kapoor and K. F. Ehmann, "The Mechanics of Machining at the Microscale: Assessment of the Current State of the Science," *Trans ASME Journal of Manufacturing Science and Engineering,* vol. 126, p. 666–678, 2004.

[38] J. A. Arsecularatne, "On Tool-Chip Interface Stress Distributions, Ploughing Force and Size Effect in Machining," *International Journal of Machine Tool and Manufacturing,* vol. 37, pp. 885-899, 1997.

[39] J. A. Arsecularatne, "Size effect and Tool Geometry in Micromilling of Tool Steel," *Precision Engineering,* vol. 33, p. 402–407, 2009.

[40] H. Yan, J. Hua and R. Shivpuri, "Numerical Simulation of Finish Hard Turning for AISI H13 Die Steel," *Science and Technology of Advanced Materials,* vol. 6, p. 540–547, 2005.

[41] E.-G. Ng, D. K. Aspinwall, D. Brazil and J. Monaghan, "Modelling of Temperature and Forces when Orthogonally Machining Hardened Steel," *International Journal of Machine Tools & Manufacture,* vol. 39, p. 885–903, 1999.

[42] L. Qian and M. R. Hossan, "Effect on Cutting Force in Turning Hardened Tool Steels with Cubic Boron Nitride Inserts," *Journal of Materials Processing Technology,* vol. 191, p. 274–278, 2007.

[43] Y. Huang and S. Y. Liang, "Cutting Forces Modeling Considering the Effect of Tool Thermal Property—Application to CBN Hard Turning," *International Journal of Machine Tools & Manufacture,* vol. 43, p. 307–315, 2003.

[44] T. D. Marusich, "Effects of Friction and Cutting Speed on Cutting Force," in *Proceedings of ASME Congress*, Nov. 11–16, New York, Paper No. MED-23313, 2001.

[45] K. Lui and S. N. Melkote, "Material Strengthening Mechanisms and their Contribution to Size Effect in Micro-cutting," *Journal of Manufacturing Science and*

Engineering AUGUST 2006, Vol. 128 / 731, vol. 128, pp. 730-738, 2006.

[46] D. J. Waldorf, "A Simplified Model for Ploughing Forces in Turning," *Transaction of NAMRI of SME,* vol. 32, p. 447–454, 2004.

[47] S. Afazov, S. Ratchev and J. Segal, "Effects of the Cutting Tool Edge Radius on the Stability Lobes in micro-milling," *Advanced Materials Research,* vol. 223, pp. 859-868, 2011.

[48] H. D. Habbit, B. I. Karlsson and Srrensen, "ABAQUS Online Documentation: Version 6.4-1," *ABAQUS Inc.,* 2008.

[49] S. P. F. Jasper and J. H. Dautzenberg, "Material Behavior in Metal Cutting: Strains, Strain Rates and Temperature in Chip Formation," *Journal of Materials Processing Technology,* vol. 121, pp. 123-135, 2002.

[50] V. Kalhor, Modelling and Simulation of Mechanical Cutting, Ph. D. Thesis, Lulea University of Technology, Lulea.

[51] M. Gunay, I. Korku, E. Aslan and U. Seker, "Experimental Investigation of the Effect of Cutting Tool Rake Angle on Main Cutting Force," *Journal of Materials Processing Technology,* vol. 166, p. 44–49, 2005.

[52] M. C. Shaw, Metal Cutting Principles, New York: Oxford University, 2005.

[53] Y. C. Yen, A. Jain and T. Altan, "A Finite Element Analysis of Orthogonal Machining using Different Tool Edge Geometries," *Journal of Materials Processing Technology*, vol. 146, p. 72–81, 2004.

APPENDIX

The intercept and the slope for the regression lines used in the results and discussion section are shown in the following tables:

Table A-1: The intercept and the slope for the regression lines-cutting edge I (ρ_e= 60 μm)

	Kc		*Kf*	
Feed Rate (mm/rev)	Intercept	Slope	Intercept	Slope
0.05	3273	-1.3	2287	1.5
0.07	3167	-2.2	1829	-0.5
0.1	3003	-1.4	1603	-0.8
0.14	2903	-1.8	1301	-1.5

Table A-2: The intercept and the slope for the regression lines-cutting edge II (ρ_e= 30 μm)

	Kc		*Kf*	
Feed Rate (mm/rev)	Intercept	Slope	Intercept	Slope
0.05	3347	-2.5	1473	1.2
0.07	3029	-1.9	1362	-0.2
0.1	2997	-2.4	1263	-0.7
0.14	2803	-2.2	1156	-1.4